

# Efficient Simulation and Optimization of Simulated Moving Bed Chromatography Processes

#### Dissertation

zur Erlangung des akademischen Grades

#### Doktoring en ieur in

(Dr.-Ing.)

von M.Sc. Rojiar Pishkari

geb. am 27. May 1987 in Tehran

genehmigt durch die Fakultät für Elektrotechnik und Informationstechnik der Otto-von-Guericke-Universität Magdeburg.

Gutachter:

Prof. Dr.-Ing. Achim Kienle

Prof. Dr.-Ing. Andreas Seidel-Morgenstern

Promotionskolloquium am 04.07.2025

### **Abstract**

#### **Abstract**

Chromatography is a powerful separation technique that has been used on the preparative scale in a wide range of industries, including the chemical, pharmaceutical, and food industries. It allows the separation of molecules that are temperature sensitive and/or have similar physical properties such as stereoisomers or enantiomers and are therefore difficult to separate with other types of processes. For continuous process operation, simulated moving bed (SMB) technology was introduced by Broughton et al. in 1961 [11]. The main advantages of SMB processes compared to the classical batch processes are increased productivity and reduced solvent consumption. Since SMB processes are relatively expensive, model-based design and optimization play an important role. For this purpose, triangle theory has been developed [81]. It is based on an idealized model, which assumes isothermal operation, and constant flow rates, axial dispersion is neglected, and thermodynamic equilibrium is assumed between the liquid and the solid phase. Further, simulated moving bed operation is approximated by the assumption of a true moving bed operated under steady-state conditions, which is valid if the number of columns is high. Under these assumptions, an analytical solution to the design problem is possible for certain classes of equilibrium relations and binary separation problems with total separation. For a moderate number of columns, incomplete separation, and/or separation problems with more than two fractions usually a numerical approach is applied. Due to the presence of sharp concentration fronts, the numerical solution is often challenging and can be computationally expensive. In this thesis, the analytical approach is extended to the dynamic simulated moving bed model. Like the corresponding steady-state solution, It is based on the method of characteristics and first applied to processes with linear adsorption isotherms in chapter 3 of this thesis. The method is based on a discretization of the concentration coordinate instead of a discretization of the spatial coordinate, which is applied in the classical method of line approaches. Inside the columns, concentration values are propagated with characteristic velocity and new positions in space are calculated cyclically at selected time points. This method is exact for linear isotherms, the discretization of concentrations is only used for the representation of the solution and for evaluating the coupling conditions between the columns. Application is demonstrated for a binary separation in a 4-zone process and a center-cut separation in an 8-zone Simulated Moving Bed chromatography (SMB) process. In the center-cut separation, an intermediate component is isolated from a multi-component mixture. It is shown, that the computational effort can be reduced by more than a factor of 100 compared to the classical cell model which represents a first-order finite volume discretization scheme in space. In the fourth chapter, an extension to nonlinear isotherms is discussed. In the first step, a non-linear non-competitive Langmuir isotherm is considered. It is shown that the solution effort increases due to possible shock formation for non-linear isotherms. As a result of the shock formation, the method is no longer exact anymore but depends on the discretization of the concentration coordinate. Different strategies for capturing the shock formation are proposed and compared with each other in terms of accuracy and efficiency. Due to the limited applicability of the analytical approach to nonlinear isotherms, a different approach is then proposed in Chapter 5 for the optimization of SMB processes with competitive isotherms based on surrogate models. The approach is demonstrated for a binary separation process with competitive Langmuir isotherms. The method is iterative. In each iteration, artificial neural networks are fitted to the reference model based on randomly distributed sampling points around the optimal solution of the previous iteration based on the previous iteration's results. Maximum productivity under a certain purity requirement is obtained at the end of the process. The method is particularly attractive for processes with a high number of stages but reduced product purities, where classical triangle theory cannot be applied. Such situations may arise for a given plant with highly efficient columns for applications with moderate purity requirements, where product purities can be relaxed to increase productivity. In these cases, the proposed approach is also much faster than the numerical optimization of the full model. In this thesis, the focus is on local optimization. Even higher potential for improvement by surrogate-based optimization can be expected for deterministic global optimization, which is therefore becoming more and more attractive for the optimization of complex chemical processes like SMB processes.

### Zusammenfassung

Die Chromatographie ist ein leistungsfähiges Trennverfahren, das im präparativen Maßstab in einer Vielzahl von Industriezweigen eingesetzt wird, unter anderem in der Chemie-, Pharma- und Lebensmittelindustrie. Sie ermöglicht die Trennung von Molekülen, die temperaturempfindlich sind und/oder ähnliche physikalische Eigenschaften haben, wie z. B. Stereoisomere oder Enantiomere, und die daher mit anderen Verfahren nur schwer zu trennen sind. Für den kontinuierlichen Prozessbetrieb wurde 1961 von Broughton et al. die Simulated-Moving-Bed-Technologie (SMB) eingeführt [11]. Die Hauptvorteile von SMB-Prozessen im Vergleich zu den klassischen Batch-Prozessen sind die höhere Produktivität und der geringere Lösungsmittelverbrauch. Da SMB-Prozesse relativ teuer sind, spielen die modellbasierte Prozessgestaltung und Optimierung eine wichtige Rolle. Zu diesem Zweck wurde die Dreiecks-Theorie entwickelt [81]. Sie basiert auf einem idealisierten Modell, das von einem isothermen Betrieb und konstanten Durchflussraten ausgeht, die axiale Dispersion vernachlässigt und thermodynamisches Gleichgewicht zwischen der festen und der flüssigen Phase annimmt. Außerdem wird an Stelle eines simulierten Gegenstromes ein echter Gegenstrom der festen Phase angenommen, was aber nur bei einer relativ hohen Anzahl von Trennsäulen eine gute Näherung darstellt. Unter diesen Annahmen ist eine analytische Lösung des Auslegungsproblems für bestimmte Klassen von Gleichgewichtsbeziehungen und binären Trennproblemen mit vollständiger Trennung möglich. Bei einer mäßigen Anzahl von Trennsäulen, unvollständiger Trennung und/oder Trennproblemen mit mehr als zwei Fraktionen wird in der Regel ein numerischer Ansatz verwendet. Aufgrund des Auftretens steiler Konzentrationsfronten ist die numerische Lösung oft eine Herausforderung und kann rechenintensiv sein. In dieser Arbeit wird der analytische Ansatz auf das dynamische Prozessmodell mit simuliertem Gegenstrom erweitert. Wie die entsprechende stationäre Lösung des idealisierten Modells mit echtem Gegenstrom basiert er auf der Methode der Charakteristiken und wird zuerst in Kapitel 3 dieser Arbeit auf Prozesse mit linearen Adsorptionsisothermen angewandt. Die Methode basiert auf einer Diskretisierung der Konzentrationskoordinate anstelle einer Diskretisierung der Raumkoordinate, wie sie bei den klassischen Linienmethoden angewendet wird. Innerhalb der Säulen wandern die Konzentrationswerte mit charakteristischer Geschwindigkeit. Zu ausgewählten Zeitpunkten werden zyklisch neue Positionen in den Säulen berechnet. Diese Methode ist exakt für lineare Isothermen. Die Diskretisierung der Konzentrationen wird nur für die graphische Darstellung der Lösung und für die Auswertung der Kopplungsbedingungen zwischen den Säulen verwendet. Die Anwendung wird für eine binäre Trennung in einem 4-Zonen-Prozess und eine so genannte Center-Cut-Trennung in einem 8-Zonen SMB-Prozess demonstriert. Bei der Center-Cut-Trennung wird eine Zwischenkomponente aus einem Mehrkomponentengemisch isoliert. Es wird gezeigt, dass der Rechenaufwand im Vergleich zum klassischen Zellenmodell, das ein Diskretisierungsschema erster Ordnung im Ort darstellt, um mehr als einen Faktor 100 reduziert werden kann. Im vierten Kapitel wird eine Erweiterung auf nichtlineare Isothermen diskutiert. In einem ersten Schritt werden nicht-lineare, nicht-kompetitive Langmuir-Isothermen be-Es wird gezeigt, dass der Lösungsaufwand aufgrund einer trachtet. möglichen Schockbildung bei nichtlinearen Isothermen zunimmt. Als Folge der Schockbildung ist die Methode nicht mehr exakt, sondern hängt von der Diskretisierung der Konzentrationskoordinate ab. Es werden verschiedene Strategien zur Erfassung der Schockbildung vorgeschlagen und in Bezug auf Genauigkeit und Effizienz miteinander verglichen. Aufgrund der begrenzten Anwendbarkeit des analytischen Ansatzes auf nichtlineare Isothermen wird dann in Kapitel 5 ein alternativer Ansatz für die Optimierung von SMB-Prozessen mit konkurrierenden Isothermen auf der Grundlage von Ersatzmodellen vorgeschlagen. Der Ansatz wird für einen binären Trennungsprozess mit konkurrierenden Langmuir-Isothermen demonstriert. Die Methode ist iterativ. In jeder Iteration werden künstliche neuronale Netze an das Referenzmodell auf der Grundlage zufällig verteilter Stichprobenpunkte um die optimale Lösung der vorherigen Iteration herum angepasst. Am Ende des Verfahrens wird so die maximale Produktivität unter vorgegebenen Reinheitsanforderungen erreicht. Die Methode ist besonders attraktiv für Prozesse mit einer hohen Anzahl von Stufen, aber geringeren Produktreinheiten, bei denen die klassische Dreieckstheorie nicht angewendet werden kann. Solche Situationen können bei einer vorhandenen Anlage mit hocheffizienten Kolonnen für Anwendungen auftreten, bei denen die Produktreinheiten gelockert werden können, um die Produktivität zu erhöhen. In diesen Fällen ist der vorgeschlagene Ansatz auch viel schneller als die numerische Optimierung des vollständigen Modells. In dieser Arbeit liegt der Schwerpunkt auf der lokalen Optimierung. Ein noch höheres Verbesserungspotenzial durch surrogatbasierte Optimierung ist für die deterministische globale Optimierung zu erwarten, die daher für die Optimierung komplexer chemischer Prozesse wie SMB-Prozesse immer attraktiver wird.

## Contents

Lis	st of	Figures	xiii
Lis	st of	Tables	xix
Αd	crony	ms	xxi
N	omen	clature	xxii
1	Intr	oduction	1
	1.1	Chromatographic separation	1
	1.2	Simulated moving bed chromatography	3
	1.3	Center-cut separation	7
	1.4	State of the art and motivation	10
	1.5	Objectives and outline	14
2	The	oretical background	17
	2.1	Adsorption	19
	2.2	Model equation	22
	2.3	Triangle theory based on true moving bed chromatography	26
	2.4	Cell model	33
	2.5	Cell model for 8-zone SMB with raffinate and extract recycle	36
3	Ana	lytical solution for linear adsorption isotherms	41
	3.1	Adsorption isotherm	41
	3.2	Method of characteristics	42
	3.3	Implementation of analytical solution	43
	3.4	One column simulation	45

	3.5	4-zone SMB simulation	51
	3.6	8-zone SMB with raffinate recycle simulation	59
	3.7	Summary	71
4	Арр	proximate solution for nonlinear non-competitive adsorp-	
	tion	isotherms	73
	4.1	Non-linear adsorption isotherm and wave theory	73
	4.2	One column simulation	77
	4.3	4-zone SMB simulation	81
	4.4	Summary	85
5	Opt	imization of SMB processes using surrogate models	87
	5.1	Optimization description	88
		5.1.1 Purity	89
		5.1.2 Productivity	91
	5.2	Full-model equations and optimization	92
	5.3	Surrogate model	96
		5.3.1 Artificial neural network	97
	5.4	Algorithm development and dynamics	97
	5.5	Summary	102
6	Con	clusions and perspectives	103
	6.1	Analytical solution	103
	6.2	Approximate solution	104
	6.3	Surrogate-model optimization	105
Bi	bliog	raphy	107

# List of Figures

1.1	a. Schematic of a True Moving Bed, b. Schematic of a	
	Simulated Moving Bed	7
1.2	The chromatogram shows a hypothetical mixture contain-	
	ing three fractions. Fraction A is the first eluting fraction,	
	fraction B is the intermediate fraction, and fraction C is	
	the target	8
1.3	Cascades of independently operated 4-zone Simulated Mov-	
	ing Bed units for the separation of the ternary mixture	9
2.1	Chromatographic column structure	20
2.2	Single column chromatographic process schematic for math-	
	ematical description	23
2.3	Areas of separation obtained for linear isotherms	29
2.4	Areas of separation obtained for non-linear isotherms	32
2.5	Cascade of continuous stirred tanks (CSTs) in which ad-	
	sorbent and solvent are in equilibrium	34
2.6	8-zone SMB with raffinate recycle	36
2.7	8-zone SMB with extract recycle	39
3.1	Linear and nonlinear isotherm for one component [73]	42
3.2	Schematic illustration of (a) one-column and (b) two-column	
	chromatography with recycle configuration	45
3.3	Internal concentration profile of one component inside one	
	column solved by (a) Analytical solution (b) Cell model	
	with 100 grid points, (c) Cell model with 10000 grid points	47

3.4	Comparison of the computational time in case of the cell model for one column	48
3.5	Internal concentration profile of one component inside two- column configuration solved by (a) Analytical model (b) Cell model with 100 grid points, (c) Cell model with 10000 grid points	50
3.6	Comparison of the computational time in case of the cell model for two columns in series	51
3.7	Schematic illustration of 4 zone simulated moving bed chromatoghraphy	52
3.8	Internal concentration profile of binary mixture at the end of the cycle inside 4-zone SMB. The feed enters the system at point 0, the raffinate is removed at point 100 or 1000, and the extract is removed at point 300 or 3000. The solvent enters at point 200 or 2000. (a) Cell model with 100 grid points. (b) Cell model with 1000 grid points (c) Analytical model	55
3.9	Comparison of the computational time in case of cell model and analytical model for 4-zone SMB	56
3.10	Outlet concentrations from analytical solution (a1) First component in extract port and first run. (a2) First component in extract port and second run. (b1) Second component in extract port and first run. (b2) Second component in extract port and second run. (c1) First component in raffinate port and first run. (c2) First component in raffinate port and second run. (d1) Second component in raffinate port and first run. (d1) Second component in raffinate port and second run.	57

3.11	Outlet concentrations from cell model solution with 1000 cells (a1) First component in extract port and first run. (a2) First component in the extract port and second run. (b1) The second component is in the extract port and the first run. (b2) The Second component in the extract port and the second run. (c1) First component in the raffinate port and the first run. (c2) First component in the raffinate port and second run. (d1) The second component is in the raffinate port and the first run. (d1) The second component is in the raffinate port and the	
	second run.	58
3.12	Schematic illustration of 8-zone simulated moving bed chromatography	60
3.13	Internal concentration profile of ternary mixture inside a 8-zone SMB (a) Cell model with 100 grid points. (b) Cell model with 1000 grid points (c) Analytical model	63
3.14	Comparison of the computational time in case of numerical discretization method and analytical solution for 8 zone SMB and ternary separation	64
3.15	Outlet concentration profiles using an analytical solution.  (a1) Extract1 first run, (a2) Extract1 second run with 0.5 gr/l increase in the feed concentration, (b1) Extract2  first run, (b2) Extract2 second run with 0.5 gr/l increase in the feed concentration, (c1) Raffinate2 first run, (c2)  Raffinate2 second run with 0.5 gr/l increase in the feed concentration	65
3.16	Outlet concentration profiles using cell model. (a1) Extract1 first run, (a2) Extract1 second run with 0.5 gr/l increase in the feed concentration, (b1) Extract2 first run, (b2) Extract2 second run with 0.5 gr/l increase in the feed concentration, (c1) Raffinate2 first run, (c2) Raffinate2 second run with 0.5 gr/l increase in the feed concentration	66

3.17	Internal concentration profile of 5 component mixture inside 8-zone SMB (a) Cell model with 100 grid points. (b) Cell model with 1000 grid points (c) Analytical model	67
3.18	Comparison of cell and analytical model computational time for 5 component separation using 8 zones SMB	69
3.19	Outlet concentration profiles using cell model. (a1) Extract1 first run, (a2) Extract1 second run with 0.5 gr/l increase in the feed concentration, (b1) Extract2 first run, (b2) Extract2 second run with 0.5 gr/l increase in the feed concentration, (c1) Raffinate2 first run, (c2) Raffinate2 second run with 0.5 gr/l increase in the feed concentration	70
3.20	Outlet concentration profiles using analytical solution (a1) Extract1 first run, (a2) Extract1 second run with 0.5 gr/l increase in the feed concentration, (b1) Extract2 first run, (b2) extract2 second run with 0.5 gr/l increase in the feed concentration, (c1) Raffinate2 first run, (c2) Raffinate2 second run with 0.5 gr/l increase in the feed concentration	71
4.1	Characteristic patterns of behavior for linear compared to a nonlinear single solute or noncompetitive adsorption isotherms. The first column illustrates the type of isotherm, the second column shows the behavior during the loading of an empty bed, the third column shows the behavior during regeneration of a fully loaded bed with pure solvent. [24]	74
4.2	Characteristic curves in the z-t plane for linear adsorption isotherms (a) compared to nonlinear adsorption isotherms (b) with spreading waves (c) self-sharpening waves	76
4.3	Characteristic curves in the z-t plane with shock formation. Solid lines are characteristic velocities, and dashed lines are shock velocities between neighboring concentration values.	77
	uon varuos	1 1

4.4	The characteristics plot for two concentration values with	
	different catch up points. a) Catch up point coincides with	
	given time point $t_3$ . b) Catch up point in the interval $t_3-t_4$	79
4.5	Comparison of the cell model (solid red line) with the	
	approximate solution (blue dashed line) with $3$ and $17$	
	discretization points in the concentration vector	81
4.6	Schematic illustration of 4 zones simulated moving bed	
	chromatography	82
4.7	Concentration profile of a binary mixture separation using	
	the approximate model (a) and cell model (b)	84
4.8	Computational time for reaching cyclic steady state	84
5.1	Schematic illustration of binary mixture separation using	
	4-zone SMB	93
5.2	Optimal operating point (red star) predicted by the full	
	model (numerical solution) for a minimum purity of 0.85	
	of both products. Red, blue and green lines define the	
	total separation region according to triangle theory	96
5.3	Schematic illustration of an artificial neural network	98
5.4	Optimal point reached in each iteration and the process	
	of converging towards the final optimum. The green dot	
	in the up left diagram is the starting point	101
5.5	Optimal points (x) found by surrogate model and full model.	101

# List of Tables

3.1	Model parameters and column properties	46
3.2	Model parameters and column properties	49
3.3	Model parameters and column properties	53
3.4	Dimensionless flow rates (m-values)	54
3.5	Model parameters and column properties	61
3.6	Arbitrary adsorption Henry coefficient of the components	
	of the ternary mixture	62
3.7	Dimensionless flow rates	62
3.8	Model parameters and column properties	68
3.9	Dimensionless flow rates	69
4.1	Model parameters and column properties	85
4.2	Dimensionless flow rates	85
5 1	Comparison of the computational time	102

### Acronyms

CPU Central Processing Unit. 50, 54

**LC** liquid chromatography. 1

**ODEs** Ordinary Differential Equations. 53, 103

 ${\bf PDEs}$  Partial Differential Equations. 34, 103

**SMB** Simulated Moving Bed chromatography. iv, viii, xiv-xvi, 4–10, 14, 17, 18, 26–30, 35–38, 51, 55, 59, 62–64, 66, 69, 81, 85, 89–93, 95, 98, 103, 104

**TMB** true moving bed. 5, 6, 26–28

### Nomenclature

 $\Delta t$  Time step  $\dot{V}$  Volume flow-rate

 $\epsilon$  Porosity

 $A_c$  Cross sectional area of the column

 $c_{feed}$  Concentration of the feed flow

 $c_i$  Concentration of solute i in the solvent

 $D_{ax}$  Axial diffusion coefficient

 $H_i$  Solid phase isotherm adsorption (Henry constant)

*i* Specific solute

 $k_i$  Liquid phase isotherm adsorption

 $L_c$  Length of the column

lb Lower bound

 $m_k$  Dimensionless flow-rate ratio

Pr Productivity

 $Pu_E$  Extract purity

 $pu_R$  Raffinate purity

Q Flow-rate

- $q_i$  Concentration of solute i in the adsorbent
- $t_{sw}$  Switching time
- ub Upper bound
- v Interstitial velocity
- $V_c$  Volume of the column
- $x_{opt}$  Optimal point
- z Z coordinate

### **CHAPTER 1**

### Introduction

### 1.1 Chromatographic separation

Liquid chromatography (LC) is a crucial separation technique widely used for the purification of various substances. Its versatility allows it to be applied at different scales depending on the intended purpose. On a smaller scale, it is often used for analytical purposes. However, it can also be adapted for larger-scale operations for preparative purposes. This dual functionality makes it an important tool in both research and industrial applications [73].

The chromatography process is conducted by passing the mixture through a column containing a mobile phase and a stationary phase. liquid chromatography (LC) is based on the principle of selective interaction between the stationary phase and the components of the mixture being separated. As the mixture travels through the column, the stationary phase interacts differently with each component. This difference in interaction causes the components to separate, allowing them to be individually analyzed or collected.

Most stationary phases consist of a solid material, such as silica gel or a resin, coated onto the surface of small particles or packed into a column. The mobile phase consists of a liquid solvent that is used to transport the mixture through the column. As the mixture moves through the

column, the components with stronger interactions with the stationary phase move more slowly and remain in the column longer than those with weaker interactions. This difference in retention causes the components to separate and exit the column at different times, resulting in the separation of the mixture into individual components. There are several mechanisms used in the chromatographic separation process, but these can all be broken down into three basic elements:

Solutes - In the process, solutes are chemical components that are separated from one another. A suitable solvent is used to inject a mixture of at least two desired components into a chromatographic column.

Adsorbent – The stationary phase provides selective affinity for the different solutes, it makes it possible to separate them. Hence, it must at least meet two requirements: first, it must be stationary, at least for the duration of the relevant process. In addition, it must be capable of separating solutes with different affinities. As long as they are mechanically attached to a support material, liquid adsorbents can also be used as long as they are not flowing out of the chromatographic system during the separation process.

Solvent(desorbent) – It is the mobile phase that drives the separation of the solutes by providing the convective flow of solutes. There are several forms of it (gas, liquid, or even as a supercritical fluid [17, 18, 15]) provided it can flow through a packed bed. As with gradient chromatography and displacement chromatography, its composition does not have to remain constant during the separation process.

As mentioned, chromatographic separation involves solutes, solvents, and adsorbents. Despite this, they do not represent the entire experimental setup. There is still much more to say about the valves, detectors, pumps, and control systems that make modern chromatography possible, but these will be left out in this work.

As of today, examples of chromatography application are found in the fields of enantiomer separation [74, 9, 53], sugar separation [12, 21], petroleum derivative separation [44, 30, 8], protein separation [16, 84,

10] and even isotope separation [3, 43]. There are different types of liquid chromatography, including reversed-phase chromatography, normal-phase chromatography, ion-exchange chromatography, and size-exclusion chromatography. [73]. Each type of chromatography uses a different stationary phase and mobile phase to achieve separation based on different chemical and physical properties of the components of the mixture and the type of solid phase applied.

The development of innovative processes relies heavily on theoretical modeling and process simulation. These tools are crucial for gaining a deep understanding of transport phenomena and optimizing processes. By creating models that simulate real-world processes, researchers can predict potential outcomes and identify areas for improvement. Furthermore, these simulations allow for the optimization of various process parameters, leading to more efficient, cost-effective, and sustainable operations [73].

### 1.2 Simulated moving bed chromatography

The simplest application of the chromatographic principle is single-column chromatography. A column is usually packed with an adsorbent bed, and equipped with a pump, and detectors. A mixture of solutes is first introduced into the column, followed by the pumping of solvent free solution. As the solutes exit the column, they are collected sequentially, ideally well separated. The entire procedure can be repeated after regeneration of the column with solute-free solvent. Continuous operation and complex process layouts are not used with batch chromatography. Scaling-up is usually achieved by using larger columns and/or parallel processing units. It has been possible to improve batch chromatographic separation by improving hydraulic systems (such as pumps, valves, and detectors), using new solvents, and adsorbents, and in particular, reducing the size of adsorbent particles [22]. Several continuous and counter-current variations of the classical batch chromatographic process have been proposed to reduce solvent and adsorbent consumption [22, 76, 73, 61].

However, simulated moving bed (SMB) chromatography offers several benefits over batch chromatography. Here are some of the benefits of SMB chromatography:

Higher productivity: SMB chromatography is a process that enables continuous separation of substances, resulting in higher productivity due to reduced downtime between batches. This leads to faster and more efficient separations. Since this process operates continuously, there is minimal need for cleaning and setup in between, which in turn reduces the amount of waste generated by these processes.

Higher purity: The continuous nature of SMB chromatography also allows for tighter control over separation conditions, resulting in higher purity products.

Reduced solvent consumption: SMB chromatography typically uses less solvent than batch chromatography, which can reduce costs and make the process more environmentally friendly.

Reduced waste: SMB chromatography produces less waste than batch chromatography, which again makes the process more environmentally friendly. Some continuous chromatography systems are designed to allow for the continuous recycling of solvents and other consumables. This closed-loop system reduces the need for fresh solvents, further minimizing waste generation. Continuous chromatography systems typically operate with a steady-state flow, which allows for better control of solvent usage. In batch chromatography, the solvent is often used in excess to ensure complete elution. Continuous systems optimize solvent consumption, leading to less solvent waste.

Scalability: SMB chromatography is more easily scalable, making it suitable for both laboratory and industrial-scale separations.

Overall, SMB chromatography provides a more efficient, cost-effective, and environmentally friendly alternative to batch chromatography for the separation of complex mixtures. Since this continuous process is not cheap as well, modeling and simulating has a significant role in optimizing the process.

In simulated moving bed chromatography a Counter-current movement of the solid and liquid phase is approximated by cyclic switching of the inlets and outlets shown in Figure 1.1.

In counter-current operation, the mobile phase moves in the opposite direction to the stationary phase, meaning the two phases flow against each other. This setup maximizes separation efficiency, making it possible to separate complex mixtures with high levels of purity. The counter-current movement maintains a significant concentration gradient between the mobile and stationary phases, leading to improved resolution. Figure 1.1 illustrates a somewhat theoretical concept of an ideal counter-current system, known as a true moving bed (TMB). In this model, the solid phase circulates continuously at a constant flow rate, which is a key aspect of the concept. [73]

This configuration provides faster separations and allows for higher throughput, as the mobile phase can be processed more quickly. [73]

In the SMB chromatographic separation process, there are four external streams: the feed inlet, which introduces the mixture of components to be separated, the solvent inlet, which provides the mobile phase, the extract outlet, containing the more retained component, and the raffinate outlet, which becomes enriched with the less retained component. Based on the flow rates of the liquid phase, the process is divided into four distinct sections or zones within the system, each serving a specific and vital role in the overall separation process.

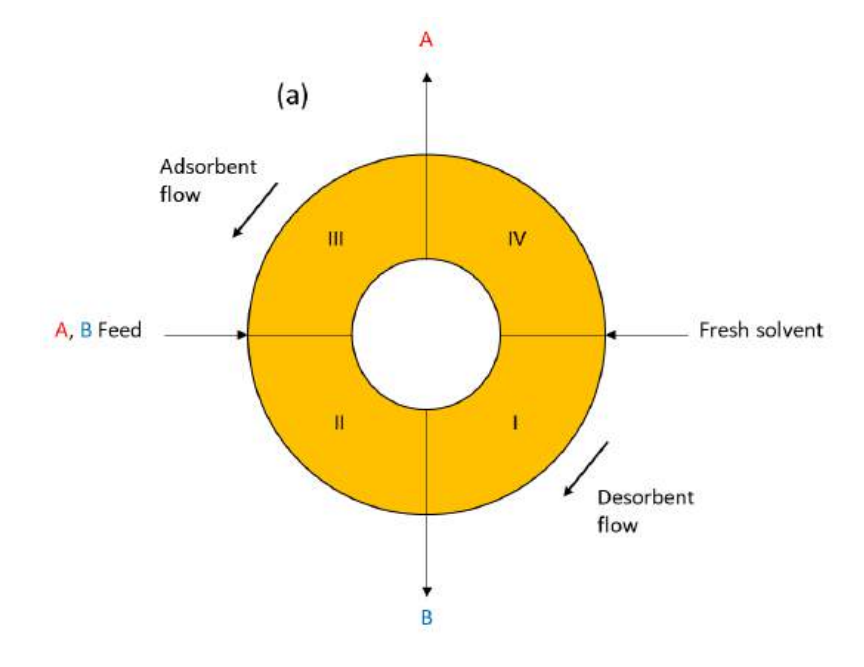
The actual separation of the two solute fractions primarily takes place in sections II and III. In these zones, the more retained component is adsorbed by the solid phase, which moves counter-currently to the liquid phase and is eventually transported to the extract port. At the same time, the less retained component is desorbed and carried by the moving liquid phase toward the raffinate port. This selective movement between the phases ensures that the desired components are separated with high precision and purity.

Additionally, section I of the system plays a crucial role in regenerating

the solid phase. An eluent stream is introduced in this section to desorb the strongly adsorbed components from the solid phase, allowing the solid to be reused in subsequent separation cycles. This regeneration step is essential to maintaining the efficiency and continuity of the separation process, ensuring that the solid phase remains active and capable of further adsorption in the next cycle. [73]

The feed mixture can be entirely separated into two pure products with the right choice of internal fluid flow rates in sections I–IV and the stationary phase velocity. SMB process operating conditions and flow rates are determined using triangle theory developed by Migliorini et al. [56] based on the TMB. This method allows the choice of proper flow rates for the TMB. A detailed explanation of the theory can be found in Chapter 2.

Due to the design of the traditional 4-zone SMB configuration, a single target solute can be isolated from a complex mixture if it is the first or last component to elute. To achieve this, it is necessary to feed the mixture into an SMB system as presented in Figure 1.1, between zones II and III. When the switching time and the solvent flow rates are chosen correctly, the net flow of most adsorbing solutes likely continues to flow in the direction of adsorbent flow and the net flow of the weakest adsorbing solutes moves in the direction of solvent flow. In zone I, the solvent flow rate must be chosen high enough to elute all strongly adsorbing solutes from the adsorbent and recover them in the extract port. It is critical to set the solvent flow in zone IV small enough that weakly adsorbing solutes are entirely removed from the solvent and recovered in the raffinate port between zones III and IV [5, 81].



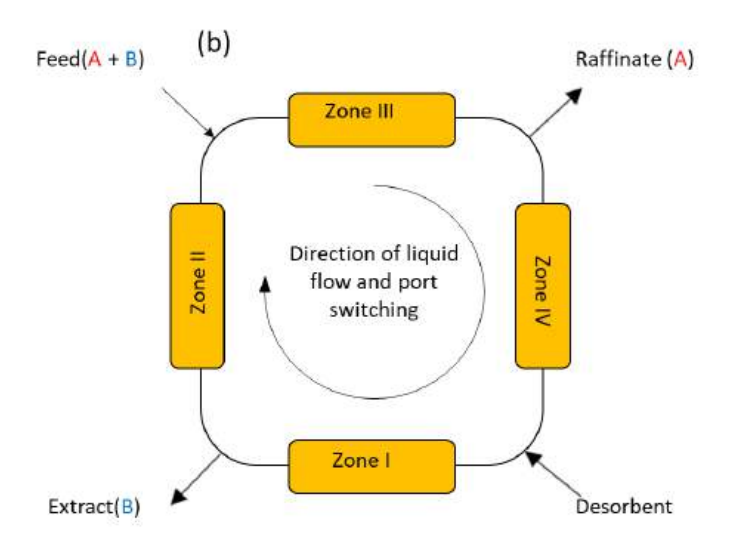


Figure 1.1: a. Schematic of a True Moving Bed, b. Schematic of a Simulated Moving Bed

### 1.3 Center-cut separation

It is essential to highlight a major drawback of the classical SMB system: the target solute must be either the one with the strongest affinity or the weakest affinity for successful isolation [1, 2].

However, in most cases, the target solute is part of an intermediate elut-

ing fraction, which is why it is necessary for the mixture to be separated into three fractions, as depicted in Figure 1.2, to be able to isolate the target.

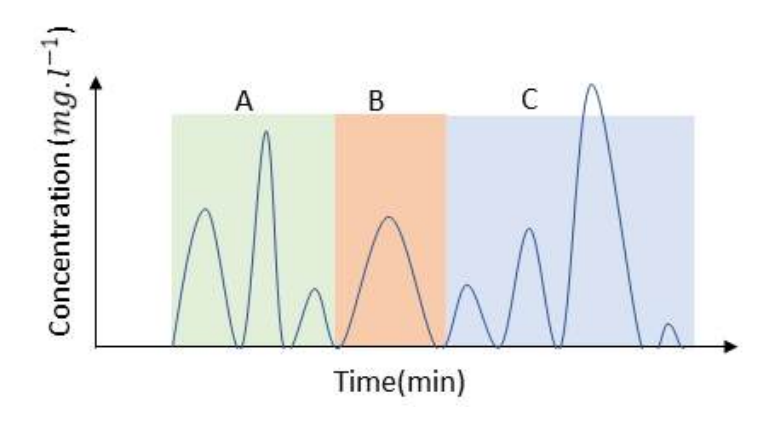


Figure 1.2: The chromatogram shows a hypothetical mixture containing three fractions. Fraction A is the first eluting fraction, fraction B is the intermediate fraction, and fraction C is the target.

Various SMB variants have been developed to separate ternary mixtures. Nikolaos et al. [60] compared different configurations of 4-zone and 5-zone SMB units using the equilibrium model, while other researchers have explored different SMB cascade arrangements for multi-component separation [32, 59, 58, 25, 83, 39]. Figure 1.3 shows a cascade of two 4-zone SMB units, separating a ternary mixture.

In addition to the three columns intermittent SMB [29, 28] proposed for ternary and pseudo ternary separations, other interesting configurations have been proposed as well, such as the five zone SMB [60, 57, 31]. There have been dynamic models and optimization algorithms employed to make realistic comparisons between the different arrangements of SMB columns [1, 2, 63, 10, 32, 39]. Additionally, several promising semi-continuous configurations have been proposed and extensively analyzed for executing center-cut separations [63, 4, 26, 47].

The continuous SMB processes mentioned above belong to the class of Center cut SMB processes. They provide powerful and versatile approaches that can be used for a wide range of conditions, including the

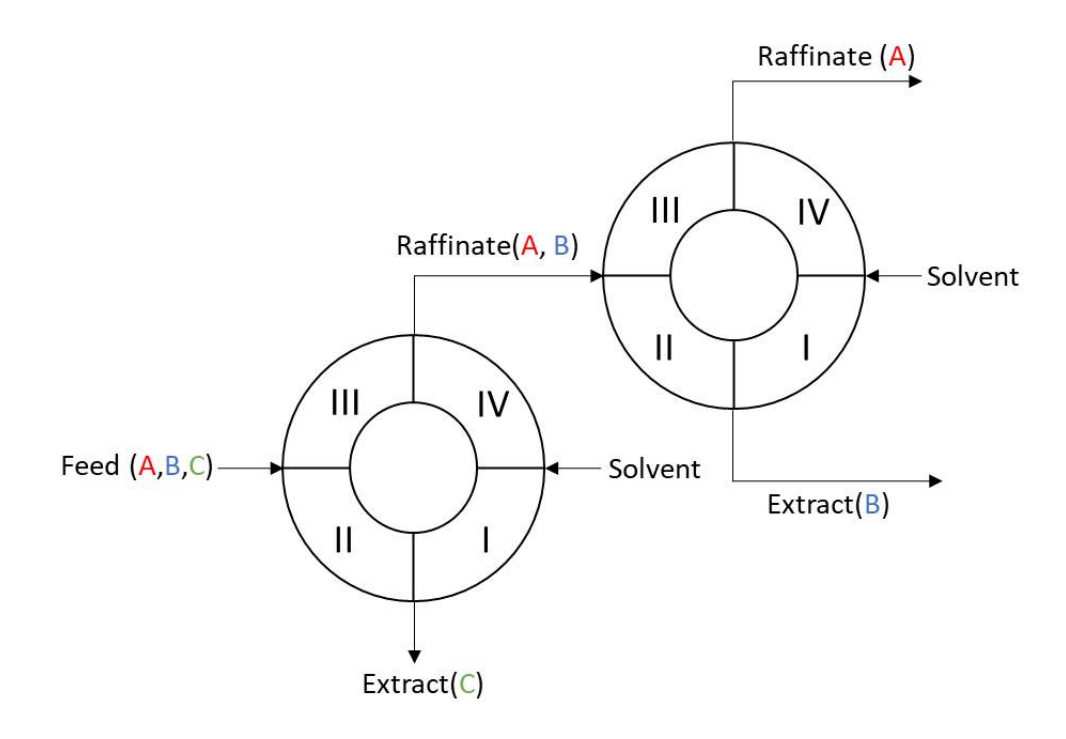


Figure 1.3: Cascades of independently operated 4-zone Simulated Moving Bed units for the separation of the ternary mixture.

purification of biopharmaceuticals, the separation of natural products, and the purification of industrial chemicals. It is particularly useful for the purification of high-value compounds, where a high degree of purity is required.

One of the advantages of center cut SMB chromatography is that it can handle large volumes of feed, and can be easily scaled up to an industrial scale. It is also very efficient in terms of solvent usage and waste generation, making it a more environmentally friendly option compared to traditional batch chromatography.

Overall, center cut SMB chromatography is an advanced and sophisticated technique that offers many advantages over traditional batch chromatography methods. It is an ideal solution for the purification of high-value compounds, where high purity and high yield are required.

#### 1.4 State of the art and motivation

As explained previously, the chromatographic process involves the separation of two or more chemical compounds present in liquid form within a solid adsorbent [23]. Depending on the two phases in the system, isotherms can be linear or nonlinear [23]. With the development of highly efficient columns and sophisticated detection systems over the last decades, liquid chromatography has become an increasingly important industrial separation technology.

Although it can be applied at a large scale, its production costs are often high, because of the high costs of packing materials and solvents [22]. A significant improvement in the economic performance of the process has been achieved with the use of SMB chromatography.

This dissertation began with a brief overview of chromatographic processes. Batch chromatography and the development of continuous chromatography have been explained.

Mathematical modeling of SMB chromatography and model-based design is important to understand the process deeply and determine complex interactions within the SMB system, including mass transfer, adsorption, and elution behavior [73]. Simulation of the process beforehand can identify the most efficient configurations, operating conditions, and process parameters for improved performance. An efficient mathematical model can lead to reduced experimental time and cost. Moreover, modeling encourages innovation by providing a platform for exploring novel configurations, materials, and operating strategies in SMB chromatography, leading to advancements in separation science and technology. The next chapter will be followed by a mathematical description of adsorption isotherms, design, and simulation of SMB processes.

The optimization and simulation of SMB processes can be computationally intensive, making it challenging to predict the performance of different process configurations and identify optimal operating conditions. A difficult task is determining the operating conditions, which is possible by the triangle theory under idealized condition [81, 55] that

will be explained in the next chapter as well.

The mathematical modeling of these processes usually results in partial differential equations (PDEs) [73]. Various models are used, depending on the assumptions made during modeling, such as equilibrium models, which assume thermodynamic equilibrium between the liquid and solid phases, or mass transfer models, which consider finite mass transfer resistance between both phases. In both scenarios, numerical solutions of the associated PDE systems are commonly used for simulating the process. Typically, simulating chromatographic columns numerically presents challenges, particularly because of the presence of steep concentration fronts. This has been a focal point in numerous research papers such as '[52, 51].

Fast and reliable methods are essential for real-time control and optimization of chromatographic processes. In practical applications, the method of lines (MOL) [85] is commonly employed to solve the system of partial differential equations (PDEs) using finite differences (FDs), finite elements (FEM), or finite volumes (FVM) for spatial discretization. A straightforward approach involves utilizing first-order finite volume discretization, resulting in widely used cell models, which can then be tackled using standard integrators. Accuracy and efficiency can be improved through the adoption of advanced high-resolution schemes and adaptive grids [48].

For instance, the CADET toolkit developed by Leweke ae al. [49] has a high accuracy and speed. In addition, Javeed et al. [27] present a high-resolution semi-discrete flux-limiting finite volume method designed to solve nonlinear equilibrium dispersive chromatography models. This method successfully mitigates numerical oscillations, maintains solution positivity, and precisely captures sharp discontinuities in chromatographic fronts, even on coarse grids. Lee et al. [46] have used an active counteraction scheme to improve the accuracy of the mixing cell model, making it applicable to various chromatographic configurations. The space-time conservation element/solution element (CE/SE) method, which is an explicit approach for solving systems of first order

hyperbolic partial differential equations, was introduced in Chernev et al. [13].

In the case of minimal axial dispersion, the equilibrium model allows for an analytical solution under specific conditions: piecewise constant initial and boundary conditions, and certain linear and nonlinear adsorption isotherms, such as the commonly used Langmuir isotherm. This analytical method forms the basis of the equilibrium theory [68, 54], which has emerged as a vital tool for conceptualizing chromatographic process design. An analytical solution for linear ideal SMB chromatography was introduced by Zhong et al., which is valid for binary mixture SMB chromatography and can describe the start-up of the process with empty columns [87].

A simplified algorithm for dynamic modeling chromatographic separation processes was introduced by Dünnebier et al., based on the nonlinear wave theory for an ideal chromatographic column and the Langmuir isotherm [19].

In this work, I present an innovative analytical approach to streamline and accelerate the simulation of linear adsorption isotherms in SMB chromatography systems. Extending from the approach proposed by Zhong et al., our efficient algorithm boasts notably enhanced speed while ensuring sharp and accurate propagation fronts. It is successfully applied to both 4- and 8-zone SMB chromatography systems featuring a centercut recycle design. Furthermore, its application is extended to a five-component mixture separation using an 8-zone SMB setup, yielding notably satisfactory results when compared to the conventional cell model. The method is versatile and capable of not only addressing startup scenarios but also accurately computing concentration profiles during other transient scenarios.

The preceding methodology is expanded to nonlinear non-competitive adsorption isotherm. Although this extension is not precise, it provides a commendable approximation of the solution within a reasonable time-frame. The approach is applied to a 4-zone SMB system and is validated by the cell model result. Once more, a substantial difference in computa-

tional time is observed. Despite their simplicity and speed, both methods have limitations, which eventually lead to surrogate-based optimization being implemented for optimizing the SMB chromatography process.

An integral aspect of the present work lies in leveraging cutting-edge design optimization techniques and computational capabilities. Through these means, one can markedly enhance the efficiency of separation processes in SMB chromatography by simply changing or modifying the process condition. Various valuable studies have been conducted in this field, employing a range of methodologies including Genetic Algorithms and diverse discretization techniques for their calculations [82, 36].

In this study, we aimed to circumvent numerical solutions of the rigorous model once more, choosing instead a data-driven approach to optimize the SMB system. Subsequently, we compared the outcomes with those derived from the numerical model.

To maximize economic potential, optimal operational parameters balancing productivity and solvent usage must be identified while meeting purity standards. Initially, the well-established triangle theory by Storti et al. serves as a preliminary tool for identifying these conditions, assuming a true moving bed process without axial dispersion and with thermodynamic equilibrium between solid and liquid phases [81]. Depending on application specifics, relaxing purity criteria can increase productivity. Kaspereit et al. proposed an extension of the triangle theory for this purpose, however with limitations and reliance on the same simplifications and assumptions [34]. Zhang et al. utilized genetic algorithms to optimize productivity and purity dynamically in SMB processes, comparing results with the Varicol process, although with high computational time [86]. Li et al. employed surrogate models, including proper orthogonal decomposition (POD) for cost-efficient reduced-order models and a coarse model. However, due to the complexity of SMB models, rigorous numerical optimization proves time-intensive [50].

In this work, we suggest a surrogate optimization approach similar to Kessler et al. [38], employing a simplified feed-forward artificial neural network for surrogate-based iterative optimization, requiring minimal data and enhancing numerical efficiency. The adoption of this novel approach significantly accelerated the optimization process, yielding results that exhibited good agreement with the numerical model. Such promising outcomes suggest that this method may represent a superior option for optimizing SMB systems.

#### 1.5 Objectives and outline

The primary aim of this thesis centers on new efficient methodologies tailored for the model-based analysis of chromatographic processes with both linear and non-linear (non-competitive) adsorption isotherms. A novel simulation algorithm for SMB processes with linear and non-linear adsorption isotherm is presented, which significantly reduces computational time and resources while maintaining high accuracy.

The algorithm employed for linear isotherms is grounded in an analytical solution derived from the underlying partial differential equations, employing the method of characteristics. This method illuminates the propagation dynamics of specific component concentrations within the chromatographic system.

To exemplify its efficacy, we showcase its application across various scenarios. Initially, we demonstrate its utility in binary mixture separation using 4-zone and ternary mixture separation using 8-zone SMB chromatography processes with center-cut separation configurations. Subsequently, we extend its application to a more complex setting, addressing a five-component mixture within an 8-zone SMB system. Once more, we compare the algorithm's outcomes against those generated by the cell model, thereby offering a comprehensive evaluation of its performance across diverse chromatographic scenarios.

Further, this work introduces an approximate solution designed for the complexity of non-linear and non-competitive adsorption isotherms, making use of the inherent dynamics governing the propagation of select component concentration values within the chromatographic column. To effectively represent this solution and evaluate the coupling conditions

across columns, a discretization of concentration values is necessitated. While the method does not furnish an exact solution, its precision is tightly associated with the intensity of discretization employed. Notably, the variations in velocities inherent to different concentration values lead to the formation of shocks, wherein higher concentration values propagate faster than smaller counterparts during loading an empty bed, prompting the significance of exploration of their spatiotemporal occurrences. Addressing this challenge entailed not only tracking the emergence and transit times of these shocks and concentration values within the current column but also their seamless integration into subsequent columns.

To underscore the practical utility of this approach, we showcase its application across both single columns and 4-zone SMB configurations. Compared to the prevalent discrete cell model, our proposed method markedly reduces the computational burden while retaining a commendable level of accuracy, thus declaring a promising method for chromatographic analysis.

In the end, the binary mixture separation process flow rates are optimized. The isotherm is Langmuir and competitive.

The ultimate aim of this endeavor terminates in the optimization of the SMB process, with a specific focus on maximizing productivity while adhering to predetermined purity constraints. Central to achieving this objective is the optimization of flow rates within the system. The limitation that the two previous methods for simulating the process with Langmuir adsorption isotherms have, underscore the necessity for an alternative approach.

Recognizing these constraints, we choose the adoption of a surrogate model, strategically chosen to accelerate and enhance the optimization process. By leveraging the versatility and efficiency afforded by this surrogate model, we aim to streamline the optimization efforts, thereby bringing us closer toward the ultimate goal of enhancing SMB process productivity while maintaining requisite purity levels.

A systematic iterative method is implemented to optimize SMB Chromatography with Langmuir adsorption isotherms, using a surrogate-based optimization strategy. Throughout each iteration, artificial neural networks are fitted utilizing randomly distributed sampling points around the optimal point attained in the previous iteration. This surrogate-based optimization technique offers a notable advantage in terms of efficiency over the full-blown model's numerical optimization process employed, particularly in scenarios involving highly efficient chromatographic columns.

This thesis is based on the following three articles:

 Fast and accurate simulation of simulated moving bed chromatographic processes with linear adsorption isotherms Pishkari, R. and Kienle, A.
 In Computer Aided Chemical Engineering (Vol. 48, pp. 487-492). Elsevier 2020

2. Fast and Accurate Solution for Simulation of Linear and non-Linear Adsorption Isotherm Simulated Moving Bed Chromatography Process using Dispersion Free column Pishkari, R. and Kienle, A. In preparation

3. Optimization of Simulated Moving Bed Chromatographic Processes using Surrogate Models

Pishkari, R. Fechtner, M. Kessler, T. and Kienle, A. In Computer Aided Chemical Engineering (Vol. 52, pp. 343-348). Elsevier 2023

#### **CHAPTER 2**

### Theoretical background

Mathematical modeling of simulated moving bed chromatography SMB is a crucial aspect of process design and optimization for this separation technique.

Mathematical modeling of SMB involves the development of mathematical equations that describe the dynamic behavior of the process. This includes the mass balance equations for the components in the feed and the two phases. In addition, the equations that describe the movement of the phases within the chromatography column are provided. These equations are solved numerically to predict the performance of the SMB system, including breakthrough curves, product purity and yield, and residence time distribution.

The thermodynamics of the system plays an important role in the view of process dynamics. This involves the determination of the distribution coefficients, which describe the affinity of each component for the two phases. These coefficients can be estimated experimentally or calculated using adsorption isotherm models.

Finally, the mathematical model must take into account the design parameters of the SMB system. These include the flow rate of the feed, the flow rate of the solvent, and the geometry of the column. These parameters can be optimized to maximize the efficiency and performance of the SMB system.

In conclusion, mathematical modeling is an essential tool for the design, optimization, and control of SMB processes. The models developed allow for a deeper understanding of the underlying physics and chemistry of the system and provide valuable information for the improvement of SMB performance.

To solve these equations, various numerical methods can be used, including finite difference methods, finite element methods, and differential equation solvers. The choice of method depends on the complexity of the equations and the desired accuracy of the solution.

Once the equations are solved, the performance of the SMB system can be predicted, including breakthrough curves, product purity and yield, and residence time distribution. The numerical approach also allows for the optimization of design parameters, such as the flow rate of the feed, solvent, and the geometry of the column. The main design parameters of the SMB process are the flow rates in different sections and the switching time. This will improve the efficiency and performance of the SMB process.

In summary, the numerical approach is a powerful tool for the analysis and optimization of SMB processes. It provides a detailed understanding of the behavior of the system and allows the identification of the key parameters that impact performance. This information can be used to design more efficient and effective SMB systems and to improve the separation performance of existing systems. Nevertheless, numerical approaches are computationally expensive, so this thesis aims to simplify and speed up this simulation.

In special cases also an analytical solution of the underlying model equation is possible. The analytical solution uses the method of characteristics (MOC) to solve partial differential equations, which describe the propagation of selected concentration values [68].

The analytical method offers both speed and accuracy in simulating chromatographic columns with linear adsorption isotherms under the ideal equilibrium model. It is particularly well-suited for highly efficient chromatographic columns characterized by minimal axial dispersion and sharp concentration gradients. The method is precise, with discretization of concentrations utilized solely for graphical representation and evaluation of coupling conditions between columns, without compromising accuracy.

In the case of multiple components, concentration profiles are transformed into a multi-dimensional tensor and component positions are determined based on individual propagation velocities. To calculate concentration profiles in subsequent time steps, new positions for concentration values are first computed. Node balances at column entrances are assessed, and resultant values are propagated into the column to fill gaps in the concentration vector from the left.

#### 2.1 Adsorption

In chromatography, the retention of solutes is differentiated by the adsorption process, which ultimately allows them to be separated. Modeling chromatographic separations requires an understanding of the thermodynamic equilibrium between the solvent and the adsorbent. It is called an adsorption isotherm if adsorption occurs at a constant temperature.

Typically, the adsorption isotherm  $q_i(\mathbf{c})$  represents the equilibrium composition of component i in the solid phase, and it generally depends on the composition of the fluid phase.

A schematic of a chromatographic column can be seen in Figure 2.1. Inside the column, the variable  $\varepsilon$  represents the porosity.

To accumulate molecules on solid surfaces, most chromatographic processes utilize the principle of adsorption. The adsorption isotherm depends on many variables, including temperature, solution ionic strength, solute interaction, pressure, PH, etc [78]. Porous and lumped adsorption isotherm models can broadly be classified [61]. Based on the pore size distribution of the adsorbent particles, three or possibly more phases may

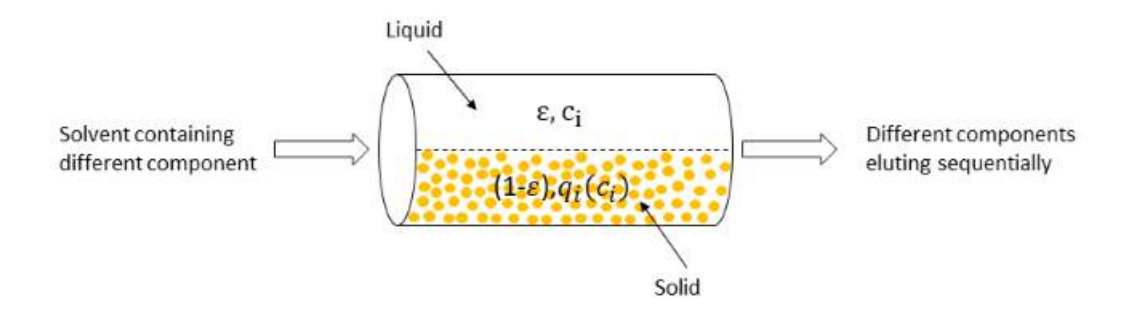


Figure 2.1: Chromatographic column structure

be taken into account: the solvent, the solid phase, and an intragranular stagnant fluid phase. The second category of adsorption isotherm models simplifies the mathematical description of the adsorbent to a homogeneous state.

Due to the principle of adsorption, most chromatographic processes operate by the deposition and accumulation of molecules on solid surfaces. A relevant industrial example of this is the adsorption of pollutants from waste air or water onto activated carbon, which illustrates the first two phase combinations. Adsorption occurs at a molecular level when the adsorbent surface forms binding forces with the molecules of the fluid phase. There are different types and strengths of binding forces. Bindings can be divided into two basic types.

- 1) Physical adsorption, or physisorption, involves physical binding due to the van der Waals or electrostatic forces. These forces are usually weaker than the chemical binding forces described below and allow physisorbed molecules to retain their chemical identity.
- 2) Chemical adsorption or chemisorption is the strongest type of binding. It is caused by valence forces, which are equivalent to chemical bonds, mainly covalent bonds [73].

There are also favorable and unfavorable adsorption isotherms. During favorable adsorption isotherms, i.e., when their curves are convex, the derivative of the adsorption isotherm function decreases as the concentration increases. This is typically caused by over-saturation of the adsorbent surface. In contrast to this, when adsorption isotherms are

unfavorable, the derivative of the adsorption isotherm function over increasing concentrations increases. This leads to a concave adsorption isotherm curve, typically observed when the adsorbed solutes interact synergistically. Adsorption isotherms can also have inflection points, causing them to have concave and convex regions. It is possible for the resulting curve to be defined by a series of multi-layer adsorption steps, depending on the mechanisms involved [61, 72].

Special cases of the adsorption isotherms considered in this thesis are:

1)Linear adsorption isotherm: for this isotherm, once the concentration of the solute in the mobile phase surpasses certain limits, further increments no longer lead to an increase in the amount adsorbed onto the stationary phase. Only within the initial low-concentration range of the mobile phase is there a linear correlation observed.

Within the initially linear segment of the adsorption isotherm, the connection between concentrations in the mobile and stationary phases, denoted as c and q respectively, is delineated by Henry's law:

$$q_i(c_i) = H_i c_i \tag{2.1}$$

 $H_i$  is known as the Henry constant in the linear adsorption isotherm.

2) Langmuir isotherm (competitive): Based on a homogeneous surface saturation model, the Langmuir isotherm equation (2.2) is the archetypal favorable adsorption model. It has proven highly effective in describing experimental data because it is thermodynamically consistent and tends to form a straight line at low concentrations, a characteristic frequently observed in various adsorption systems [72].

$$q_i(\mathbf{c}) = \frac{H_i c_i}{1 + \sum_{j=1}^n k_j c_j}$$
 (2.2)

As a special scenario, we also consider the non-competitive Langmuir isotherm, it is calculated by the following formula:

$$q_i(c_i) = \frac{H_i c_i}{1 + k_i c_i} \tag{2.3}$$

In this instance, individual components within the liquid solution do not influence each other's adsorption onto the solid phase.

3) Bi-Langmuir isotherm (competitive): A second term can be added to the Langmuir approach to generate the bi-Langmuir model for adsorbents with energetically heterogeneous adsorbents, which is often used to describe the adsorption equilibrium of enantiomers on chiral adsorbents.

$$q_i(\mathbf{c}) = \frac{H_{1,i}c_i}{1 + \sum_{j=1}^n k_{1,j}c_i} + \frac{H_{2,i}c_i}{1 + \sum_{j=1}^n k_{2,j}c_j}$$
(2.4)

A more accurate fit to experimental data can be obtained using alternative variations of the Langmuir isotherm, such as the Toth and Hill isotherms. These modifications incorporate additional terms into the original function, enabling a more effective representation of deviations from ideality. [73].

#### 2.2 Model equation

Physio-chemical complexity and the number of significant process properties determine the mathematical complexity of a chromatographic model. There are many different types of modeling approaches, including many analytical solutions comprehensively summarized in monographs by [70], [75], [23], and [22], as well as in various review articles. The following assumptions are applied in the remainder.

- 1. Thermodynamic equilibrium between the solid and liquid phases.
- 2. The adsorbent bed is homogeneous and packed with spherical particles of constant diameter.
- 3. The density and viscosity of fluids are constant.
- 4. The radial distribution is negligible.
- 5. It is an isothermal process.
- 6. Transport resistance inside the particles is neglected.

#### 7. The flow rate of the fluid phase is constant [73].

In consequence, one-dimensional material balances are used to describe chromatographic columns [73]. Detailed descriptions of models can be found in [22]. In this thesis, a single tubular packed-bed column of length L and with a cross-sectional area  $A_c$  is described at first.

The assumptions underlying this single-column process model are as follows. By injecting fluid into the column with a feed concentration  $c_{feed}$  of target components that may vary with time t and a constant volumetric flow rate  $\dot{v}$ , the fluid will act as the mobile phase for the separation process. In the column, the direction of fluid flow determines the spatial coordinate z as shown in Figure 2.2. There is a concentration c of target components in the fluid in the column.

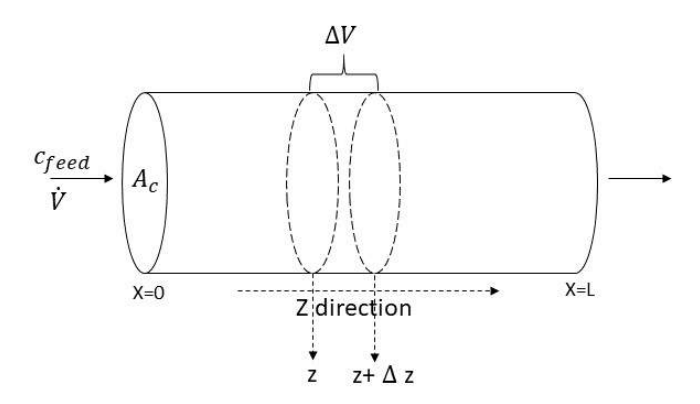


Figure 2.2: Single column chromatographic process schematic for mathematical description

In addition, no chemical reactions occur in the fluid phase. There is a mass transfer from the fluid phase to the solid phase based on the adsorption mechanism between the target components and the solid phase. This mass transfer is assumed to be small when compared to the convective transport in the fluid phase, so it is assumed that the interstitial velocity  $v = \frac{\dot{V}}{\varepsilon A}$  is constant in the fluid phase.

Inter- and intraparticle volumes are determined by the total porosity  $\varepsilon$  of the solid phase. There is no transport resistance inside the adsorbent. Generally speaking, porous particles are rigid, uniformly sized, and uni-

formly packed. Consequently, the total bed porosity  $\varepsilon$  is constant. Furthermore, no chemical instability or degradation is assumed for the solid phase. As a result, there are no chemical reactions in the solid phase. In the final assumption, the process is assumed to be isothermal. Therefore, it is possible to omit energy balances.

The local mass balance when  $\partial z$  and  $\partial t$  are arbitrarily small can be expressed as follows. Under these assumptions, the model equation can be obtained in differential form as [73]:

$$\frac{\partial c_i}{\partial t} + \frac{(1-\varepsilon)}{\varepsilon} \frac{\partial q_i(c_i)}{\partial t} + \frac{\dot{V}}{\varepsilon A} \frac{\partial c_i}{\partial z} = D_{ax} \frac{\partial^2 c_i}{\partial z^2}$$
 (2.5)

The term  $\frac{\dot{V}}{\varepsilon A}$  is equivalent to the average linear velocity of the solvent in the packed bed (interstitial velocity). Thus, this equation can be written as follows [73]:

$$\frac{\partial c_i}{\partial t} + \frac{(1-\varepsilon)}{\varepsilon} \frac{\partial q_i(c_i)}{\partial t} + v \frac{\partial c_i}{\partial z} = D_{ax} \frac{\partial^2 c_i}{\partial z^2}$$
 (2.6)

One of the most commonly used mathematical representations of a chromatographic column is this equation, often referred to as the equilibrium-dispersive model. Its reliability in explaining concentration profiles in finely packed beds stems from the simplification of solute diffusivity into a one-dimensional process. A further reduction of Equation 2.6 to the ideal model can be obtained by neglecting the dispersion in addition to the previous assumptions:

$$\frac{\partial c_i}{\partial t} + \frac{(1-\varepsilon)}{\varepsilon} \frac{\partial q_i(c_i)}{\partial t} + v \frac{\partial c_i}{\partial z} = 0$$
 (2.7)

In the general case (e.g., competitive Langmuir isotherm) when equilibrium has been established, the time derivative of the loading can be expressed by the slope of the isotherm and the time derivative of all components in the liquid phase:

$$q_i(c_1, c_2, ..., c_n)$$
 (2.8)

$$\frac{\partial q_i}{\partial t} = \sum_j \frac{dq_i}{dc_j} \cdot \frac{\partial c_j}{\partial t} \qquad j = 1, ..., n$$
 (2.9)

For the decoupled Langmuir isotherm, when equilibrium is reached, the rate of change of loading of one component can be defined by the rate of change of the relevant component in the liquid phase.

$$q_i(c_i) \tag{2.10}$$

$$\frac{\partial q_i}{\partial t} = \frac{dq_i}{dc_i} \cdot \frac{\partial c_i}{\partial t} \tag{2.11}$$

According to Equation 2.1, if  $q_i$  and  $c_i$  have a linear relationship, Equation 2.7 for the linear isotherm case can be simplified to [73]:

$$q_i = H_i(c_i) (2.12)$$

$$\frac{\partial q_i}{\partial t} = H_i \frac{\partial c_i}{\partial t} \tag{2.13}$$

$$\frac{\partial c_i}{\partial t} \left( 1 + \frac{1 - \varepsilon}{\varepsilon} H_i \right) + v \frac{\partial c_i}{\partial z} = 0 \tag{2.14}$$

For the non-competitive Langmuir isotherm, the relationship between the component's loading and its concentration is described as follows:

$$q_i = \frac{H_i c_i}{1 + k_i c_i} \tag{2.15}$$

$$\frac{\partial q_i}{\partial t} = \frac{H_i}{(1 + k_i c_i)^2} \cdot \frac{\partial c_i}{\partial t}$$
 (2.16)

Initial and boundary conditions for the chromatographic column are necessary to solve systems of partial differential and algebraic equations. A set of initial conditions defines the values for concentration and loading at time t=0, which corresponds to the startup phase. It is typically

assumed that the columns are not preloaded, meaning their initial values are zero. [73]:

$$\begin{cases}
c_i = c_i(t=0) = 0 \\
q_i = q_i(t=0) = 0
\end{cases}$$
(2.17)

The integration of Equations 2.7 is normally carried out by using the following boundary conditions, in which  $c_{in,i}(t)$  describes the concentration profile at the inlet.

$$\begin{cases}
c_i(z=0,t) = c_{in,i}(t) \\
\frac{\partial c_i(z=L,t)}{\partial z} = 0
\end{cases}$$
(2.18)

For all models that do not include dispersion, the boundary condition is  $c_i(z=0,t)=c_{in,i}(t)$ . In the case of highly efficient columns, the differences between the solutions for various boundary conditions are generally negligible [22]. Different boundary conditions can be readily assessed within numerical simulations [73].

## 2.3 Triangle theory based on true moving bed chromatography

In this section, we describe the conditions under which SMB units operating parameters are designed under ideal conditions, i.e., disregarding axial dispersion and mass transfer resistance, therefore assuming infinitely efficient columns. Triangle theory was developed as an elegant technique to simplify the choice of proper operating parameters like flow rates of the ideal TMB [14]. Besides the fluid phase, the solid phase is also moving at a steady state, allowing continuous separation in the TMB system. In the binary separation case, two inlets - feed and adsorbent - and two outlets - extract and raffinate - are used to provide a complete separation of mixtures composed of two target components. Due to this, the process can be divided into four sections, each called a "zone". Further developing their work on SMBs, Storti et al. [79, 81]

showed that SMBs and TMBs are equivalent under the above assumptions and if the net flow ratio between the solvent and the adsorbent in each zone k (described by  $m_k$ ) is the same. This is according to the following relation:

$$m_k = \frac{\dot{V}_{k,smb}t_{sw} - V_c\varepsilon}{V_c(1-\varepsilon)} = \frac{\dot{V}_{k,TMB}}{\dot{V}_s}$$
 (2.19)

In this formula,  $t_{sw}$  is the switching time and the solid phase flow rate can be described as follows:

$$\dot{V}_s = \frac{V_c(1-\varepsilon)}{t_{sw}} \tag{2.20}$$

For the linear adsorption isotherm, as long as  $m_k$  is greater than the adsorption Henry coefficient of a solute, the net direction of its mass flow is the same as that of the solvent flow, since the solute mass flow caused by solvent convection is greater than the mass flow caused by adsorbed solutes. In contrast, when the adsorption Henry coefficient is greater than  $m_k$ , the solute mass flow follows in the same direction as the adsorbent flow. The solute concentration shock can be effectively squeezed between two zones when  $m_k$  is greater than the Henry coefficient of adsorption in one zone and lower in the neighboring one [25]. There are a number of ways in which these solvent-adsorbent flow ratios can be selected in all zones. By choosing the right combination of solvent-adsorbent flow ratios in every zone, it is possible to separate solutes with different Henry coefficients by compressing their concentration fronts at the interfaces between the zones and collecting them purely at the outlet [72].

Based on Equation 2.19, which defines a dimensionless flow rate  $m_k$ , and using the equilibrium model (Equation 2.14) and an adsorption Henry coefficient  $H_i$  in zone  $k(v_{i,k})$ , we can determine the velocity of a solute i front or rear concentration shock when it exhibits a linear adsorption isotherm [72].

$$v_{i,k} = \frac{(Fm_k + 1)L}{(FH_i + 1)t_{sw}} \tag{2.21}$$

L is the column length, F is the phase ratio of the column (determined by  $\frac{1-\varepsilon}{\varepsilon}$ , and  $t_{sw}$  is the switching interval of the SMB process.

Additionally, in a real SMB system, there are dead volumes between the zones, as opposed to a TMB system. In SMB the pumps, frits, connections, tubing, and valves between the columns cause dead volumes [73]. It is still inevitable that dead volumes will exist even in an optimized system, even if the dead volumes are reduced. In the case where the dead volumes between the zones are constant and there is no severe back-mixing within them (which is a reasonable assumption for capillary tubes), then it is possible to use the method proposed by Katsuo et al [35]. to account for the delay in the break-through curves that resulted from the extra volume that had to percolate. Nowak et al. [62] modified the original formula to incorporate the extra retention time resulting from the dead volumes into the adsorption Henry coefficient.

In Equation 2.19,  $\dot{V}_{k,smb}t_{sw}$  shows the volume of liquid phase passing through the column in one cycle, Consequently, the flow ratios involved in separation and regeneration inside the system are dependent on these two. The flow ratios in zones II and III determine the separation performance of the feed mixture, while those in zones I and IV determine the regeneration performance. Around the flow ratios  $m_2$ ,  $m_3$ , and  $m_4$ ,  $m_1$ , two parametric domains are defined. In the triangle theory, the flow ratios are described without taking the dead volumes and the nonlinearities of the system into consideration, such as the sensitivity of the column efficiencies on the zone flow rates and the column kinetics. Thus, these regions serve only as a guide to orientation. In the literature, dead-volume effects have been reported over separation regions [35]. In a four-zone SMB unit with a linear adsorption isotherm, Figure 2.3 shows the operating ranges of dimensionless flow rates. The vertical axis represents dimensionless  $m_I$  and  $m_{III}$ , while the horizontal axis represents dimensionless  $m_{II}$  and  $m_{VI}$  for systems operating with linear adsorption isotherms.

Figure 2.3 depicts the parameter ranges for qualitative separation of

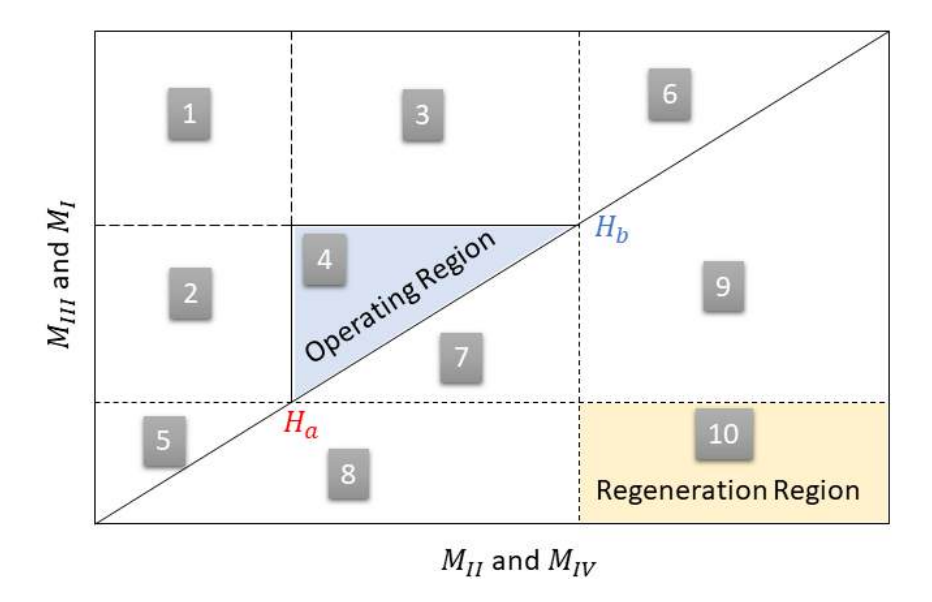


Figure 2.3: Areas of separation obtained for linear isotherms.

extract and raffinate fractions using a four-zone SMB. The triangular shape of the operating region, as shown in the diagram, is a result of linear adsorption isotherms and was first presented by Storti et al. in 1993 as the "triangle theory" [81]. This diagram is used to predict dimensionless flow rates for SMB measurement, and since its invention, SMB units have been successfully operated using this methodology. It has been expanded to other variants, adsorption isotherms, and operating conditions, as cited in sources [22, 60, 37, 62, 63, 77, 34].

The triangular region labeled as "4" in blue shows all the possible combinations of dimensionless flow rates  $m_{II}$  and  $m_{III}$  that, when used with the dimensionless flow rates  $m_I$  and  $m_{IV}$  in the yellow region (called the regeneration region), can effectively separate the two different fractions. The feed stream, which consists of solutes a and b, is continuously separated into two streams: the extract stream, which contains solute b, and the raffinate stream, which contains solute a.

The operation in the different regions in Figure 2.3 can be described below:

#### 1. Region 1: No pure outlets.

- 2. Region 2: Pure raffinate only.
- 3. Region 3: Pure extract only.
- 4. Region 4: Total separation.
- 5. Region 5: Fresh Solvent in the raffinate.
- 6. Region 6: Fresh feed in the extract.
- 7. Region 7: Incomplete regeneration of both phases.
- 8. Region 8: Incomplete regeneration of the solid phase.
- 9. Region 9: Incomplete regeneration of the liquid phase.
- 10. Region 10: Total regeneration.

For every colored region, there exists an operating point that, when located within or on the tip of it, results in complete separation and regeneration. The optimal operating points, located at the edges of the colored regions, offer the highest productivity, the lowest solvent consumption, and therefore, the most favorable operational costs for the SMB. These optimal operating points must satisfy certain conditions for successful total separation and complete regeneration:

$$H_B \le m_1 < \infty \tag{2.22}$$

$$H_A \le m_2 \le m_3 \le H_B \tag{2.23}$$

$$\frac{-\varepsilon}{1-\varepsilon} \le m_4 \le H_A \tag{2.24}$$

Outside the triangle, purity can be lower than that inside the triangle. In the  $m_2$ ,  $m_3$  diagram, the diagonal line indicates the region with the highest solvent consumption and lowest productivity, where the feed flow rate is zero. It is not feasible to operate in the region below the diagonal unless the plant configuration allows the reversal of flow in the zones of the  $m_2$ ,  $m_3$  diagram.

The minimum flow ratios, which can be negative, can be calculated using Equation 2.19 when cyclic volumetric flow rates are zero.

As a means of ensuring a safe separation, it must meet the conditions outlined in Equations 2.25 and 2.26. Solvents or feed injected into the system may flood the extract if the following criteria are not met.

$$m_2 \le H_B \tag{2.25}$$

$$m_3 \ge H_A \tag{2.26}$$

If regeneration conditions based on Equations 2.22 and 2.24 are not met, then incomplete regeneration of the liquid and/or solid phase may take place (regions 7, 8, 9). Thus, the concentration profiles could break through from zone IV to zone I, resulting in a negative impact on the whole separation process.

In the linear case, the triangle shape remains constant but in the Langmuir case, it varies according to the concentrations of the components in the feed mixture. Figure 2.4 illustrates the separation regions for a Langmuir isotherm separation process.

Below are the explicit boundaries of the triangle-shaped separation region in the  $(m_2, m_3)$  diagram illustrated in Figure 2.4. Below is the formula for calculating the triangle's tip [56]:

$$w = \left(\frac{\omega_B H_A}{H_B}, \frac{\omega_B [H_B (H_A - \omega_B) + (H_A - H_B)]}{H_A (H_B - \omega_A)}\right)$$
(2.27)

In the above quadratic equation,  $\omega_A$  and  $\omega_B$  are the roots:

$$(1 + k_A C_A + k_B C_B)\omega^2 - [H_A(1 + k_B C_B) + H_B(1 + k_A C_A)]\omega + H_A H_B = 0$$
(2.28)

Although the above equations are derived through a complex mathematical procedure, the final result is simply a set of algebraic expressions that

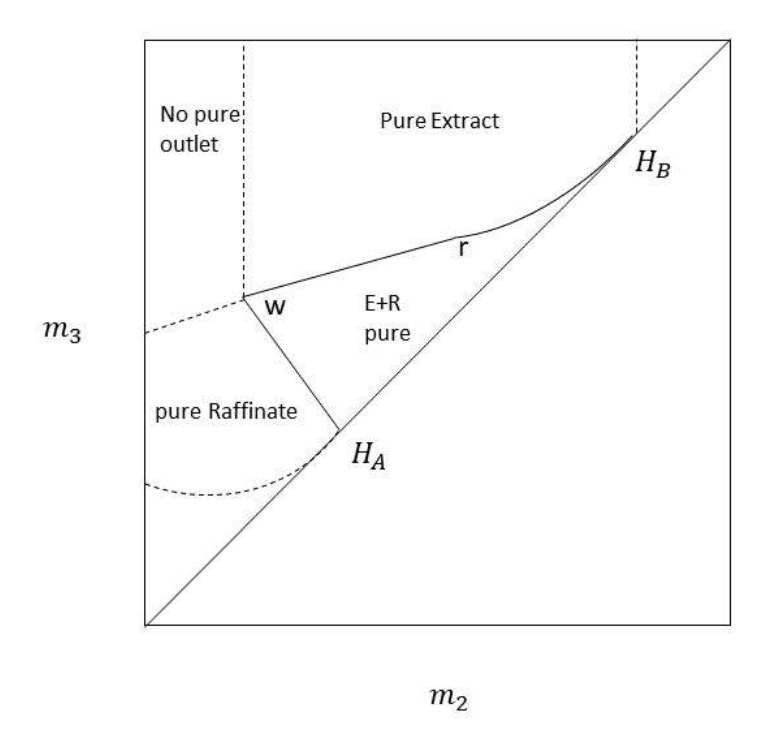


Figure 2.4: Areas of separation obtained for non-linear isotherms.

can be easily applied. Furthermore, the topological structure of the separation regions in the  $(m_2, m_3)$  plane illustrated in Figure 2.4 is close to that achieved in the linear case [56].

Moreover, the complete separation region is surrounded by three different separation regions in the nonlinear case as well. The region of pure raffinate can be found in the lower-left corner of the  $(m_2, m_3)$  diagram, as shown in Figure 2.4 which is followed by the regions of no pure outlet and pure extract that can be found proceeding clockwise from the lower left corner of the  $(m_2, m_3)$  diagram. There are, however, some significant differences between the two models; for example, the boundaries of the complete separation region in the Langmuir model depend on the feed composition and the constraints on the flow-rate ratios as opposed to the linear isotherm [55].

Often, sub-optimal operating points are determined using the safety margin method, directly affecting the separation productivity and solvent consumption. The following expressions give the dimensionless flow rate

ratios between zones 1 and 4 before the safety margin [56]:

$$m_1 = H_B \tag{2.29}$$

$$m_4 = \frac{1}{2}(m_3 + H_A + k_A C_A(m_3 - m_2)) - ((m_3 + H_A + k_A C_A(m_3 - m_2))^2 - 4m_3 H_A)^{\frac{1}{2}}$$
(2.30)

The Langmuir isotherm approaches the linear isotherm when the feed concentration tends to zero, and the flow-rate calculation is the same as the linear case. In both situations, triangle theory can be a valuable guide. It is possible to determine optimal operating points for the plant based on information about the dead volume and the plant itself to increase the probability of an initial satisfactory separation. As soon as the operating points have been determined, the switching time is calculated in such a way that the feed and maximum productivity of the plant is reached while the effects of dead volumes are minimized as much as possible. The internal and external flow rates can be obtained by knowing the column switching time.

#### 2.4 Cell model

The basic idea behind the cell model is to divide the chromatographic system into discrete elements or cells, each representing a small volume or section of the chromatographic column. These cells are used to simulate the movement of solutes as they interact with the stationary phase and the mobile phase.

Cell models are often used in conjunction with numerical methods and computer simulations to predict chromatographic performance under different conditions, such as varying mobile phase composition, flow rates, and column geometries. By adjusting model parameters and inputs, one can optimize separation conditions to achieve desired separation efficiency and resolution.

This method involves conceptualizing the column as a series of interconnected equilibrium continuous-stirred tanks (CSTs), in which solvent and adsorbent are in equilibrium [22] giving rise to the equilibrium stage or plate models. Rather than devising dynamic microscopic balances, the column is depicted as a sequence of a finite number n of identical cells. Each cell contains a mixture of liquid and solid phases, with both phases thoroughly mixed, and a continuous stream of mobile phase flows steadily through a series of N ideally stirred tanks (CSTs). Each tank has a total volume of  $\frac{V_c}{n}$ . Within each tank, a fraction  $(1 - \varepsilon)$  is filled with the solid phase, while the concentration within the liquid remains consistent between the solid phase and the pore phase [73].

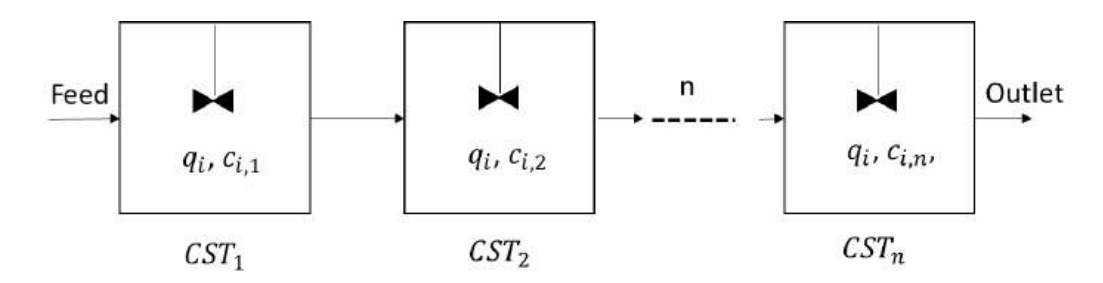


Figure 2.5: Cascade of continuous stirred tanks (CSTs) in which adsorbent and solvent are in equilibrium.

The cell model represents a first order finite volume discretization of the Partial Differential Equations (PDEs) model (2.7) with negligible axial dispersion. It can be directly obtained by balancing finite cells and is used as the reference model in this work.

By neglecting the diffusion term and spatial discretizing in the z direction, the mass balance of solute i in the  $j^{th}$  cell of the zone k and the general Langmuir adsorption isotherm can be described by:

$$\frac{\partial c_{i,j}}{\partial t} + F \frac{\partial q_i(\mathbf{c}_{i,j})}{\partial t} + v_k(c_{i,j} - c_{i,j-1}) = 0$$
 (2.31)

Where  $\frac{(1-\varepsilon)}{\varepsilon}$  is replaced by F and  $v_k = \frac{\dot{V}_k n}{V_c}$ .  $v_k$  has the dimension of  $\frac{1}{s}$  which is different from the interstitial velocity used in partial differential equation. When considering linear isotherms, the formulation can be expressed as follows:

$$\frac{\partial c_{i,j}}{\partial t} + FH_i \frac{\partial c_{i,j}}{\partial t} + v_k (c_{i,j} - c_{i,j-1}) = 0$$
 (2.32)

where  $H_i$  corresponds to the adsorption Henry coefficient of the solute i. Rearranging the Equation 2.32 results in:

$$\frac{dc_{i,j}}{dt} = \frac{v_k}{(1+FH_i)}(c_{i,j-1} - c_{i,j}); \quad j = 1....n$$
 (2.33)

For the nonlinear, noncompetitive Langmuir adsorption isotherm, where the adsorption of one component does not influence the adsorption of others, the formula can be modified to:

$$\frac{dc_{i,j}}{dt} = \frac{v_k}{(1 + F\frac{H_i}{(1 + b_i c_i)^2})} (c_{i,j-1} - c_{i,j}); \quad j = 1....n$$
 (2.34)

Taking the feed port as the starting point and continuing in the direction of the solvent flow, the subscript j indicates the position of the considered cell. In the zone k, the volumetric solvent flow rate is given in  $l.min^{-1}$  by  $v_k$ ,  $c_{i,j}$  is the concentration of the solute i in any particular cell, in  $mg.l^{-1}$ , and, the chromatographic column volume is shown by  $V_c$ . n is the total number of cells in each zone.

SMB internal concentration profiles can be calculated by integrating Equations (2.31) for each of the n cells and changing the boundary condition of the columns periodically after each cycle [63]. This was accomplished using MATLAB in this dissertation. The differential equations of the cells where solvent flows into the system (often called nodes) must be adjusted to take into account either the dilution or concentration caused by the injection of solvent or the feed stream to properly model the SMB process.

This system reaches a cyclic steady state after a certain number of cycles [41]. The repetition pattern of the concentration profiles in the outlet ports during each cycle determines the cyclic steady state of the system [71, 80].

## 2.5 Cell model for 8-zone SMB with raffinate and extract recycle

Figure 2.6 illustrates an 8-zone SMB with raffinate recycle. In the first sub-unite, the ternary mixture separates into two fractions, one extract which contains solute C, and the raffinate which contains solutes A and B. The raffinate fraction would be recycled to the second sub-unit to be separated into two different fractions of A in the second raffinate and B in the second extract.

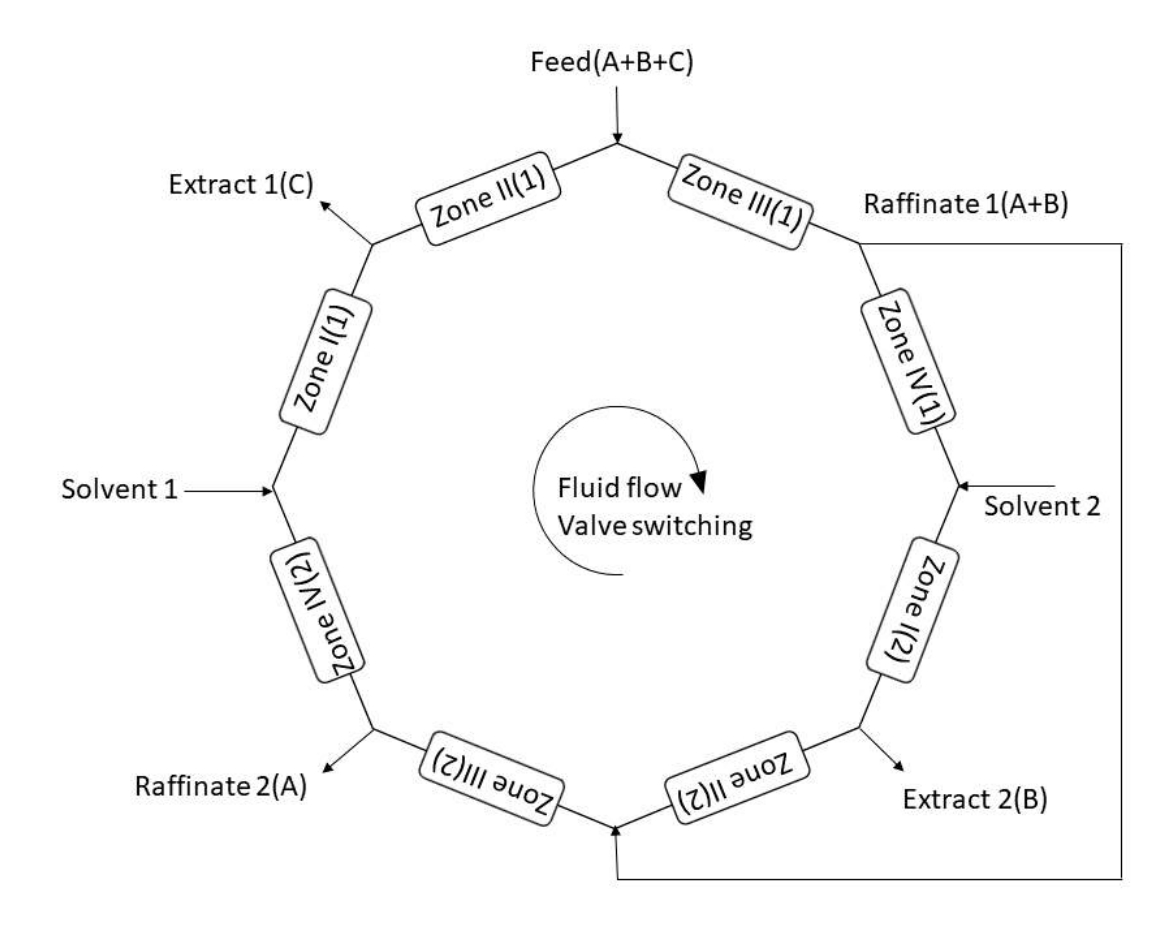


Figure 2.6: 8-zone SMB with raffinate recycle

Every column is divided into cells in the SMB simulation, with n representing the number of cells per zone or column, which can range from hundreds to thousands. The result is large and sparse equation systems.

In this work, they are solved using ODE solvers in MATLAB. Equation 2.31 can be implemented to any cell in the 8-zone SMB which does not have any neighboring cells that need extra equations and different mass balances nor inlet and outlet ports.

In each cell, the adsorbent and solvent are in equilibrium, and the solutes are partially adsorbed onto the adsorbent surface and partially dissolved in the solvent. The mass balance of one solute in the  $j^{th}$  cell and j = 1, ..., n which is located in the  $k^{th}$  zone or column, can be expressed as the following [7]:

At the feed inlet port:

$$\frac{dc_{i,2n+1}}{dt} = \frac{v_{III,1}}{(1+F\frac{\partial q_i}{\partial c_i})} \left(\frac{1}{v_{III,1}} (v_{II,1}c_{i,2n} + v_F c_{i,F}) - c_{i,2n+1}\right)$$
(2.35)

These equations are only valid for decoupled isotherms like linear and non-competitive Langmuir. For competitive Langmuir  $\frac{\partial q}{\partial c}$  is a matrix and division has to be replaced by multiplication with the inverse.

In the first zone or column, the cell numbers are from 1 to n. In the second zone, they are from n+1 to 2n. In the third zone, they are from 2n+1 to 3n. This continues until the eighth zone, in which the cell numbers are from 7n+1 to 8n.

At the second solvent inlet port:

$$\frac{dc_{i,4n+1}}{dt} = \frac{v_{I,2}}{(1 + F\frac{\partial q_i}{\partial c_i})} \left(\frac{v_{IV,1}}{v_{I,2}} c_{i,4n} - c_{i,4n+1}\right)$$
(2.36)

At the raffinate recycle port:

$$\frac{dc_{i,6n+1}}{dt} = \frac{v_{III,2}}{(1+F\frac{\partial q_i}{\partial c_i})} \left(\frac{1}{v_{III,2}} \left(v_{II,2}c_{i,6n} + v_{rec}c_{i,3n}\right) - c_{i,6n+1}\right)$$
(2.37)

At first, the solvent inlet port:

$$\frac{dc_{i,1}}{dt} = \frac{v_{I,1}}{(1 + F\frac{\partial q_i}{\partial c_i})} \left(\frac{v_{IV,2}}{v_{I,1}} c_{i,8n} - c_{i,1}\right)$$
(2.38)

Mathematically, setting up an SMB model involves connecting the boundary conditions of each column model, incorporating nodes that represent material balances of cell models. Inlet concentrations  $c_{in}$  represent the initial boundary conditions of the columns at the start of each section, while outlet concentrations  $c_{out}$  are the concentrations calculated at the end of each section. Intermediate node balances involve equating volume flows and assigning the outlet concentration to the inlet concentration of the subsequent column. Since SMB is a cyclic process, boundary conditions for individual columns are altered after a switching period  $t_{sw}$  [73].

Due to the strong resemblance between simulated and true countercurrent flows, TMB models are commonly used for designing SMB processes, particularly for determining optimal operating parameters such as inlet and outlet flow rates and shifting times. Operating conditions are determined in terms of m-values which are obtained from Equation (2.19), and are linked to the fluid flow rate and switching time.

When specifying the operating parameters, it is crucial to define independent variables. A typical approach involves specifying internal flow rates and the switching time (for SMB models) or solid flow (for TMB models). It's important to note that external flow rates must satisfy the overall mass balance.

SMB with 8 zones can be configured to perform ternary separation under extract recycle. Figure 2.7 demonstrates an 8-zone SMB with extract recycle. Most of the equations for the mass balances are the same as the raffinate-recycle configuration, except for the recycle part and the nodes at which it leaves and enters the system.

At the feed inlet port:

$$\frac{dc_{i,2n+1}}{dt} = \frac{v_{III,1}}{(1+F\frac{\partial q_i}{\partial c_i})} \left(\frac{1}{v_{III,1}} (v_{II,1}c_{i,2n} + v_F c_{i,F}) - c_{i,2n+1}\right)$$
(2.39)

At the second solvent inlet port:

$$\frac{dc_{i,4n+1}}{dt} = \frac{v_{I,2}}{(1+F\frac{\partial q_i}{\partial c_i})} \left(\frac{v_{IV,1}}{v_{I,2}}c_{i,4n} - c_{i,4n+1}\right)$$
(2.40)

At the extract recycle port:

$$\frac{dc_{i,6n+1}}{dt} = \frac{v_{III,2}}{(1+F\frac{\partial q_i}{\partial c_i})} \left(\frac{1}{v_{III,2}} \left(v_{II,2}c_{i,6n} + v_{rec}c_{i,n}\right) - c_{i,6n+1}\right)$$
(2.41)

At first solvent inlet port:

$$\frac{dc_{i,1}}{dt} = \frac{v_{I,1}}{(1 + F\frac{\partial q_i}{\partial c_i})} \left(\frac{v_{IV,2}}{v_{I,1}} c_{i,8n} - c_{i,1}\right)$$
(2.42)

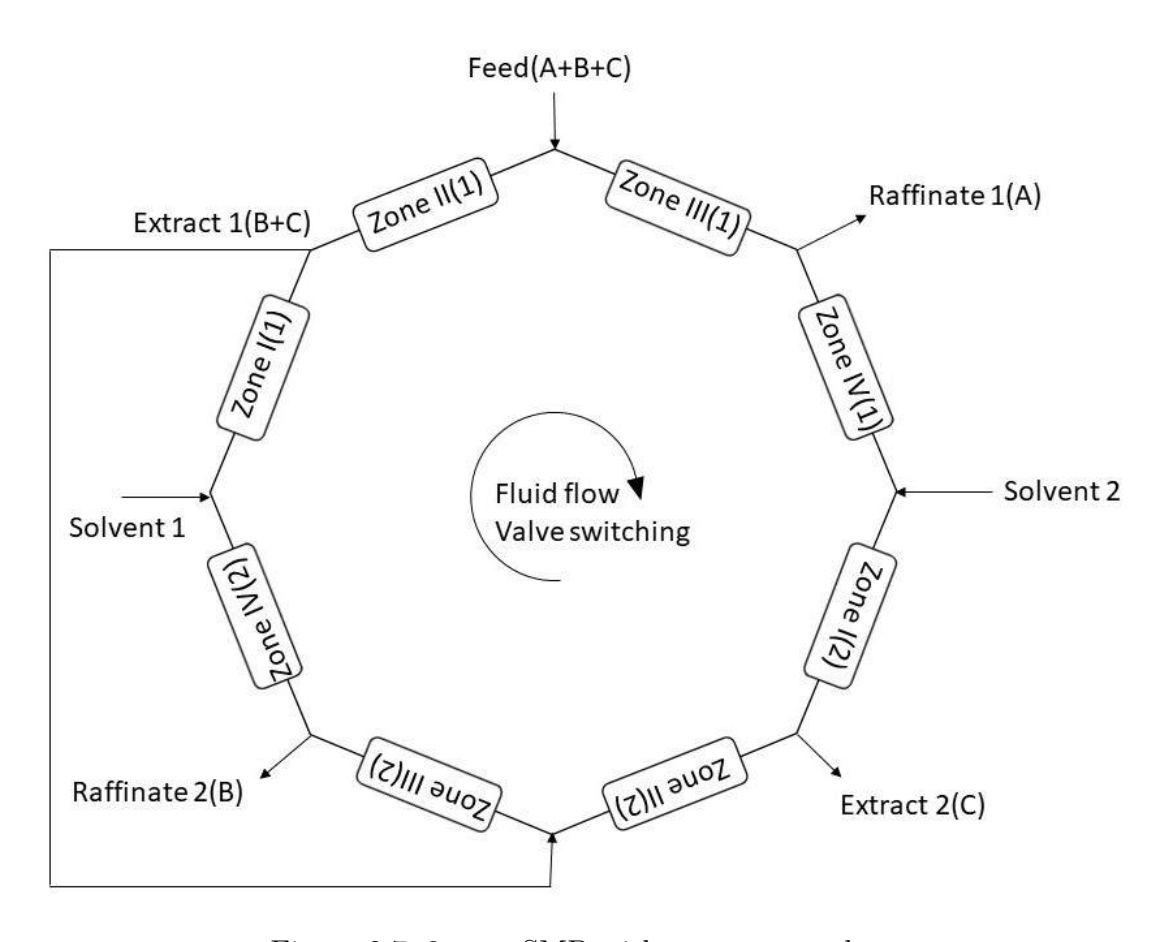


Figure 2.7: 8-zone SMB with extract recycle

#### **CHAPTER 3**

# Analytical solution for linear adsorption isotherms

#### 3.1 Adsorption isotherm

This chapter is based on the publication [66] published in Computer Aided Chemical Engineering, where the objective was to develop a rapid and precise solution for linear isotherm adsorption for SMB systems. An adsorption isotherm is a mathematical model that describes the relationship between the concentration of a solute in the mobile phase and the amount of solute adsorbed onto the stationary phase in a chromatography system.

Graphing the solid load  $q_i$  against the concentration of the solute in the fluid phase  $c_i$  under constant temperature showcases the progression of the adsorption isotherm.

The concentration of the solute in the mobile phase and the amount of solute adsorbed onto the stationary phase, c, and q, are directly proportional in the initial range of the adsorption isotherm. The adsorption coefficient H (Henry constant) is a measure of the interaction strength between the solute and the stationary phase. As the solute's concentration in the mobile phase increases so does the amount of solute adsorbed

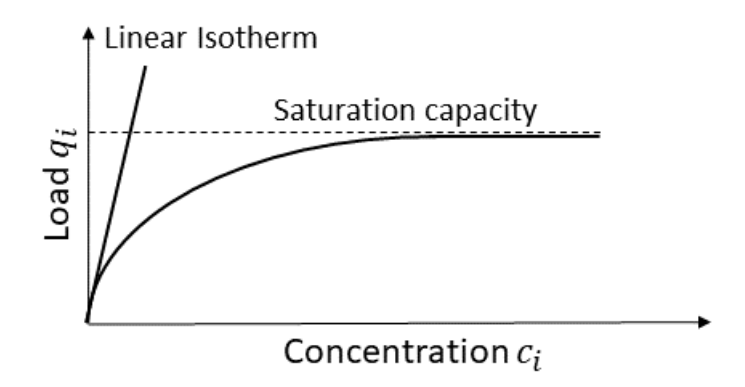


Figure 3.1: Linear and nonlinear isotherm for one component [73]

until the adsorption sites on the stationary phase are saturated. The linear adsorption isotherm assumes that the value of H is constant over the entire range of solute concentrations.

The linear adsorption isotherm can be represented mathematically by Equation 2.1 in chapter 2, where q is the amount of solute adsorbed per unit mass of the stationary phase, c is the concentration of the solute in the mobile phase at equilibrium, and H is the adsorption coefficient or the equilibrium constant [73]. The linear adsorption isotherm provides a useful starting point for understanding and optimizing chromatography systems, and it is often used as a basis for more complex adsorption models. Here it is assumed that the adsorption is decoupled and far from the saturation capacity.

#### 3.2 Method of characteristics

A powerful approach to obtaining analytical solutions for first-order partial differential equations is the method of characteristics. Due to the original model's second order in space, one is only able to apply this method when diffusion is ignored. The following partial differential equation is used as a starting point for single-component chromatography.

$$\frac{dc_i}{dt} + \frac{1 - \varepsilon}{\varepsilon} \frac{dq_i}{dt} + v \frac{dc_i}{dz} = 0 \tag{3.1}$$

Based on the following assumptions:

$$\begin{cases} q_i = q_i(c_i(t, z)) \\ c_{i,in}(t) = c_i(t, 0) \\ c_i(0, z) = c_{i,0}(z) \end{cases}$$
(3.2)

The initial concentration at t = 0 is  $c_{i,0}$ , and  $c_{i,in}$  is the boundary condition. With a slight adjustment to the terms of Equation 3.1, a solute's convectional velocity  $v_i$ , as a function of the solvent interstitial velocity  $v_i$ , the column's porosity  $\varepsilon$  and the adsorption coefficient  $H_i$  in the z direction is introduced according to Rhee et al. [69]:

$$v_{i} = \frac{dz}{dt} = \frac{\partial z}{\partial c_{i}} \frac{\partial c_{i}}{\partial t} = \frac{v}{\left(1 + \frac{1 - \varepsilon}{\varepsilon} H_{i}\right)}$$
(3.3)

As proposed by Rhee et al. [69], the method of characteristics can be applied to solve the equilibrium model. According to the solvent velocity, the adsorption isotherms, and the concentration of the solutes, it is possible to calculate the migration velocity and shape of the solute concentration shocks analytically. The front migration velocity of the process is independent of the concentration if the adsorption isotherms are in the linear domain. It can be expressed by Equation 3.1 as a function of the adsorption Henry coefficient. It is also possible to integrate the right-hand side of the second differential Equation 3.3.

$$c(t) = c_{in}, \quad z - z_0 = \frac{v}{(1 + \frac{1-\varepsilon}{\varepsilon}H_i)}(t - t_0)$$
 (3.4)

This is accomplished by selecting values for the integration constants  $c_0$ ,  $z_0$ , and  $t_0$  so that these constants satisfy either the initial condition or the boundary condition.

#### 3.3 Implementation of analytical solution

For simulating the SMB processes, the analytical solution which is obtained from Equation 3.4 is implemented in discrete form, i.e., the initial profile of each component in each column is discretized and put into a matrix form according to:

$$\begin{bmatrix} concentration \ value \ 1 & concentration \ value \ 2 \dots & concentration \ value \ n \\ position \ value \ 1 & position \ value \ 2 \dots & position \ value \ n \\ \hline (3.5) & \\ \end{bmatrix}$$

In the multicomponent case, the corresponding concentration profiles are put together in a multi-dimensional tensor form, and the positions for each component are calculated using its specific propagation velocity.

In the remainder, 100 spatial grid points are used for this purpose. Further, time is also discretized. In particular, 100 time steps per switching interval are used in this study. For the calculation of the concentration profiles in the next time step, first, new positions are calculated for the concentration values in Equation 3.5 using Equation 3.4 according to:

$$new \ position = old \ position + v_i.dt$$
 (3.6)

Afterward, the concentration vector is rearranged. Concentration values with positions beyond the actual column length are removed, and the other values are shifted to the right. Then, node balances at the entrance of the columns are evaluated, and resulting values are propagated into the column to fill the gaps in the concentration vector from the left. For this purpose, it is important to calculate at which exact intermediate time point the concentration values have left the previous column, which is again simply done by application of Equation 3.4 according to:

$$intermediate\ time\ point = old\ time\ point + (column\ length - old\ position)/v_i$$

$$(3.7)$$

Corresponding node balances are evaluated at this time point, and the propagation into the subsequent column for the remaining time of this interval is determined. In this way, the solution is exact. Discretization is done only for the graphical representation of the solution. Accuracy is not affected.

#### 3.4 One column simulation

Initially, the analytical method was applied to a single column with a single solute in order to investigate its feasibility. Simulating a single column does not require connections and node balances; therefore it is less complex than a multi-column system simulation. For a batch system with a single column, the simulation is rather straightforward, but for a continuous system also a recycling of the fluid phase needs to be considered. Even though the configuration does not make sense in reality, it was a useful starting point for implementing an easy node balance and an analytical solution. Adsorption-desorption does not change as concentration increases, since the isotherm is linear. The solvent is selectively removed at the outlet to keep the interstitial velocity constant. This configuration provides information on how the profile behaves with non-zero initial concentrations. Afterward, the configuration is extended to two columns with a recycle from the end of the second column to the beginning of the first column. An outlet is also considered at the end of the second column to balance flow rates.

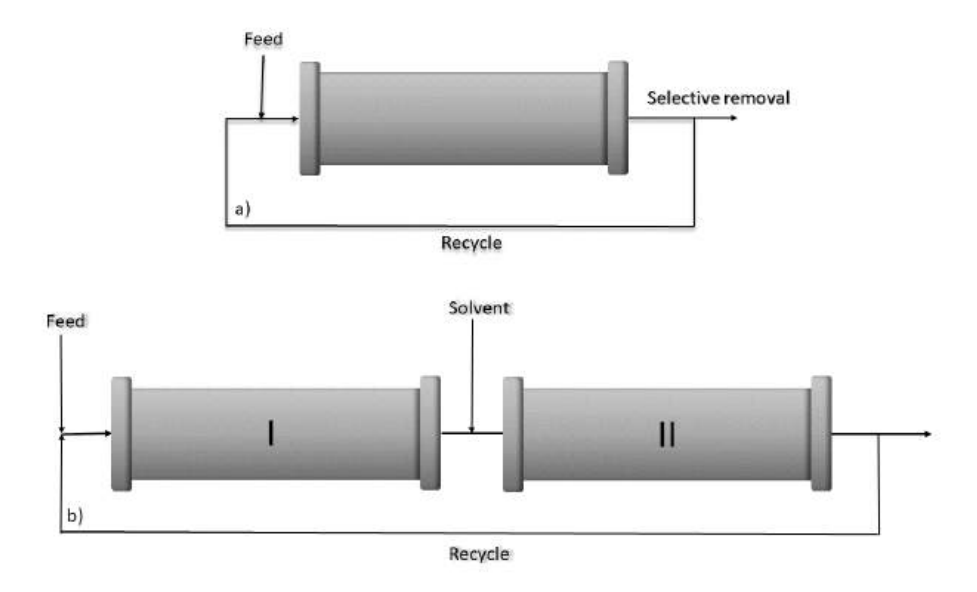


Figure 3.2: Schematic illustration of (a) one-column and (b) two-column chromatography with recycle configuration

The first configuration which contains one column and a recycle at the end of the column has a feed concentration of 3 [g/l], the internal flow rate has been considered 0.4 [ml/s] due to the pressure drop limitations. The model parameter, the constants for the adsorption, and the flow rates are given in Table 3.1.

Table 3.1: Model parameters and column properties

Parameters	Value	
Number of the column	1	
Column dimensions	$10[\mathrm{mm}]$	
Column porosity	0.75	
Henry constant	2	
Feed flow rate	$0.1[\mathrm{ml/s}]$	
Recycle flow rate	$0.3[\mathrm{ml/s}]$	
Internal flow rate	$0.4[\mathrm{ml/s}]$	
Feed concentration	3[gr/l]	

The node balance at the entry of the column is as follows:

$$c_{in} = \frac{((c_f * Q_f) + (c_r * Q_r))}{Q}$$
(3.8)

Where  $c_f$  is the feed concentration,  $Q_f$  is the feed flow rate,  $Q_r$  and  $c_r$  are the respective recycle flow rate and the recycle concentration.

The solution for the one-column chromatography with a recycle connection using ode15s solver and cell model is presented in Figure 3.3 (b) and (c) as the reference solution and the analytical model solution is given in Figure 3.3 (a). As it is shown in the Analytical model the solution is highly precise and causes no dispersion. Regarding the simulation time and CPU time, the analytical model is a bit faster but the difference is not considerable. The absolute CPU time depends on the actual hardware which is used. However, the main focus here is on the relative CPU time of different solution approaches, mainly independent of the hardware.

It should be pointed out that in the cell model to get to the high efficiency in the simulation and decrease the dispersion, the number of grid points needs to be increased noticeably to be able to have a solution close to the Analytical model like 3.3 (c). This means that the computational time will increase as well. In the case of having 10000 grid points, which is still not so close to the analytical solution the computational time is about one hour.

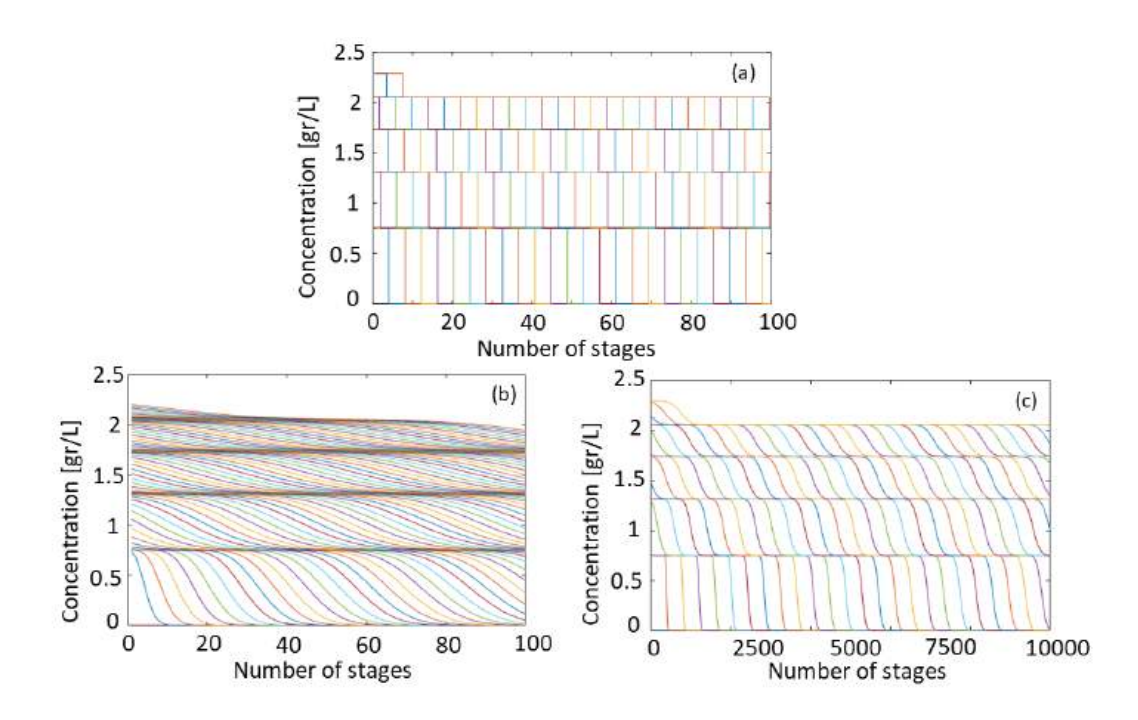


Figure 3.3: Internal concentration profile of one component inside one column solved by (a) Analytical solution (b) Cell model with 100 grid points, (c) Cell model with 10000 grid points

In Figure 3.4, computational time are given for varying numbers of grid points used in the cell model. The figure also includes a comparison of computational time with the analytical model.

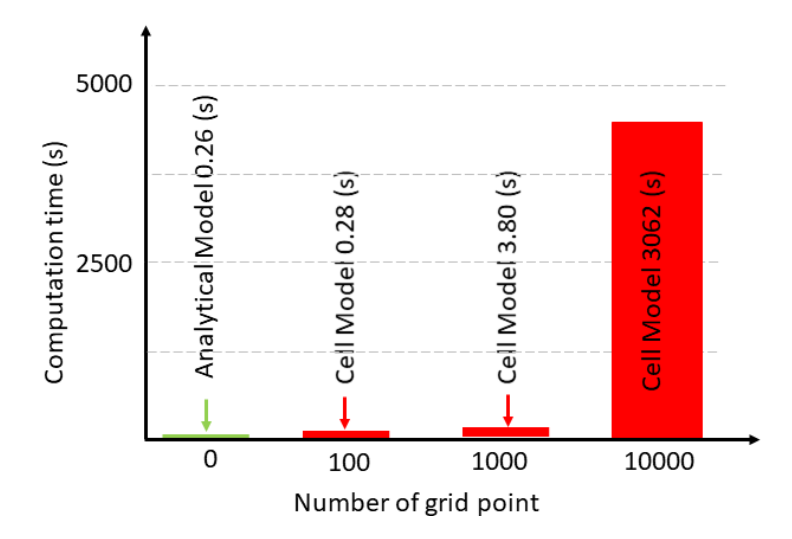


Figure 3.4: Comparison of the computational time in case of the cell model for one column

The bar chart illustrates the considerable difference in calculation time between the analytical and numerical models. Despite the fact that the numerical model with 10,000 grid points is still not as precise as the analytical model, the high calculation time indicates that the analytical solution is much more computationally efficient, especially for highly efficient columns with steep concentration fronts.

The same approach is applied to the two-column configuration, and its schematic is presented in Figure 3.2. The second configuration contains two columns connected in series and there is a recycle of the outlet of the second column to the inlet of the first column. Similar to the last configuration the inlet flow rate of the first column is 0.4 ml/s and 0.6 ml/s for the second column. The feed concentration and the model parameters are given in Table 3.2.

Table 3.2: Model	parameters and	l column	properties
------------------	----------------	----------	------------

Parameters	Value
Number of columns	2
Column dimensions	$10 [\mathrm{mm}]$
Column porosity	0.75
Henry constant	2
Feed flow rate	0.1 [ml/s]
Recycle flow rate	0.3  [ml/s]
Solvent flow rate	0.2  [ml/s]
flow rate 1	0.4  [ml/s]
flow rate 2	0.6  [ml/s]
${\rm feed\ concentration}[{\rm gr/l}]$	3 [gr/l]

Where flow rate 1 is the internal flow rate of the first column and flow rate 2 is the internal flow rate of the second column. Assuming that two columns are connected in series and the solvent is injected in between two columns and the feed to the first column which is mixed with the recycle coming from the outlet of the second column, then the inlet concentration for both columns can be obtained from the following mass balances:

$$c_{in,1} = \frac{(c_f * Q_f) + (c_{out,2} * Q_r)}{Q_1}$$

$$c_{in,2} = \frac{Q_1 * c_{out,1}}{Q_2}$$
(3.9)

$$c_{in,2} = \frac{Q_1 * c_{out,1}}{Q_2} \tag{3.10}$$

Where  $c_{in,1}$  is the inlet concentration of the first and  $c_{in,2}$  is the inlet concentration of the second column. The first internal flow rate is the summation of the feed flow rate and the recycle and the second internal flow rate is the solvent flow rate plus the outlet of the first column.

Figure 3.5(a) shows the results with 100 grid points per column using the cell model. A 10,000 grid point model has been presented in Figure 3.5(b) in order to increase the efficiency of the columns. As the number of grid points increases to infinity, the solution becomes more similar to

the analytical solution, despite a significant increase in Central Processing Unit (CPU) time. Figure 3.5(c) illustrates the second method, the analytical model solution.

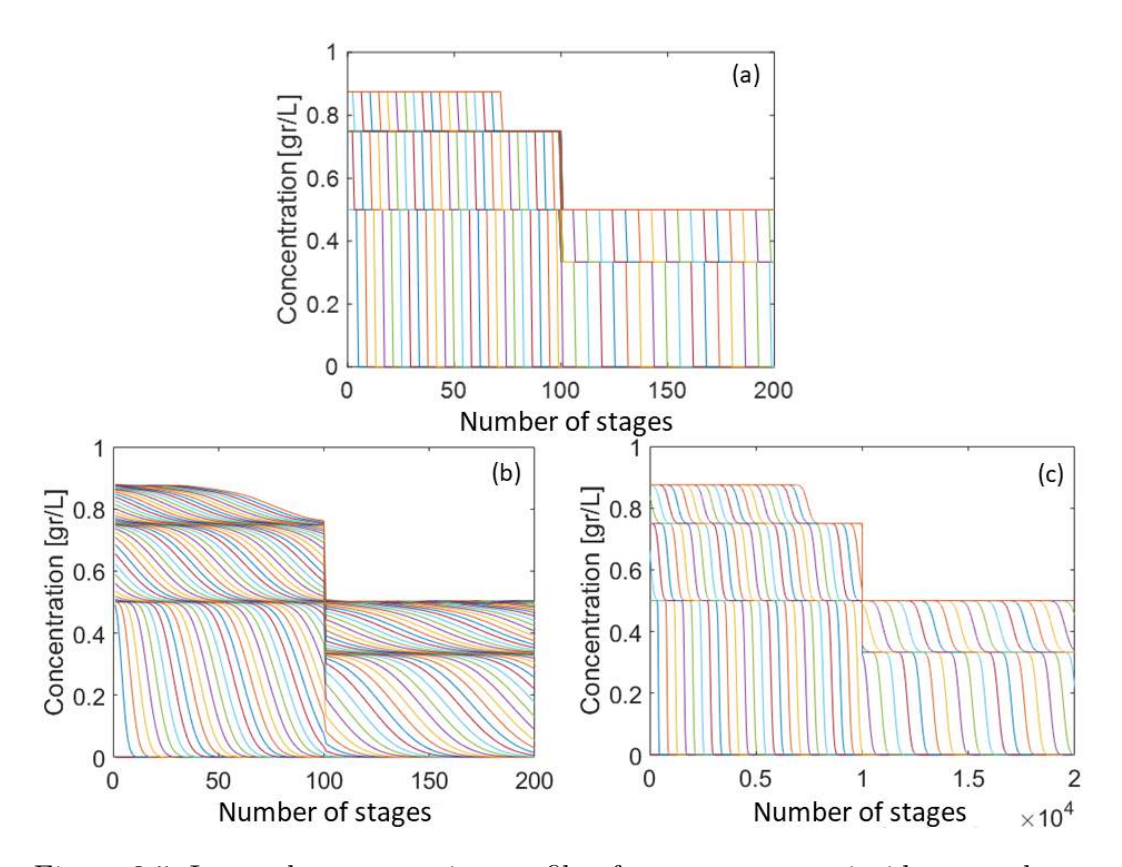


Figure 3.5: Internal concentration profile of one component inside two-column configuration solved by (a) Analytical model (b) Cell model with 100 grid points, (c) Cell model with 10000 grid points

The difference in computation time is not noticeable again with the 100 grid points, although the number of grid points needs to be increased to 10,000 in order to decrease dispersion, resulting in a very long computation time.

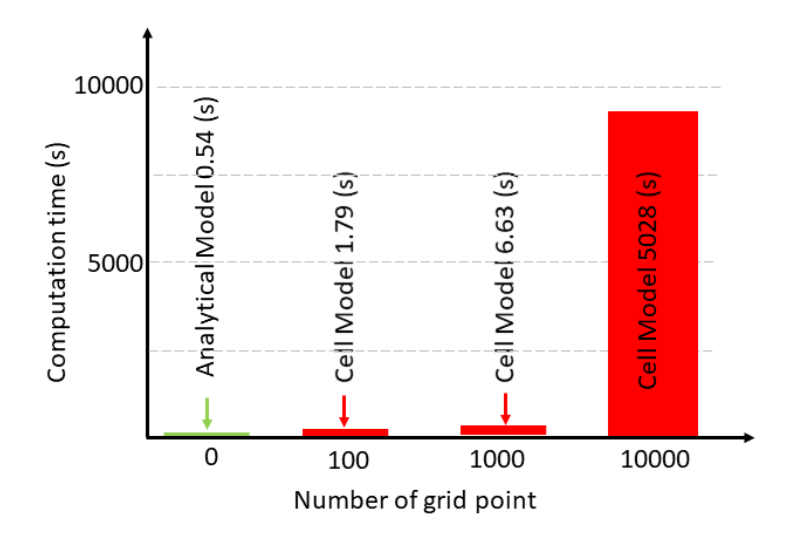


Figure 3.6: Comparison of the computational time in case of the cell model for two columns in series

## 3.5 4-zone SMB simulation

For binary mixture separation, both methods, a cell model and analytical solution are shown using a four-zone SMB. A schematic for a 4-zone SMB is shown in Figure 3.7. The feed enters the first column and the components that are less retained move faster with the fluid flow. These components can be collected at the raffinate port located at the end of the first column. It is necessary to switch the ports at the beginning of the fourth column in order to collect the most retained component, which moves slowly through the column and is captured at the very beginning of the fourth column at the extract outlet. In between column II and column III, the solvent enters the system.

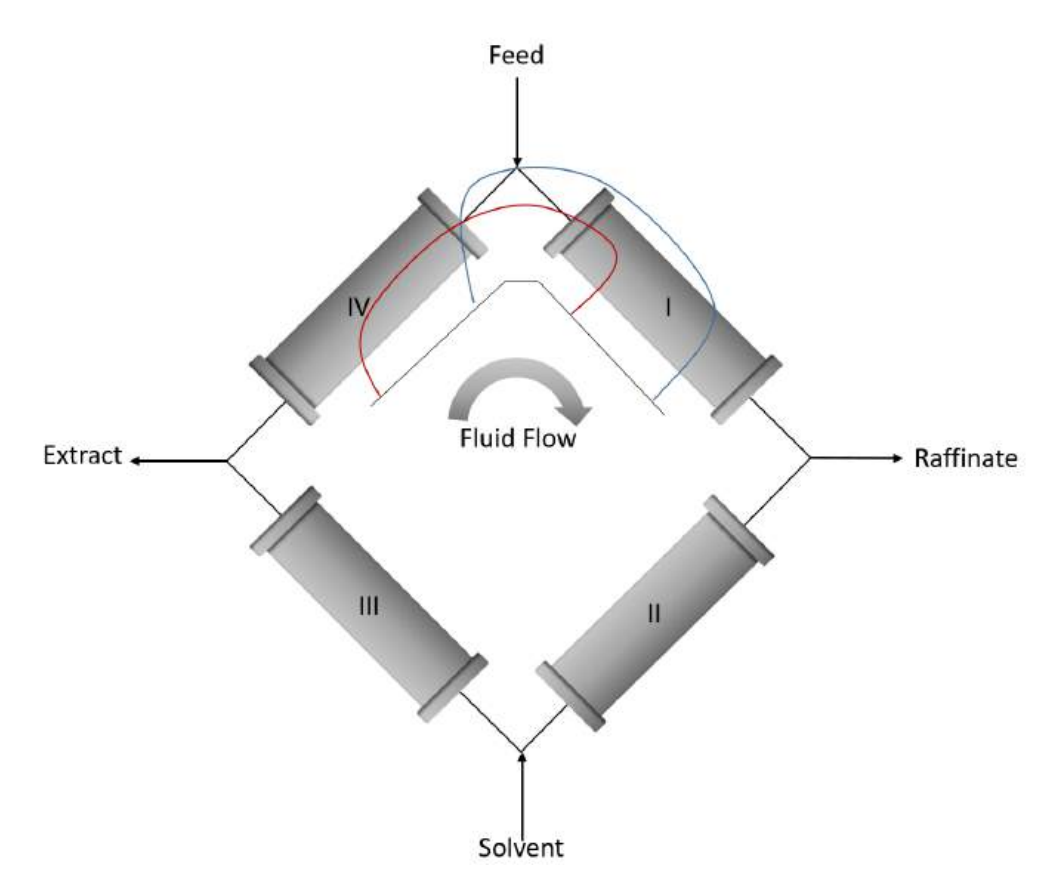


Figure 3.7: Schematic illustration of 4 zone simulated moving bed chromatoghraphy

When no solvent or feed is entering between columns, the concentration at the inlet is the same as that at the outlet of the previous column.

The mass balances at the inlet and outlet nodes are as follows:

Feed node:

$$Q_1 = Q_f + Q_4 (3.11)$$

$$Q_1 c_{i,1} = Q_f c_{f,i} + Q_4 c_{i,4n} (3.12)$$

Raffinate node:

$$Q_2 = Q_1 - Q_R (3.13)$$

$$c_{i,n+1} = c_{i,n} = c_R (3.14)$$

Solvent node:

$$Q_3 = Q_s + Q_2 (3.15)$$

$$Q_3c_{i,2n+1} = Q_sc_s + Q_2c_{i,2n} (3.16)$$

Extract node:

$$Q_4 = Q_3 - Q_E (3.17)$$

$$c_{i,3n+1} = c_{i,3n} = c_E (3.18)$$

In the cell model columns are discretized into 100 or 1,000 cells in the cell model. The Equation 2.33 is applied to each cell, and the resulting Ordinary Differential Equations (ODEs) equations are solved by the ode45 solver in MATLAB. Table 3.3 presents the operating conditions applied to both methods.

Table 3.3: Model parameters and column properties

Parameter	Value
Number of the column	4
Column dimensions	100 [mm]
Column porosity	0.75
Henry constant A	5
Henry constant B	7.5
Switching time	100 [s]
Porosity	0.75 [s]
feed concentration A	2 [gr/l]
feed concentration B	3 [gr/l]

There is a dimensionless value used to specify the ratio of the fluid flow rate to the solid flow rate. This value is indicated by the variable  $M_k$  and is defined using equation 2.19. The triangle theory is used to predict dimensionless flow rate ranges. The dimensionless flow rates used in this work are presented in Table 3.4. In the linear isotherm case,

these m-values are related to the Henry coefficients of the two components. Some safety margins were introduced to prevent breakthrough and regeneration in zones II and III [33].

Table 3.4: Dimensionless flow rates (m-values)

$m_I$	$m_{II}$	$m_{III}$	$m_{IV}$
7.5	4.5	7.7	5.0

Figure 3.8 (a) shows the profile of the concentrations with the cell model application and 100 grid points for each column at the end of each cycle. To make the column more efficient, the number of grid points was increased to 1000 in the cell model, as shown in Figure 3.8 (b). Even though the CPU time increases extremely when the number of grid points increases, the solution becomes more similar to the analytical solution after increasing the number of grid points. The second method, the analytical model solution, is shown in Figure 3.8 (c).

In this method, the solution would be a multi-dimensional matrix with two sheets (each contains one of the component's information), and two rows, the first one contains the concentration values, and the second one for the position values related to the concentration value.

Dispersion is assumed to be zero and the fronts are quite steep. There is no red component in the fourth column, and the Extract is completely pure.

Figure 3.9 shows the CPU time for the cell model with different numbers of grid points and the Analytical solution as well.

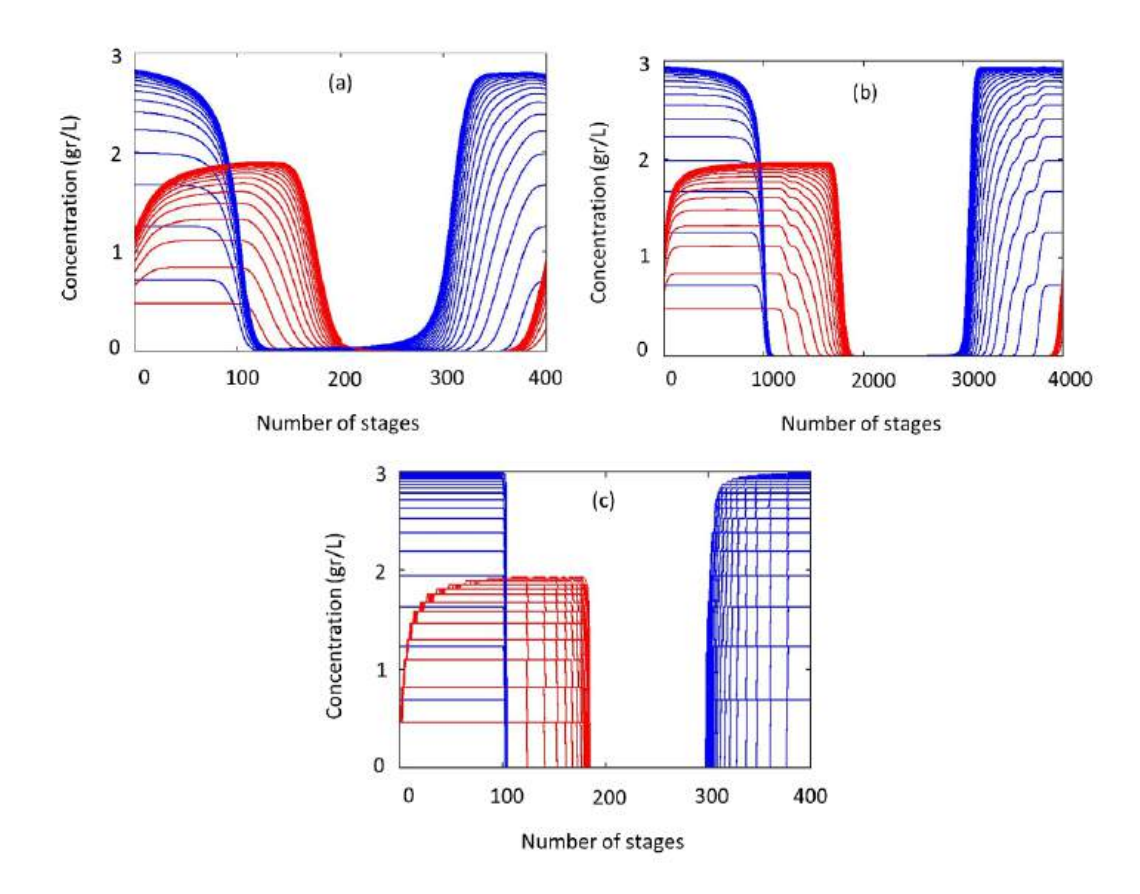


Figure 3.8: Internal concentration profile of binary mixture at the end of the cycle inside 4-zone SMB. The feed enters the system at point 0, the raffinate is removed at point 100 or 1000, and the extract is removed at point 300 or 3000. The solvent enters at point 200 or 2000. (a) Cell model with 100 grid points. (b) Cell model with 1000 grid points (c) Analytical model

The difference in the computational time in Figure 3.9 is great enough to conclude how the analytical solution can accelerate the computation. In comparison to the cell model with 100 grid points, it is about 8 times faster, and with 1000 grid points it is about 500 times faster. As the number of cells increases the plateau concentration value inside the column progressively increases and comes closer to the feed concentration. In the case of having a super efficient column which means having an infinite number of cells, the concentration value will become equal to the feed value as it is shown in Figure 3.8 (c).

Over each cycle, every outlet stream can be collected separately at each

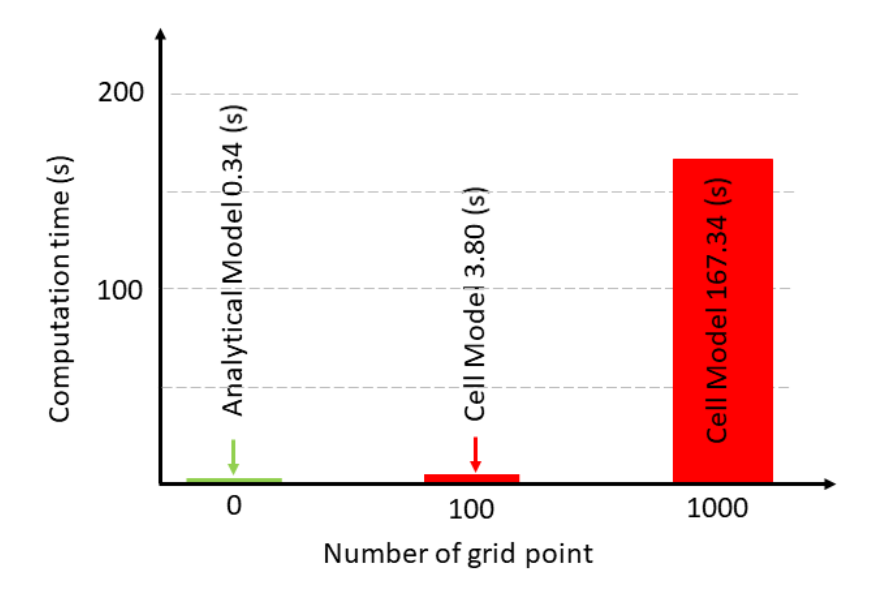


Figure 3.9: Comparison of the computational time in case of cell model and analytical model for 4-zone SMB

outlet port. The outlet stream of each port is shown in Figure 3.10 and Figure 3.11 during 20 times of switching or about four cycles, subsequently the concentration profile at the last switching is saved in the system and the feed concentration is increased and the process is running for another 20 switching time. The feed concentrations are increased by 0.5[gr/l] each. The same operating conditions are applied to test the algorithm for a transient condition where the initial concentration inside the column is not zero. This test showed that the transient condition can also be calculated. There are some differences in the outlets that are explained later. The following figures exhibit the outlet concentration at different ports and different methods.

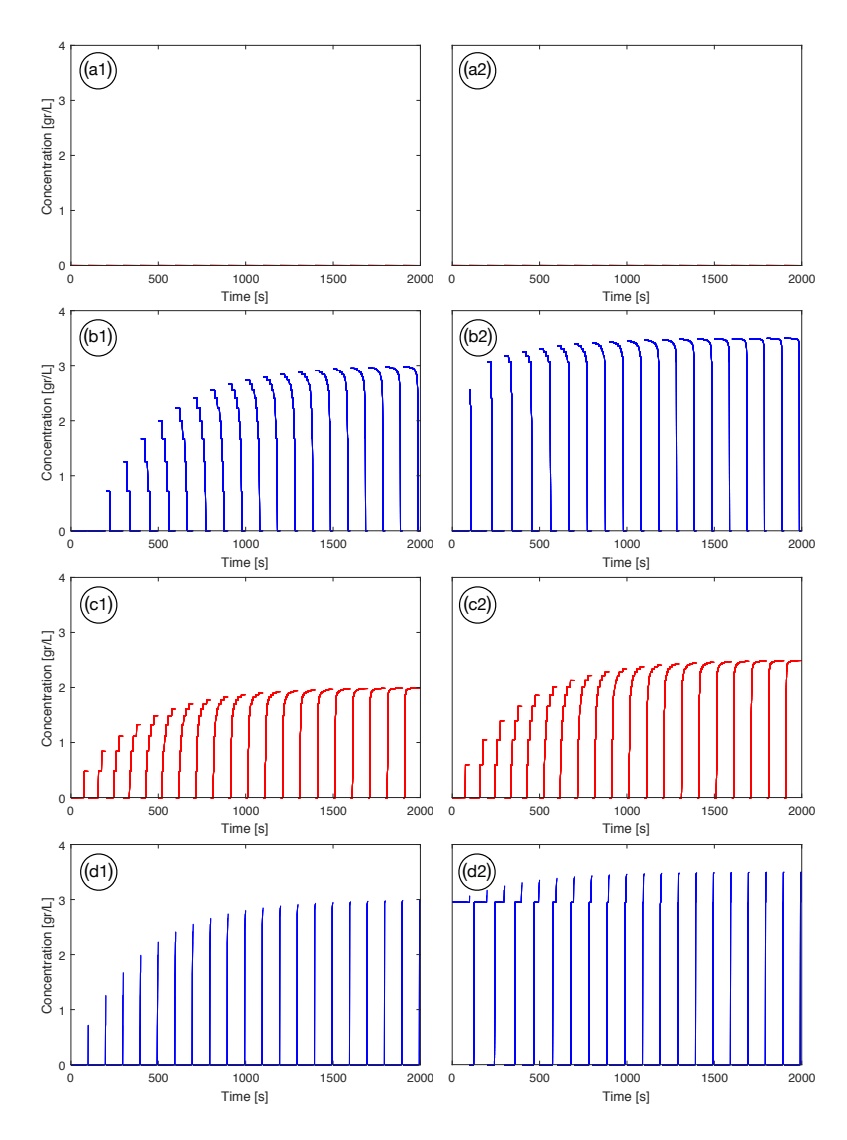


Figure 3.10: Outlet concentrations from analytical solution (a1) First component in extract port and first run. (a2) First component in extract port and second run. (b1) Second component in extract port and first run. (b2) Second component in extract port and second run. (c1) First component in raffinate port and first run. (c2) First component in raffinate port and second run. (d1) Second component in raffinate port and first run. (d1) Second component in raffinate port and second run.

Each blue or red line in the graphs represents the outlet concentration of each component during a single switching period. Once switching occurs, the outlet is drawn and then removed from memory to have faster calculations. The new line, which begins immediately after the previous one, is then drawn from the next time point. This process causes the lines to be discontinuous, but they precisely start and end at the beginning and end of each switching interval.

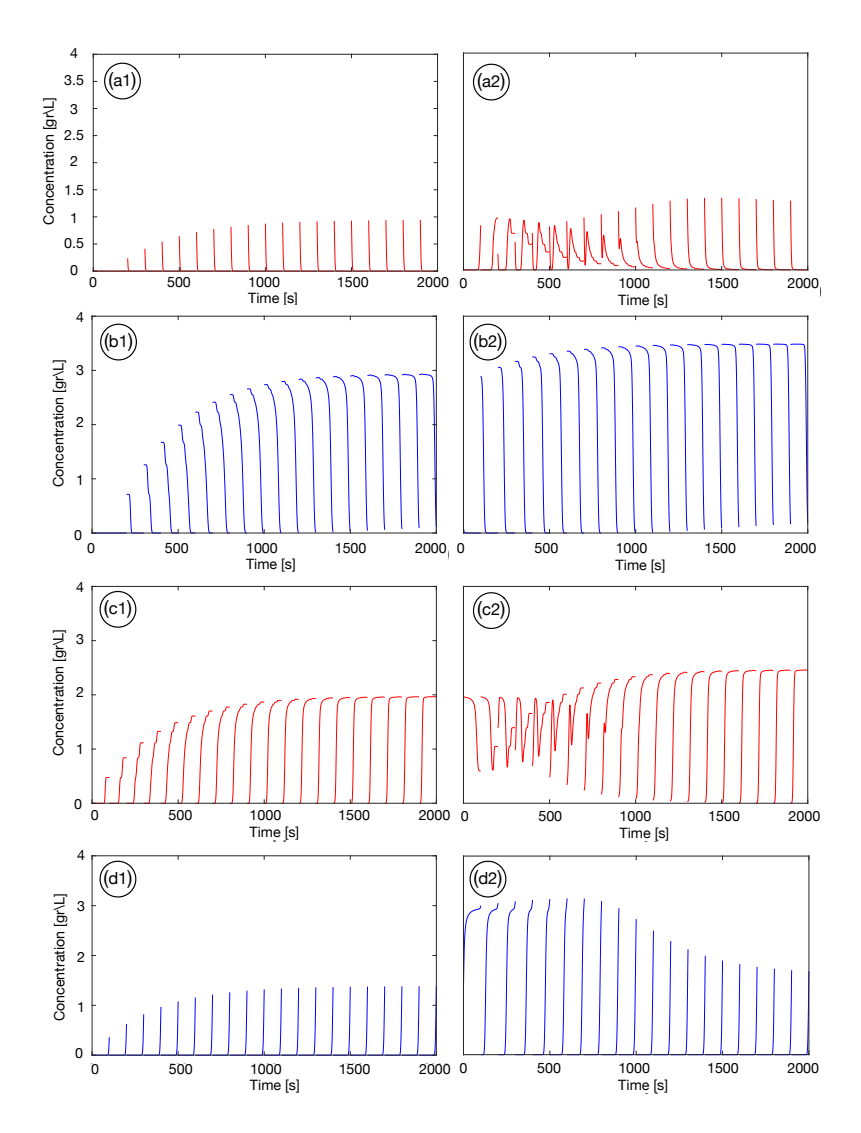


Figure 3.11: Outlet concentrations from cell model solution with 1000 cells (a1)

First component in extract port and first run. (a2) First component in the extract port and second run. (b1) The second component is in the extract port and the first run. (b2) The Second component in the extract port and the second run. (c1) First component in the raffinate port and the first run. (c2) First component in the raffinate port and second run. (d1) The second component is in the raffinate port and the first run. (d1) The second component is in the raffinate port and the second run.

The outlet concentration of the first component in the extract port differs in the cell and analytical models. The difference is due to the dispersion in the numerical model. The red component is visible at the end of the fourth zone which means that at the beginning of the cycle, it passes from the extract point and therefore, it is seen in the extract outlet. As there is no dispersion in the analytical model there is no red component at the extract port in the analytical model.

In the raffinate outlet in the cell model and second run, although the red component is expected to start from the previous value, it starts again from zero value like the first run, the reason is the steep front and ends in the analytical model. therefore, at the start of the cycle, its value is zero.

The blue component in the raffinate port and first run in the analytical model is bigger than in the cell model. The reason is the steep front in the analytical model and when the blue component is passing the raffinate port it has a bigger concentration.

# 3.6 8-zone SMB with raffinate recycle simulation

It was proposed to introduce 8 zones SMB to overcome the limitations of 4 zones SMB, such as the separation of mixtures containing more than two components [60], which is especially important when the most or least retained component is not of interest, but the middle component is of major interest. As inspired by some work done before [2, 62], the configuration used in this work has eight columns connected by capillaries in series with an inlet or outlet in between, there are several different configurations for 8-zone SMB. 8-zone center-cut SMB can have raffinate or extract recycle [77]. In this work, we have used a center-cut configuration with raffinate recycle for a 3 component mixture. As shown in Figure 3.12 there are four inlets and four outlets. There is an inlet and outlet connected to the system that serves as a recycle. Due to the recycling inside the system, there is a feed entering the second sub-system. The system can be divided into two subsystems. The upper part is the

first subsystem, and the other one is the second subsystem. The ternary mixture is entered into the middle of the first subsystem. The most retained component can be separated and exit from the extract outlet. The other two components which are less retained are recycled in the middle of the second sub-unit as feed. In the second sub-unit the other two components can be separated and exit from the extract two and raffinate two outlets.

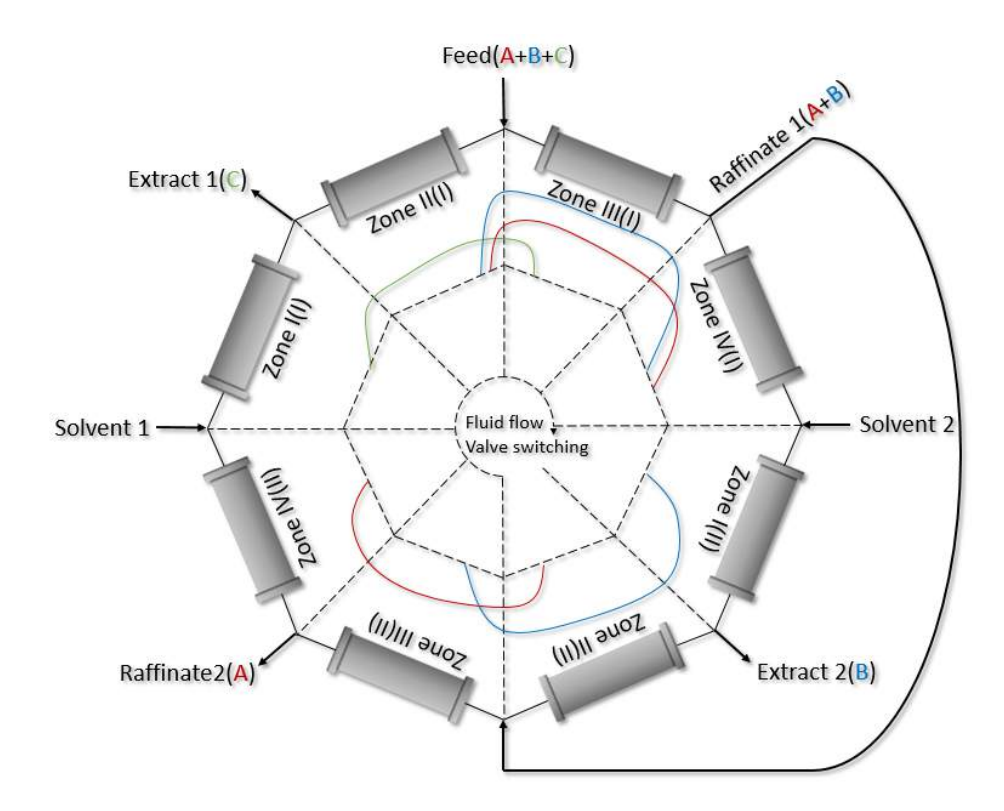


Figure 3.12: Schematic illustration of 8-zone simulated moving bed chromatography

The concentrations at the last node of each column are equal to those at the first node of the next column. In this case, dead volumes are not taken into account. Considering the outlets and inlets, the differential equations should be modified to take into account the increase in concentration caused by the injection of feed and the dilution caused by the injection of fresh solvent, in the case of the outlets and inlets.

$$\frac{dc_{i,1}}{dt} = \frac{n\dot{V}_{I(I)}}{V_c(1 + \frac{(1-\epsilon)}{\epsilon}H_i)} (\frac{\dot{V}_{IV(II)}}{\dot{V}_{I(I)}} c_{i,8n} - c_{i,1})$$
(3.19)

$$\frac{dc_{i,2n+1}}{dt} = \frac{n\dot{V}_{II(I)}}{V_c(1 + \frac{1-\epsilon}{\epsilon}H_i)} \left(\frac{1}{\dot{V}_{III(I)}} (\dot{V}_{II(I)}c_{i,2n} + \dot{V}_{f1}c_{i,2n+1}) - c_{i,2n+1}\right)$$
(3.20)

$$\frac{dc_{i,4n+1}}{dt} = \frac{n\dot{V}_{I(II)}}{V_c(1 + \frac{(1-\epsilon)}{\epsilon}H_i)} (\frac{\dot{V}_{IV(I)}}{\dot{V}_{I(II)}} c_{i,4n} - c_{i,4n+1})$$
(3.21)

$$\frac{dc_{i,6n+1}}{dt} = \frac{n\dot{V}_{III(I)}}{V_c(1 + \frac{1-\epsilon}{\epsilon}H_i)} \left(\frac{1}{\dot{V}_{III(II)}} (\dot{V}_{II(II)}c_{i,6n} + \dot{V}_Rc_{i,3n}) - c_{i,6n+1}\right) (3.22)$$

The model parameters and column characteristics are presented in Table 3.5.

Table 3.5: Model parameters and column properties

Model parameters	Values
Number of the columns	8
Column dimensions	$100[\mathrm{mm}]$
Column porosity	0.75
feed concentration A	2[gr/l]
feed concentration B	3[gr/l]
feed concentration C	4[gr/l]

The operating conditions were determined based on calculations following the approach outlined by Kessler et al. [37]. Operating conditions are presented in Table 3.6 and Table 3.7:

Table 3.6: Arbitrary adsorption Henry coefficient of the components of the ternary mixture

component	Henry constant $(H_i)$
A	1.1
В	1.7
С	2.5

Table 3.7: Dimensionless flow rates

M-value	value
$m_I(1)$	2.55
$m_{II}(1)$	1.57
$m_{III}(1)$	2.19
$m_{IV}(1)$	0.86
$m_I(2)$	1.82
$m_{II}(2)$	1.22
$m_{III}(3)$	2.55
$m_{IV}(4)$	1.01

A concentration profile inside an 8-zone SMB is shown in Figure 3.13. Figure 3.13 (a) shows a cell model with 100 grid points, Figure 3.13 (b) shows a cell model with 1000 grid points, and Figure 3.13 (c) shows the analytical model's result. It can be seen from the picture that the solution of the analytical model produces a concentration profile that appears to be more precise without any dispersion. Increasing the number of grid points to 1000 in the numerical solution resulted in the profiles becoming sharper and the level of dispersion decreased as the number of grid points increased.

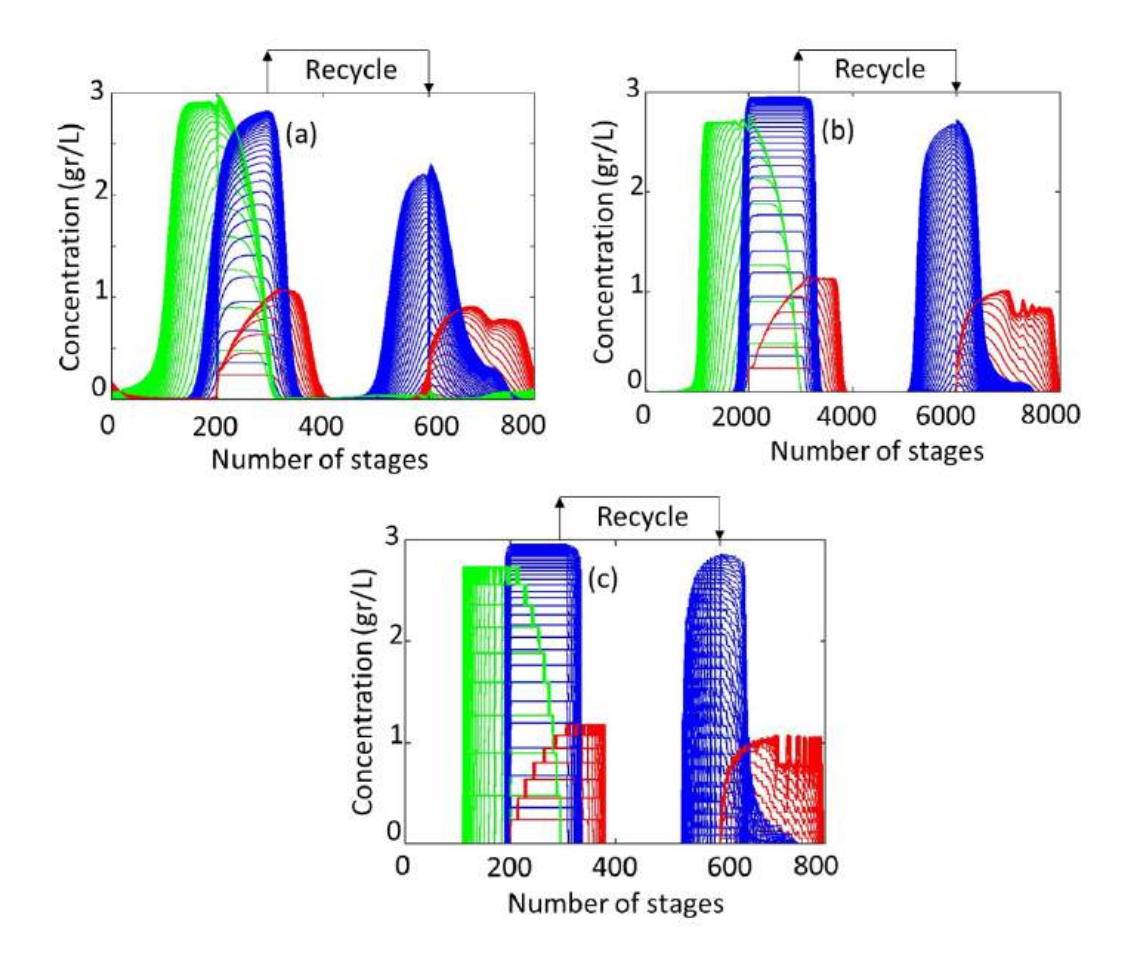


Figure 3.13: Internal concentration profile of ternary mixture inside a 8-zone SMB (a) Cell model with 100 grid points. (b) Cell model with 1000 grid points (c) Analytical model

Despite the fact that the columns would become efficient by increasing the number of grid points, the computational time is still too high to be reasonable. The time that is needed to compute the actual output for different methods with different numbers of grid points is shown in Figure 3.14.

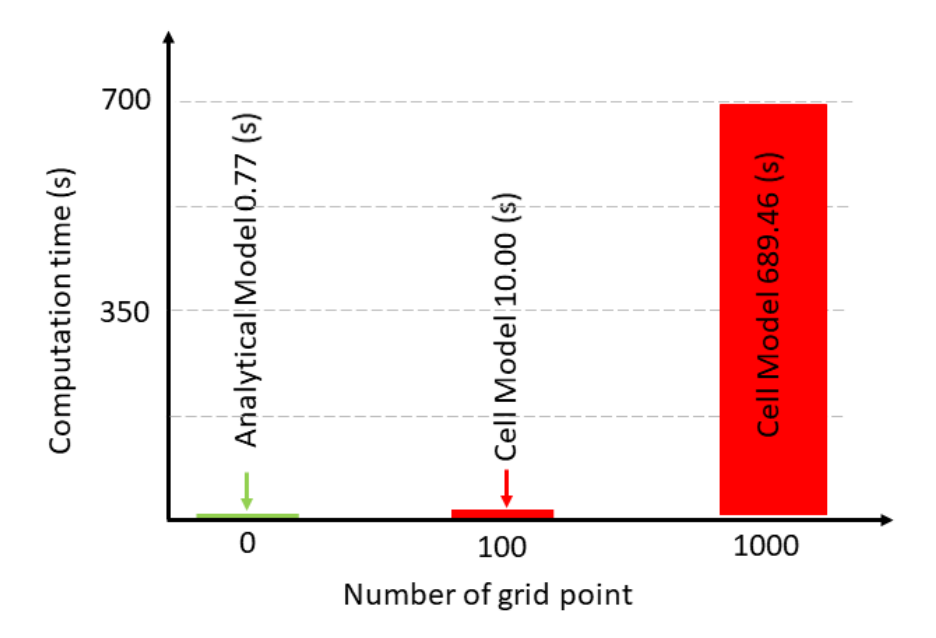


Figure 3.14: Comparison of the computational time in case of numerical discretization method and analytical solution for 8 zone SMB and ternary separation

As shown in Figure 3.14, applying 1000 grid points to the cell model increases computational time significantly. Despite the fact that it takes more than 3 days, the results are closer to the analytical solution, but the dispersion phenomenon is drastically reduced. There is a relationship between the number of grid points and the efficiency of the column when it comes to internal concentration values. Dispersion is responsible for this effect. Due to this fact, the outlet concentrations at different ports can differ if more grid points are applied. It was shown in both the 4-zone SMB and the 8-zone SMB that when grid points are around 1000, the outlet concentration of the cell model and analytical model becomes more similar. From Figure 3.14 it is obvious that applying such a huge number of grid points makes the model slow and time-consuming, thus in this case the outlet concentrations are calculated and presented using 100 grid points.

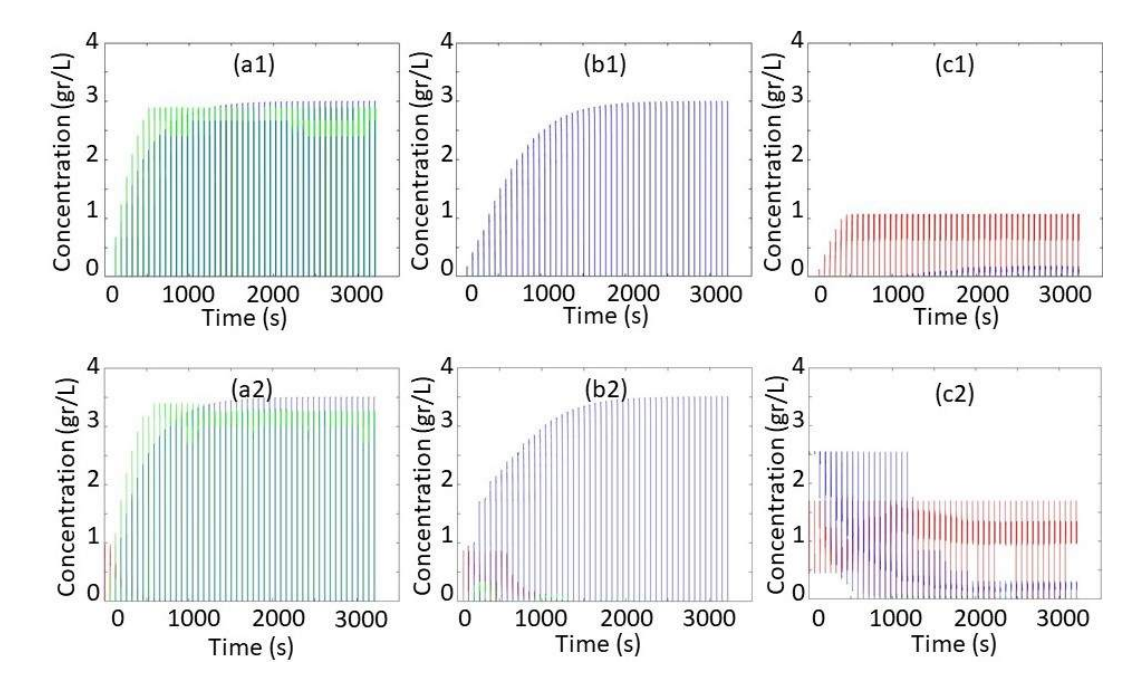


Figure 3.15: Outlet concentration profiles using an analytical solution. (a1)

Extract1 first run, (a2) Extract1 second run with 0.5 gr/l increase
in the feed concentration, (b1) Extract2 first run, (b2) Extract2
second run with 0.5 gr/l increase in the feed concentration, (c1)
Raffinate2 first run, (c2) Raffinate2 second run with 0.5 gr/l increase in the feed concentration

After the first run, the feed concentration is increased and the model continues to run with the new feed concentration and columns which are not empty. At the first run, the concentration of red, blue, and green components are respectively 2, 3, and 4 gr/l and the initial condition is zero. In the second run the initial condition is the concentration profile in the last cycle of the first run and then all the feed component concentrations are increased by 0.5 gr/l and the test is running for another 50 cycles until it reaches a steady state condition. This test was done to assure the model's accuracy with non-zero initial conditions. The test was applied to both methods, the analytical and cell model. The results almost agree and the slight difference is because of the not efficient column assumption in the cell model.

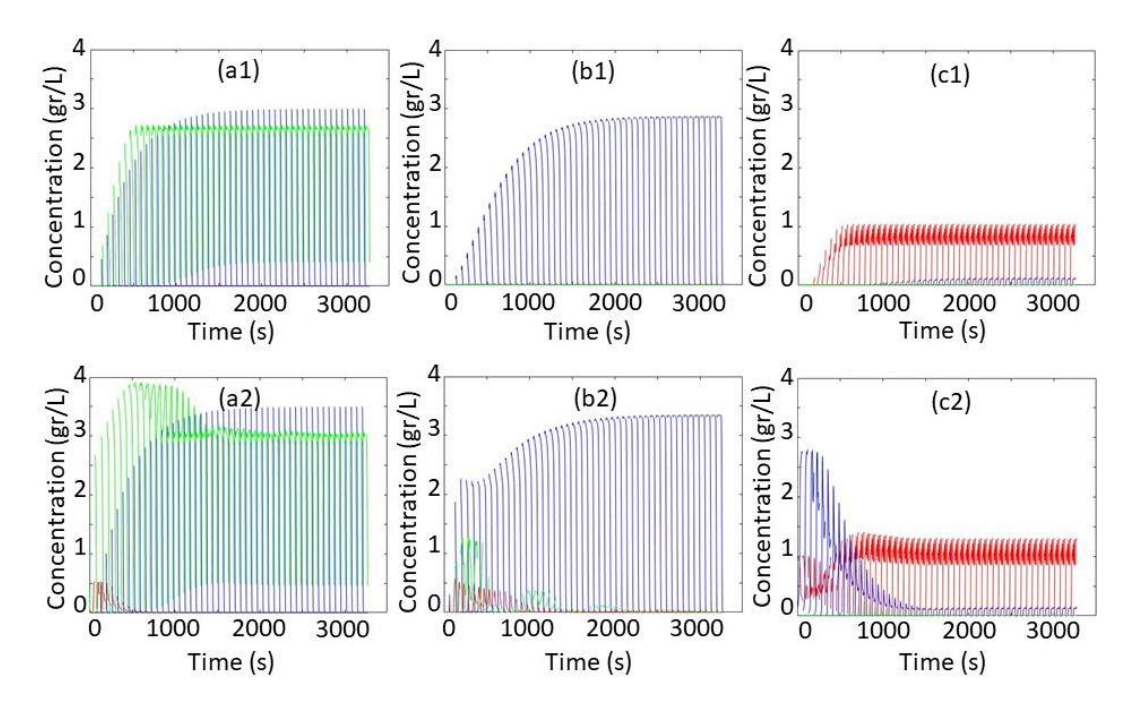


Figure 3.16: Outlet concentration profiles using cell model. (a1) Extract1 first run, (a2) Extract1 second run with 0.5 gr/l increase in the feed concentration, (b1) Extract2 first run, (b2) Extract2 second run with 0.5 gr/l increase in the feed concentration, (c1) Raffinate2 first run, (c2) Raffinate2 second run with 0.5 gr/l increase in the feed concentration

Finally, the analytical solution has been applied to the 8-zone SMB with a 5-component mixture and raffinate recycle. At the second extract port, the target component is selected; the other four components are separated at the other outlets. Each pair with the closest retention time will exit the system at the same point. Figure 3.17 shows the concentration profile inside the 8-zone SMB.

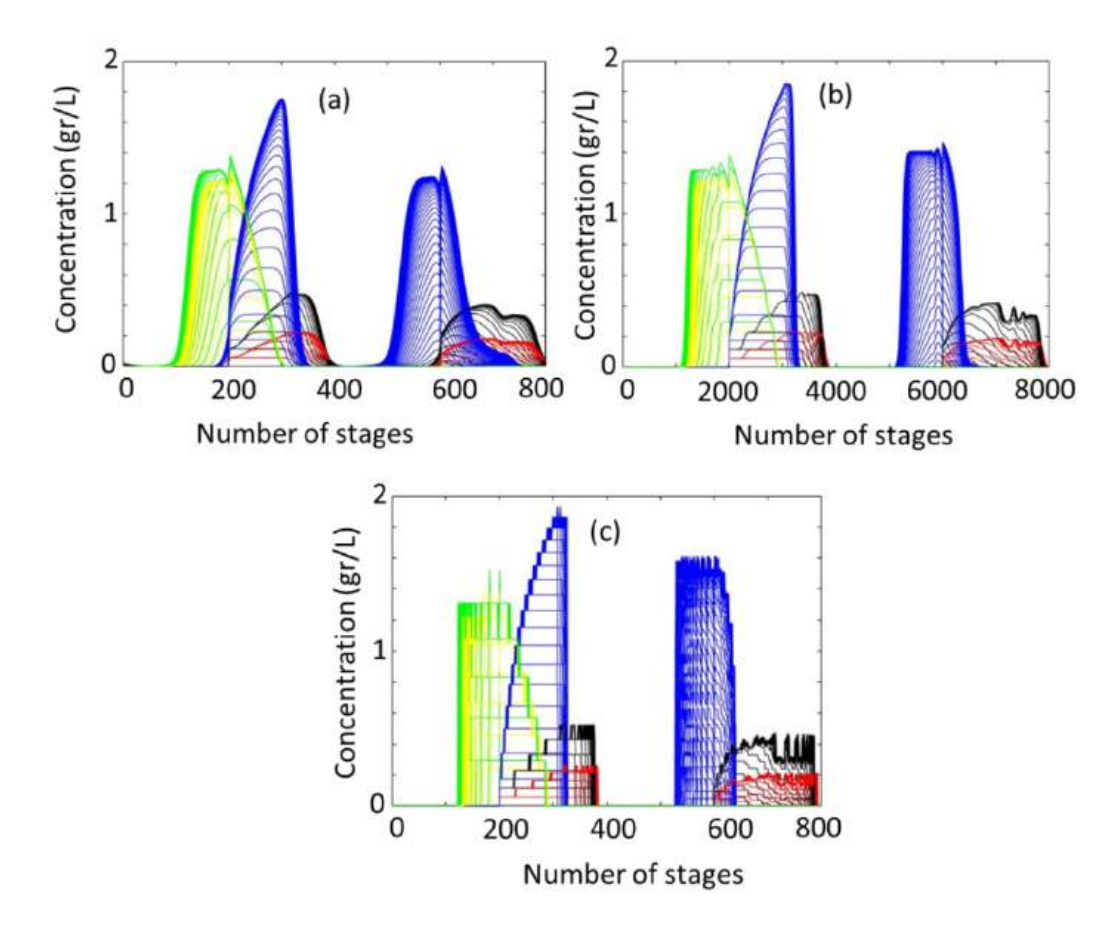


Figure 3.17: Internal concentration profile of 5 component mixture inside 8-zone SMB (a) Cell model with 100 grid points. (b) Cell model with 1000 grid points (c) Analytical model

The first two plots on the top show the concentration profiles calculated by the cell model. Sharper profiles and less dispersion are considerable in Figure 3.17 (b) compared to Figure 3.17 (a) and it is the outcome of a high number of grid points. Profiles are even sharper and more precise in Figure 3.17 (c) with applying just 100 spatial grid points which is the advantage of this solution. The products of the second raffinate and first extract port are mixtures of two components. The yellow and green components are separated in the first extract, while the target component is recycled from the first raffinate to the second sub-unit, along with the red and black components. In the second sub-unit, the blue target component leaves the system at the second extract port, and the other two are selected at the second raffinate port.

The model parameters and column characteristics are presented in Table 3.8.

Table 3.8: Model parameters and column properties

F	P-P
Parameter	8-zoe SMB
Number of the column	8
Column dimensions[mm]	$7.854[\mathrm{mm}]$
Column porosity	0.6
Henry constant A	1
Henry constant B	1.05
Henry constant C	1.575
Henry constant D	2.362
Henry constant E	2.481
cycle number	50
feed concentration A	1.5 [gr/l]
feed concentration B	2.5 [gr/l]
feed concentration C	3.5 [gr/l]
feed concentration D	4.5 [gr/l]
feed concentration E	5.5 [gr/l]

The operating conditions regarding the fluid flow rate and the switching time are given in Table 3.9 for this process.

The computational time for both methods with different numbers of grid points is presented in Figure 3.18. In the cell model, despite the fact that the column performance is more efficient by increasing the grid points, the computational time is noticeably increased. It is 1781.69 seconds, which is nearly one hour, and in comparison to the analytical model, which calculated the solution in 1.80 seconds, is quite slow.

Table 3.9: Dimensionless flow rates

M-value	value
$m_I(1)$	2.55
$m_{II}(1)$	1.57
$m_{III}(1)$	2.19
$m_{IV}(1)$	0.86
$m_I(2)$	1.82
$m_{II}(2)$	1.22
$m_{III}(3)$	2.55
$m_{IV}(4)$	1.01

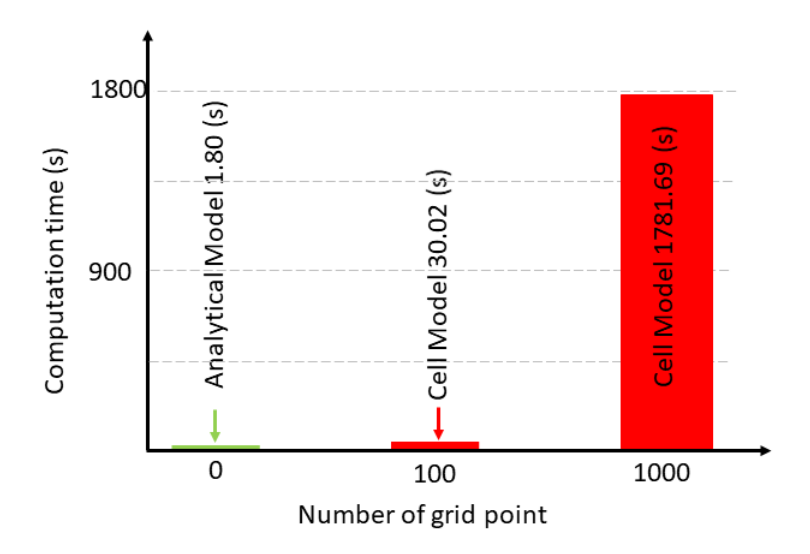


Figure 3.18: Comparison of cell and analytical model computational time for 5 component separation using 8 zones SMB

The outlet streams of the cell model and analytical solution are shown respectively in Figure 3.19 and Figure 3.20. As expected the outlet streams have higher purity than the previous section, especially on the first run. No contamination was seen in the outlet ports. The two approaches are in good agreement.

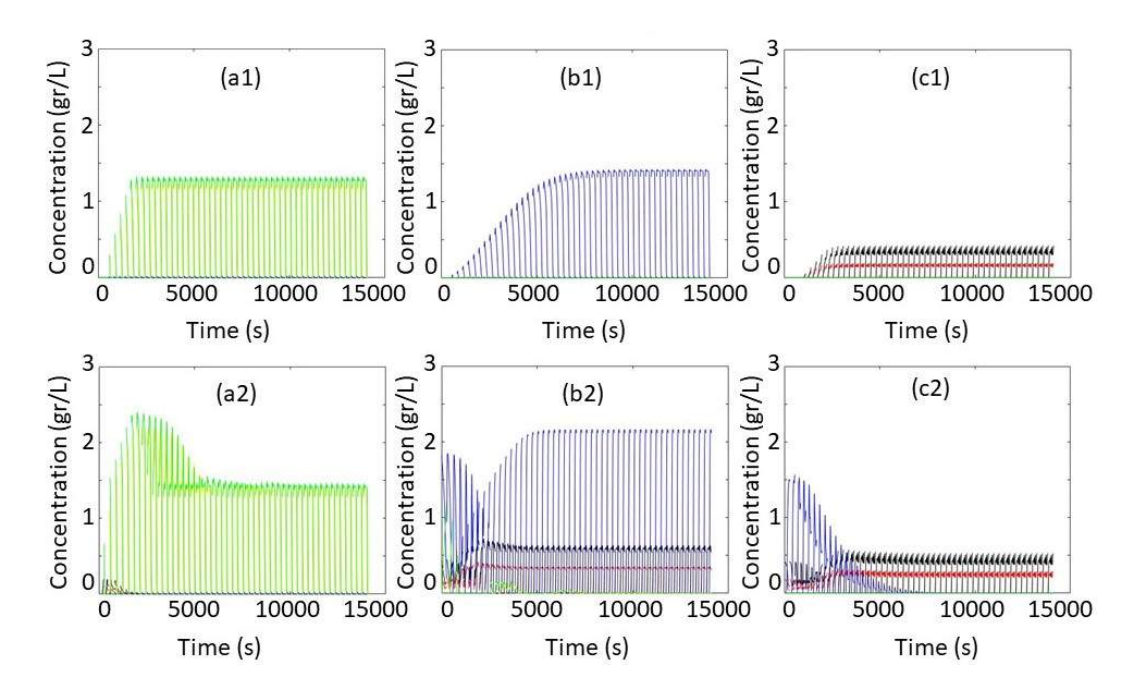


Figure 3.19: Outlet concentration profiles using cell model. (a1) Extract1 first run, (a2) Extract1 second run with 0.5 gr/l increase in the feed concentration, (b1) Extract2 first run, (b2) Extract2 second run with 0.5 gr/l increase in the feed concentration, (c1) Raffinate2 first run, (c2) Raffinate2 second run with 0.5 gr/l increase in the feed concentration

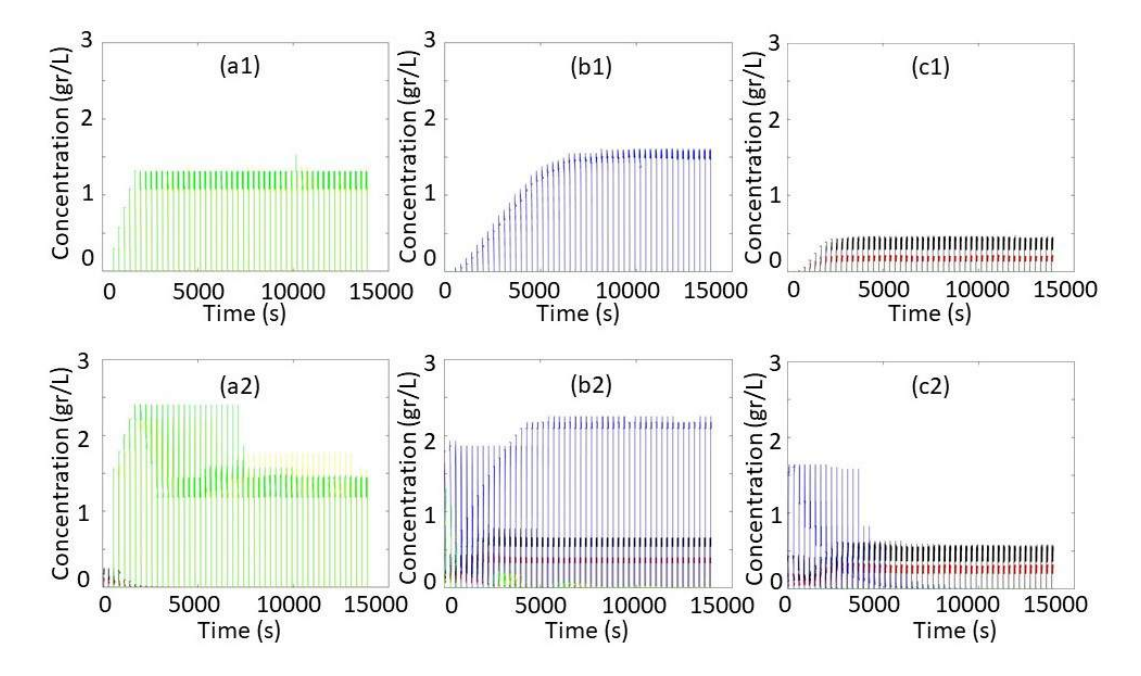


Figure 3.20: Outlet concentration profiles using analytical solution (a1) Extract1 first run, (a2) Extract1 second run with 0.5 gr/l increase in the feed concentration, (b1) Extract2 first run, (b2) extract2 second run with 0.5 gr/l increase in the feed concentration, (c1) Raffinate2 first run, (c2) Raffinate2 second run with 0.5 gr/l increase in the feed concentration

# 3.7 Summary

In this chapter, a fast and accurate method is presented for simulating chromatographic columns with linear adsorption isotherms. This method uses the ideal equilibrium model to simulate chromatographic columns. As a result, it will be most suitable for highly efficient chromatographic columns with negligible axial dispersion and steep concentration fronts. In comparison with standard approaches based on the popular cell model, it outperforms those approaches.

In the first instance, the solution was applied to a column with a recycle from its outlet. Then, it was applied to two, four, and eight SMB zones using a raffinate recycle. As mentioned earlier, the node balances and finding when the concentration values leave the columns were critical parts of the calculation of the analytical solution in all configurations. For highly efficient columns with negligible axial dispersion, the analytical method is fast in comparison to the cell model, using the ODE 45 solver and if an implicit integration scheme like ODE 15s is used, the analytical method is extremely fast.

In the end, this method is clearly superior to the numerical method, as shown by the results. In addition, the method can be easily applied to other configurations of the ternary center-cut separation process, as well as to rigorous optimization and evaluation of alternative conversion schemes for ternary center-cut separations using alternative optimization and evaluation techniques.

# **CHAPTER 4**

# Approximate solution for nonlinear non-competitive adsorption isotherms

# 4.1 Non-linear adsorption isotherm and wave theory

In the previous chapter, a powerful method for the simulation of chromatographic processes with linear adsorption isotherms was introduced. It was based on analytical insight obtained from the method of characteristics. This method can also be applied to nonlinear isotherms. In the first step, the focus in this chapter is on nonlinear noncompetitive isotherms.

For non-competitive isotherms, each solute species is independent of the others, like in linear chromatography. The main difference between linear and nonlinear chromatography is, that in linear chromatography, each concentration value of a given solute travels with the same velocity, and concentration profiles are just shifted by the characteristic propagation velocities. In contrast to this, in nonlinear chromatography, each concentration value of a given solute travels with a different velocity. Depending on the characteristic curvature of the adsorption isotherm and

the considered scenario, this may lead to self-sharpening or spreading behavior of concentration fronts. This is illustrated in Fig.4.1 according to [24].

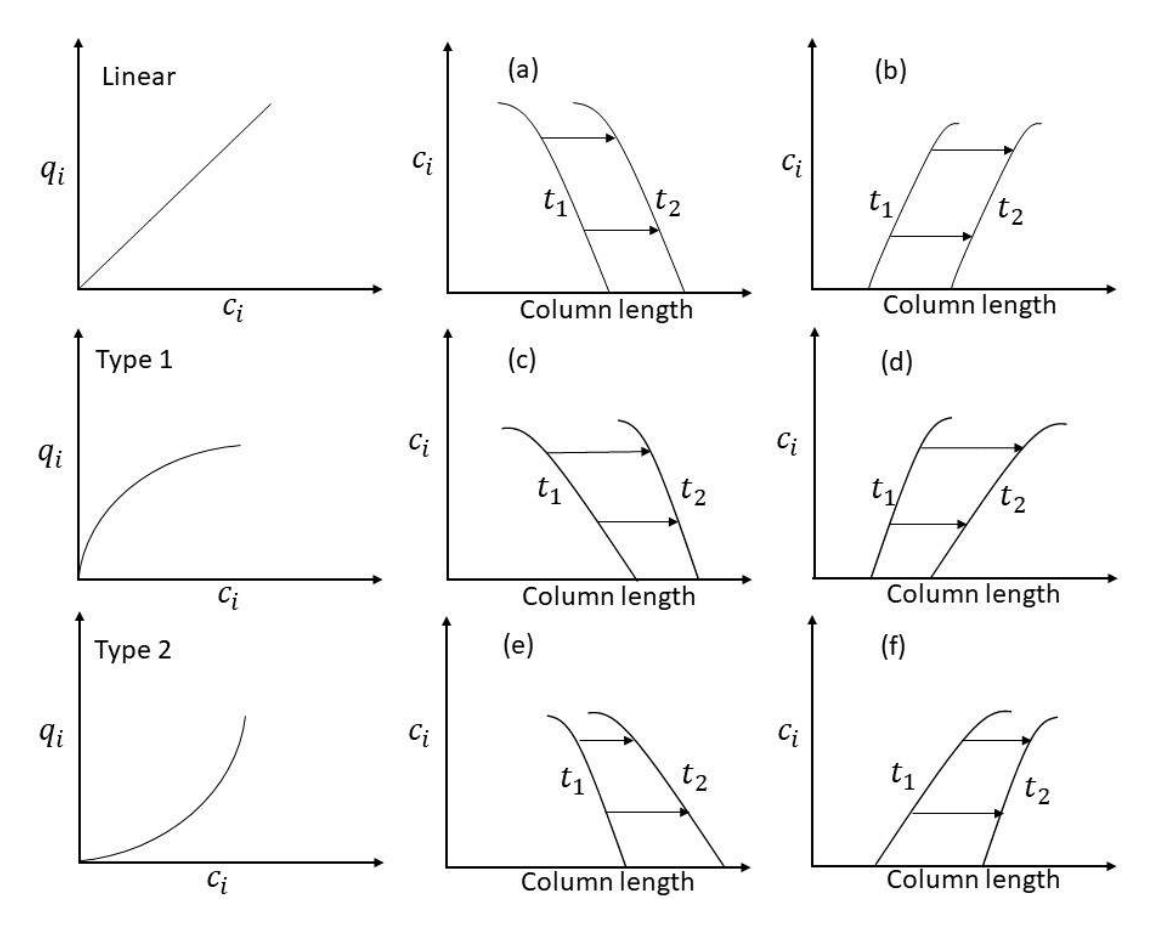


Figure 4.1: Characteristic patterns of behavior for linear compared to a nonlinear single solute or noncompetitive adsorption isotherms. The first column illustrates the type of isotherm, the second column shows the behavior during the loading of an empty bed, the third column shows the behavior during regeneration of a fully loaded bed with pure solvent. [24]

The first row in Figure 4.1 illustrates the behavior for linear isotherms. As mentioned above, concentration profiles are just shifted with characteristic velocity and do not change their shape, because of concentration independent characteristic velocity, which was derived in the previous chapter 3.3. The second row shows the characteristic behavior of concave adsorption isotherms. Noncompetitive Langmuir isotherms to be con-

sidered in this chapter belong to this class. The corresponding isotherm equations reads:

$$q_i = \frac{(a * c_i)}{1 + b * c_i} \tag{4.1}$$

The slope is:

$$\frac{dq_i}{dc_i} = \frac{a}{(1+b*c_i)^2} \tag{4.2}$$

It decreases with increasing fluid phase concentration  $c_i$  as shown in the second row in Fig. 4.1

The characteristic velocity follows from the model Equation (4.3) by differentiation and yields:

$$v_i = \frac{u_f}{(\varepsilon + (1 - \varepsilon)\frac{dq_i}{dc_i})} \tag{4.3}$$

Since  $\frac{dq_i}{dc_i}$  is decreasing with increasing fluid phase concentration, the characteristic velocity is increasing with increasing fluid phase concentration. This results in self-sharpening behavior of the concentration front during loading of an empty bed shown in Figure 4.1c and spreading behavior of the concentration front during regeneration of a fully loaded bed, shown in Figure 4.1d.

In the characteristic z,t-plane the characteristic velocity represents a straight line for a given concentration value emanating from the given initial values along the line t=0, z>0 and the given boundary conditions for z=0, t>0 [69]. In the linear case, the slope (velocity) does not depend on concentration, therefore, the characteristics are parallel. In the nonlinear case, the slope (velocity) is different for each different concentration. The characteristics are focusing for self-sharpening wavefronts and defocusing for spreading waves. Characteristics in the z,t-plane for the linear case are illustrated in Fig 4.2a, for the nonlinear case with self-sharpening waves in Fig 4.2b and the nonlinear case with spreading waves in Fig 4.2c.

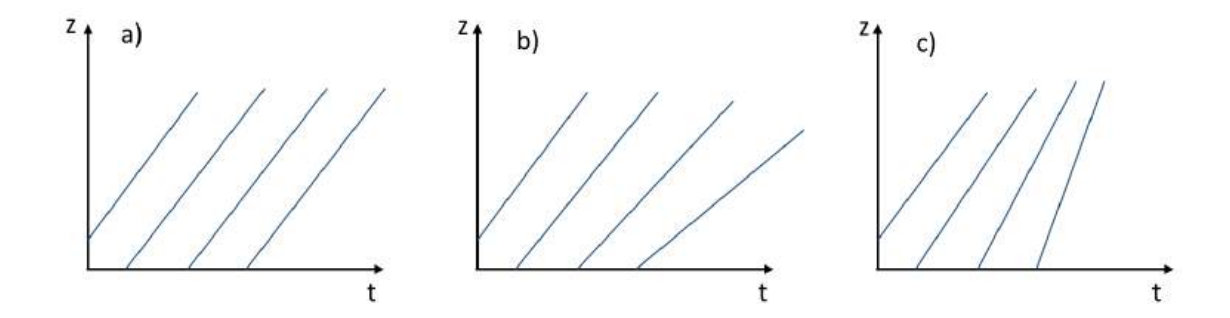


Figure 4.2: Characteristic curves in the z-t plane for linear adsorption isotherms (a) compared to nonlinear adsorption isotherms (b) with spreading waves (c) self-sharpening waves.

Self-sharpening behavior finally leads to the formation of discontinuous wave fronts, also termed shock waves. Shock waves are also obtained if the inlet concentration undergoes a discontinuous step change. In both cases, the shock velocity follows from a global material balance across the shock in an analogous form to Equation 4.4:

$$v_{shock} = \frac{v_i}{\epsilon + (1 - \epsilon) \frac{\Delta q_i}{\Delta c_i}} \tag{4.4}$$

Any concentration value within the discontinuous shock front has the same velocity. It can be shown that the shock velocity lies in between the characteristic velocities of the highest concentration value and the lowest concentration value of the shock [69].

In the z,t-plane shock formation is represented by the intersection of characteristic curves resulting in a shock curve with the slope given by the shock velocity above as illustrated in Figure 4.3 [69].

For convex isotherms, shown in the third row of Figure 4.1, characteristic patterns of behavior are opposite to the second row for concave isotherms, i.e., spreading waves during loading of an empty bed and self-sharpening waves during regeneration of a fully loaded bed.

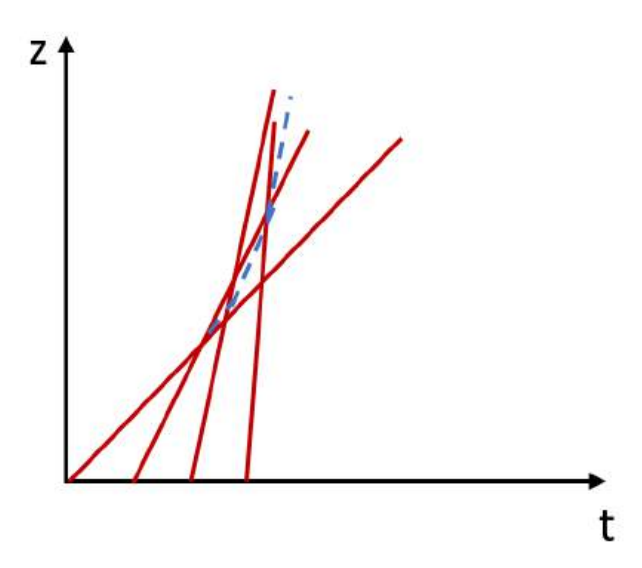


Figure 4.3: Characteristic curves in the z-t plane with shock formation. Solid lines are characteristic velocities, and dashed lines are shock velocities between neighboring concentration values.

## 4.2 One column simulation

To simulate a chromatography column, the solution is in the form of a matrix in which the first row refers to the concentration values, the second row to the velocity of that corresponding concentration value, and the third row to the position of that concentration value within the column.

$$\begin{bmatrix} concentration \ 1 & concentration \ 2 & \dots & concentration \ n \\ velocity \ 1 & velocity \ 2 & \dots & velocity \ n \\ position \ 1 & position \ 2 & \dots & position \ n \end{bmatrix}$$
(4.5)

Each time step, a new concentration value is introduced to the column, which can differ from the previous concentration value. As soon as it enters the system, its velocity is calculated, and its position inside the column is determined based on the velocity and the time step. This concentration value is inside the column and also inside the matrix if its position is smaller or equal to the column length. Matrix dimensions for this solution are not fixed and change during calculation. It is necessary

to allow for dimension changes due to shock formation, which causes some concentration values to merge. In every time step, two conditions are checked: first, if any newly calculated position exceeds the column length, then that concentration value should be removed from the column, and second, if two different concentration values have the same position or have overtaken each other.

For favorable isotherm like the noncompetitive Langmuir isotherm considered in the remainder, whenever a concentration value is bigger than the one ahead, it tends to move faster than the lower concentration value, therefore the two concentration values will catch up, and form a shock and will have the higher concentration value and the new velocity is the shock velocity of these two concentration values. The shock velocity is calculated by Equation 4.4. This means the matrix column associated with the lower concentration value would be removed.

One scenario is when the catch-up happens exactly at one of the time points known to the time vector, or in the other scenario it happens between two time points. Both cases can be seen in figure 4.4. The left column shows the catch up point that is exactly on one of the specified time points, and the right column shows the catch up point between two time points.

Assuming two different concentration value positions intersect at a known time point, the concentration values that have been at the same position at the same time point will merge and the bigger concentration value remains in the matrix. The new velocity is the shock velocity and the position is their catch up position.

The next traveling distance of the new concentration value (the bigger one) is calculated from that position using the shock velocity of the first and second concentration values. As a result, the next position for these two concentration values after their position intersect is found and exact. This corresponds to the first scenario but the other is that their position intersects between the time points specified in the time vector.

After checking the positions of the concentration values and finding the

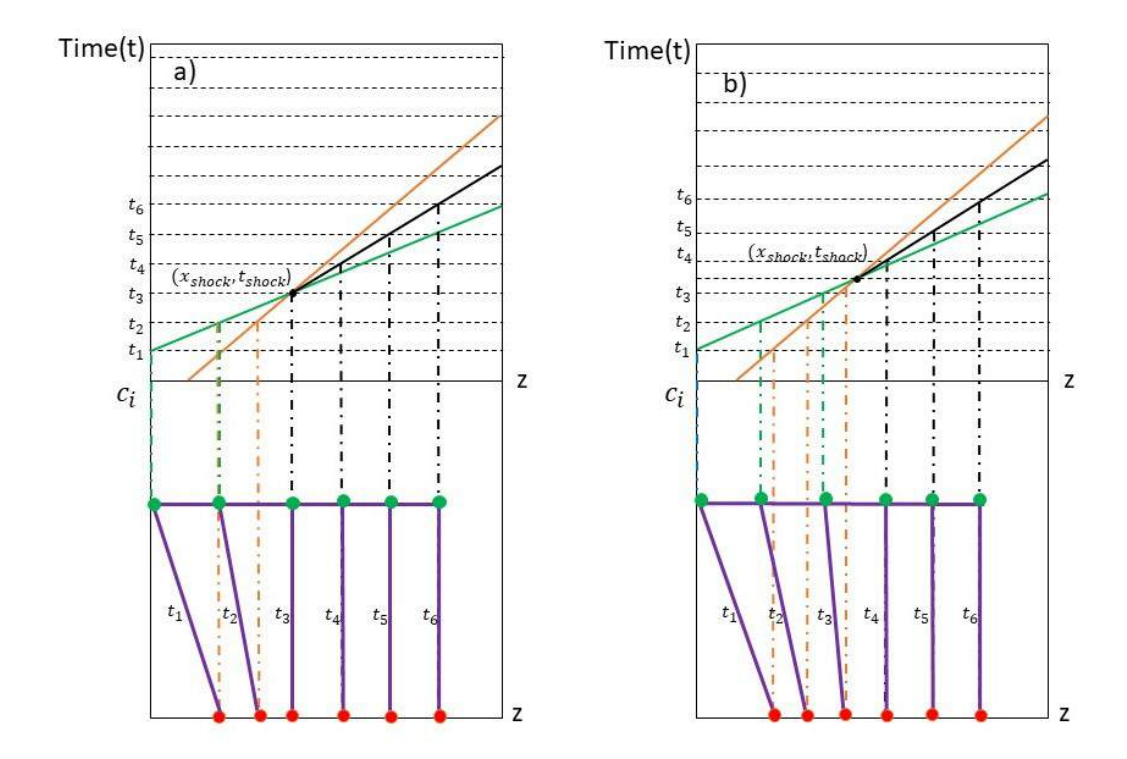


Figure 4.4: The characteristics plot for two concentration values with different catch up points. a) Catch up point coincides with given time point  $t_3$ . b) Catch up point in the interval  $t_3 - t_4$ 

time point right after the catch up, the approximate position is put into the matrix as a new position by calculating the mean distance between the previous and the current position, which is defined in Equation 4.6.

$$z_{j+1} = z_j + \frac{z_{j+1} - z_j}{2}$$
 (4.6)

 $N_t$  is a representation of the number of time points.

The shock velocity is used as velocity, and for concentration, the bigger concentration value is used and the matrix column which has the smaller concentration information will be deleted. During the calculation, the time points are fixed and remain unchanged. After this calculation, the calculated positions are checked and if they are larger than the column length, then that column of the matrix is eliminated, and the concentration value from that column of the matrix is used as a feed for the subsequent chromatography column.

To sum it up, at each time step, the velocity and position of the corresponding concentration are calculated. In the event that some concentration values overlap, they will be removed and replaced by the larger concentration value and its velocity will be the shock velocity instead. During each time step calculation, the positions are checked as well, and those larger than the column length are removed from the matrix. Their corresponding concentration value is used as feed for the next column or product for an outlet.

It is important to note that this solution is an approximate solution and its preciseness is determined by the degree of discretization of the concentration values and the time vector. A low number of discrete points indicates that the behavior of some concentration values hasn't been considered. The calculation is then excluded from some intersection points and shock formations.

Figure 4.5 illustrates the difference in the number of concentration vector discretizations. The left plot in Figure 4.5 illustrates the comparison between the cell model with 100,000 grid points and the approximate solution with a concentration vector discretized by three points. The shocks move unchanged through both solutions after they form, but there are differences in how they position themselves. This figure on the right shows a comparison between the cell model with 100,000 grid points and the approximate solution with 17 discrete points in the concentration value. Both solutions cell and the approximation method are in good agreement. Both solutions use a one-second time step.

There is a greater shock velocity between concentration values 1 and 2 when their differences are greater. As a result, when the discretization number is low, the shock velocity calculated between two concentration values is increased. Therefore, it is possible for the approximate solution to deviate from the cell model when the time step is constant.

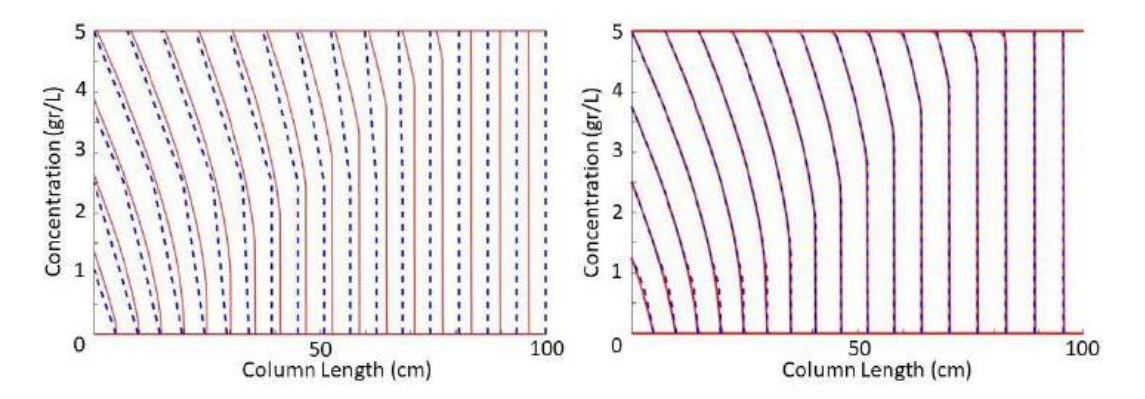


Figure 4.5: Comparison of the cell model (solid red line) with the approximate solution (blue dashed line) with 3 and 17 discretization points in the concentration vector

### 4.3 4-zone SMB simulation

Both methods, cell model and approximate solution were applied to a 4-zone binary mixture separation. The schematic of a 4-zone SMB was presented in the previous chapter in Figure 3.7. Here the configuration has a little difference in the in- and outlets from the one used in chapter 3, and it is shown in Figure 4.6. There is a feed entering between zones II and III. The less retained component is leaving the system in the raffinate port between zones III and IV. The component with the higher affinity is collected at the extract port between zones I and II. The solvent inlet is in between zones I and IV.

In the absence of feed or solvent, the concentration at the inlet of each column is the same as the concentration at the outlet of the previous column.

$$c_{i,n+1}(t) = c_{i,n}(t) (4.7)$$

The feed will be injected into the third column as soon as it has been diluted by mixing it with the outlet fraction of the second column. The following equations show the mass balances at the feed, solvent, and other connections.

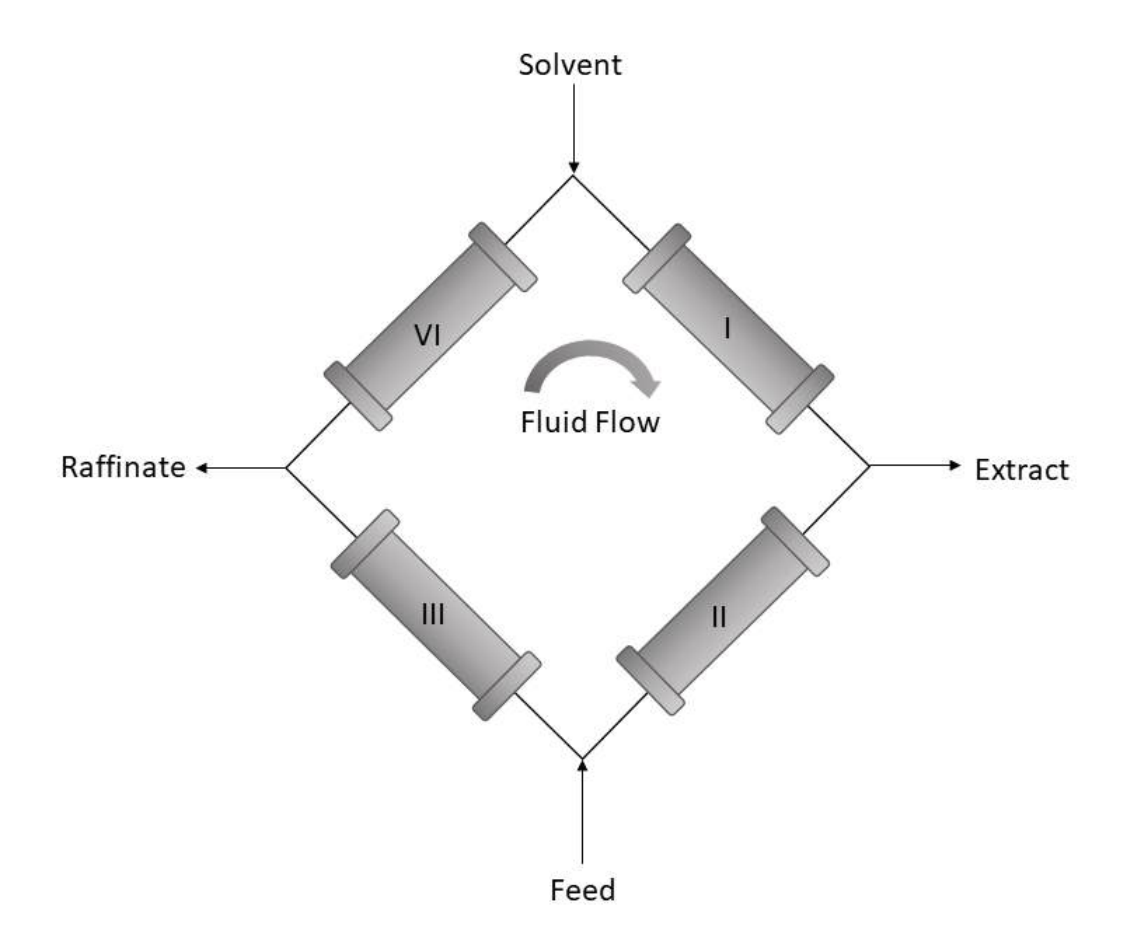


Figure 4.6: Schematic illustration of 4 zones simulated moving bed chromatography

Solvent node:

$$Q_1 = Q_S + Q_4 (4.8)$$

$$Q_1 c_{i,1} = Q_4 c_{i,4n} + Q_S c_{iS} (4.9)$$

Raffinate node:

$$Q_3 = Q_4 + Q_R (4.10)$$

$$c_{i,3n} = c_{i,3n+1} = c_R (4.11)$$

Feed node:

$$Q_3 = Q_F + Q_2 (4.12)$$

$$Q_3 c_{i,2n+1} = Q_2 c_{i,2n} + Q_F c_F (4.13)$$

Extract node:

$$Q_2 = Q_1 - Q_E (4.14)$$

$$c_{i,n+1} = c_{i,n} = c_E (4.15)$$

 $Q_S$  and  $c_{iS}$  are the solvent flowrate and component I concentration in the solvent (which is usually zero) respectively,  $Q_R$  and  $c_R$  are related to raffinate,  $Q_E$  and  $c_E$  are from the extract, and  $Q_F$  and  $c_F$  are the feed flowrate and concentration.

Based on the approximate solution, the solution for a multiple column configuration is two cell matrices each with four matrices in a row. Each matrix has three rows and a variable number of columns. At every time point, the entry concentration of each matrix is calculated. Based on the entry concentration, the isotherm q and its derivative are calculated using Equations 4.1 and 4.2. The derivative of the isotherm is used to calculate the velocity of the relevant concentration value. Each concentration value's position inside the column is calculated using its velocity. In each time step, positions are checked and if concentration values are outside the columns, they are removed. Their new position in the next column is calculated based on their leaving time. Cell matrix elements that are four matrixes are replaced in the switching direction at the end of each cycle. The simulation runs for 40 cycles to reach a cyclic steady state condition. Figures 4.7 (a) and (b) show the concentration profiles obtained by the approximate and numerical solutions, respectively. Due to a proper discretization of the concentration vector in the approximate solution, the profiles obtained by both solutions appear to be in good agreement.

The operating conditions and the dimensionless flow rates which are from Futterer's dissertation [20], are given in Table 4.1 and 4.2 respectively.

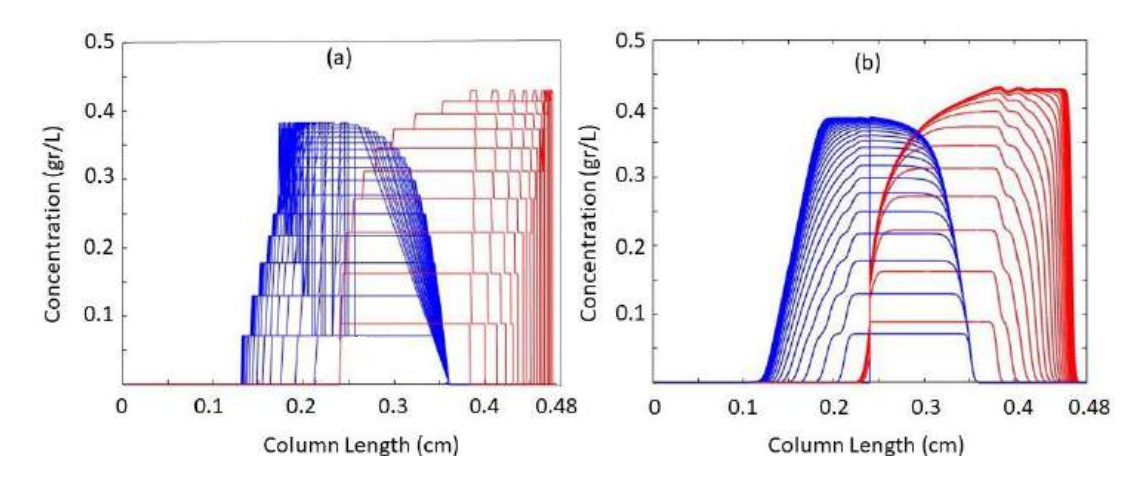


Figure 4.7: Concentration profile of a binary mixture separation using the approximate model (a) and cell model (b)

Profiles of approximate solution concentrations show no dispersion, and fronts are steep. Figure 4.8 shows CPU times. In contrast to a cell model with 1000 stages, the approximate solution takes significantly less time to calculate. In addition, the profiles are in good agreement with the cell model with 1000 stages per column.

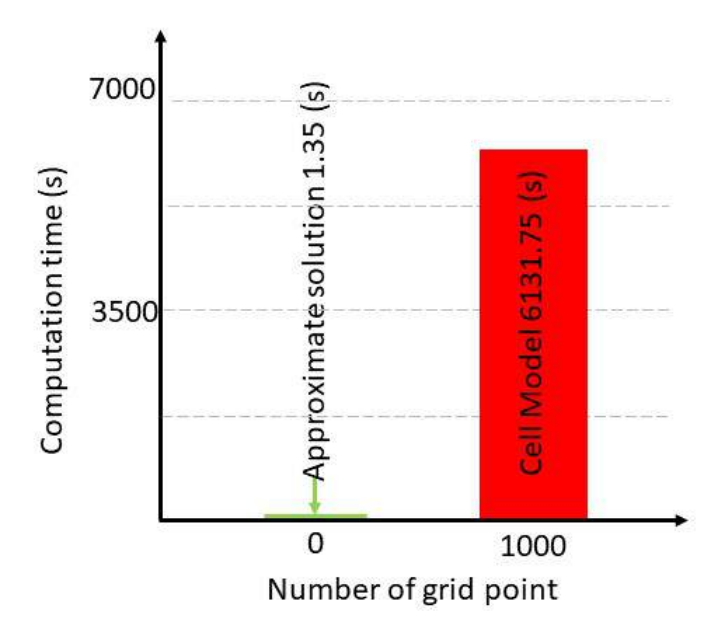


Figure 4.8: Computational time for reaching cyclic steady state

Table 4.1: Model parameters and column properties

Parameter	4-zone SMB
Number of columns	4
Column diameter[mm]	20 [mm]
Column porosity	0.7404
Henry constant A	7.5
Henry constant B	5
Retention factor A	0.3
Retention factor B	0.15
number of cycles	40
feed concentration A	0.4 [gr/l]
feed concentration B	0.5 [gr/l]

Table 4.2: Dimensionless flow rates

m_I	m_II	m_III	m_IV
7.62	4.97	6.66	4.46

#### 4.4 Summary

This chapter presents a novel method for simulating the non-linear, non-competitive chromatographic process.

For the purpose of assessing its accuracy, the method was applied to single-column chromatography and 4-zone SMB, however, it can be applied to other chromatographic configurations as well.

In terms of concentration profiles and calculation time, the results were compared with the popular cell model. The approximate method's precision increases with increasing number of discrete time and concentration values.

The results indicate that both methods have a reasonable agreement in terms of both single-column configurations as well as 4-zone SMB configurations. In spite of that, the computational time for the approximate method is much smaller compared to that of the cell model, while the approximate method is capable of detecting all the details of the concentration profile. Chromatographic columns with high efficiency and negligible axial dispersion are suitable for this method. The cell model in this work is solved using the ODE45 solver built-in function in MAT-LAB, which is much faster than other implicit integral solvers such as ODE15s.

An extension to full-blown nonlinear competitive adsorption isotherms is much more challenging due to the interactions of different solute species. Therefore, we follow a different approach here for competitive nonlinear isotherms using machine learning of surrogate models from the reference model. The approach will be presented in the next chapter.

## **CHAPTER 5**

# Optimization of SMB processes using surrogate models

This chapter is based on the publication [65] on optimizing SMB processes using surrogate models.

The economic potential of the SMB process is maximized by finding optimal operating conditions regarding productivity and solvent consumption. Additionally, the process needs to fulfill certain purity requirements. For total separation, the well-known triangle theory developed by Storti et al. [81] can be used in a first approximation to identify the optimal operating conditions. It is based on the assumptions of a true moving bed process, neglects axial dispersion, and assumes thermodynamic equilibrium between the solid and the liquid phase. Productivity can be increased substantially if purity requirements can be relaxed, which depends on the specific type of application. For reduced purity requirements, [34] presented an extension of the triangle theory. However, the extension is involved, has limitations and is based on the same simplifying assumptions as mentioned above. By using genetic algorithms, [86] has optimized the productivity and purity of the SMB process based on a dynamic model, and compared it to the Varicol process, however computational time is rather high. In [50], a surrogate model was used to optimize SMB processes. They used two different types of surrogate models. The proper orthogonal decomposition (POD) method is employed to derive cost-efficient reduced-order models (ROMs) for the SMB process and the other one is a coarse model. To create a low-fidelity DAE model, they applied the Finite Element Method to the SMB model with coarser spatial discretization. In this thesis, a numerical optimization of a more detailed model is proposed instead. Due to the complexity of the used SMB model, rigorous numerical optimization is highly time-consuming. This paper adapts the methodology from [38] to develop a surrogate-based iterative approach by using a simple feed forward artificial neural network, requiring only minimal data, thereby increasing its numerical efficiency.

An overview of the theoretical background for optimization and the neural network used as a surrogate model is provided in this chapter. It is important to mention that the model is dynamic and the optimization is done for a cyclic steady state SMB process.

#### 5.1 Optimization description

This study used the 2021 version of MATLAB's optimizer toolbox (Math-Works, 2023), which has linear and nonlinear solvers. In this case, we are using the Matlab built-in function fmincon. Optimization problems considered in this work can be formulated as follows:

$$min J(x),$$

$$h(x) = 0,$$

$$g(x) \le 0 \quad x_i \in R$$

$$lb_i \le x_i \le ub_i, \quad for \ i = 1, 2,$$

The optimizer starts at  $x_0$  which is the initial guess of the optimization variables and tries to find the minimum x of the function subject to the inequalities  $g(x) \leq 0$ .

In addition, lower and upper bounds should be defined for the design variables in x, so that the solution is always in the range of  $lb \leq x_i \leq ub$ .

Assume J(x) is the objective function, h(x) is the equality constraint, such as material balances, and g(x) is the inequality constraint, such as purity requirements, and x are the decision variables.

Productivity for a given minimum purity is the objective function to be maximized. We use m-values, the dimensionless ratios between liquid and solid phase flow rates as our decision variables. It is possible to maximize productivity by maximizing the difference between  $m_3$  and  $m_2$ , which is equivalent to finding the operating point farthest from the diagonal  $m_2 = m_3$ . The separation diagram and its different areas were explained before in Chapter 2 and Figure 2.4.

#### 5.1.1 Purity

In SMB chromatography, purity signifies how effectively the target molecule is isolated from unwanted substances or other molecules in the feed mixture. The level of purity is relatively important in different industries or fields. For example, the quality and safety of the final product in the pharmaceutical industry is highly dependent on purity.

The purity of the SMB chromatography process is influenced by several factors. One factor is the selectivity of the adsorbent used in the chromatographic system. The ability of the adsorbent to differentiate between the target component and contaminants is called selectivity. An adsorbent with high selectivity is ideal for favorable adsorption of the desired molecule while effectively minimizing the presence of impurities. [73].

Another crucial factor is the operating conditions, which include parameters like flow rates, temperature, and pressure gradients all of which play a significant role in the separation process and final purity in SMB chromatography. To enhance selectivity and separation efficiency, it is essential to determine optimal conditions. Adjusting flow rates is particularly important when dealing with mass transfer resistance, as it can help improve overall purity. [6].

The third is the column efficiency. The efficiency of the chromatographic

columns used in SMB plays a crucial role in achieving high purity. High efficiency columns have a high number of theoretical plates, which contributes to better separation and improved purity [73].

The form of the input mixture is essential to take into account. The content of the feed, including the proportion of the desired substance and contaminants, along with the duration and timing of injection, can influence the overall level of purity [45].

Finally, Elements such as the number of zones, column configuration, and switching strategy directly affect the separation efficiency and purity. Proper optimization and the design of the system play a crucial role in effective separation and maximum purity[40].

Various analytical techniques, such as high-performance liquid chromatography (HPLC) or mass spectrometry (MS), are employed to evaluate the purity achieved in SMB chromatography. These techniques help quantify the amount of the target component and impurities present in the separated fractions, allowing for an assessment of the purity level.

It's important to note that achieving high purity in SMB chromatography is a complex task that requires careful consideration of all the factors mentioned above. Process development, optimization, and continuous monitoring are essential to ensuring consistent and reliable separation with high purity throughout the chromatographic operation.

During cyclic steady-state, the purity of raffinate and extract streams is defined as follows:

$$Pu_{R} = \frac{\int_{t}^{t+t^{*}} c_{B}^{R} dt}{\int_{t}^{t+t^{*}} c_{A}^{R} dt + \int_{t}^{t+t^{*}} c_{B}^{R} dt}$$
 (5.1)

$$Pu_E = \frac{\int_t^{t+t^*} c_B^E dt}{\int_t^{t+t^*} c_A^E dt + \int_t^{t+t^*} c_B^E dt}$$
 (5.2)

These equations use the numerator to represent the amount of the target component collected in the product stream within a switching cycle, and the denominator as a measure of the total of the two components collected together [67].

#### 5.1.2 Productivity

In SMB, productivity represents the effectiveness and yield of the separation process. The goal is to maximize the recovery of the target compound during operation. Enhancing productivity is beneficial, as it boosts throughput, shortens processing duration, and optimizes economic efficiency.

Productivity (PR) is unquestionably the key economic indicator. For complete separations, it is generally defined as the quantity of feed processed per unit mass of the stationary phase within a given time frame.

$$PR = \frac{Q_F c_F^t}{(1 - \varepsilon)\rho_s V_t} \tag{5.3}$$

Assume that  $c_F^t$  is the total concentration of the feed,  $\rho_s$  represents the density of the stationary phase, and  $V_t$  represents the total volume of the columns in the unit. Combining this equation with the definition of  $m_j$  from Equation 5.3 can be written as:

$$PR = \frac{c_F^t(m_3 - m_2)}{\rho_s t^s \sum_{i=1}^4 S_i}$$
 (5.4)

The number of columns in section j of the unit is  $S_j$ . According to the above definition, the maximum productivity is achieved by maximizing the difference between  $m_3$  and  $m_2$ , i.e., by choosing an operating point that is farthest from the diagonal [67].

It is essential to recognize that although productivity is a crucial factor in SMB, it must be carefully balanced with purity and yield to achieve an efficient separation process. In most cases, lowering purity standards can significantly enhance performance metrics, including higher productivity[34].

#### 5.2 Full-model equations and optimization

Chromatographic columns are described using the equilibrium dispersion model.

$$\varepsilon \frac{\partial c_i}{\partial t} + (1 - \varepsilon) \frac{\partial q_i}{\partial t} + \varepsilon v \frac{\partial c_i}{\partial z} = D_{ax} \varepsilon \frac{\partial^2 c_i}{\partial z^2}$$
 (5.5)

v is the interstitial velocity, and  $D_{ax}$  refers to the dispersion coefficient, which includes all band-broadening effects and is neglected in this calculation. Furthermore,  $c_i$  is the fluid phase concentration of component i, while  $q_i$  is the solid phase concentration and  $\varepsilon$  is the volume fraction of the liquid phase. The following formula describes the Langmuir adsorption isotherm which is used in the remainder.

$$q_i = \frac{H_i c_i}{1 + \sum_{i=1}^{n_c} b_i c_i} \tag{5.6}$$

 $H_i$  and  $b_i$  represent the adsorption constants of each component, and  $n_c$  indicates the number of components. Since the model assumes thermodynamic equilibrium between the two phases,  $q_i$  depends on the fluid phase composition. Assuming a binary 4-zone SMB chromatography separation, the aim is to optimize productivity under reduced purity requirements in a cyclic steady-state SMB.

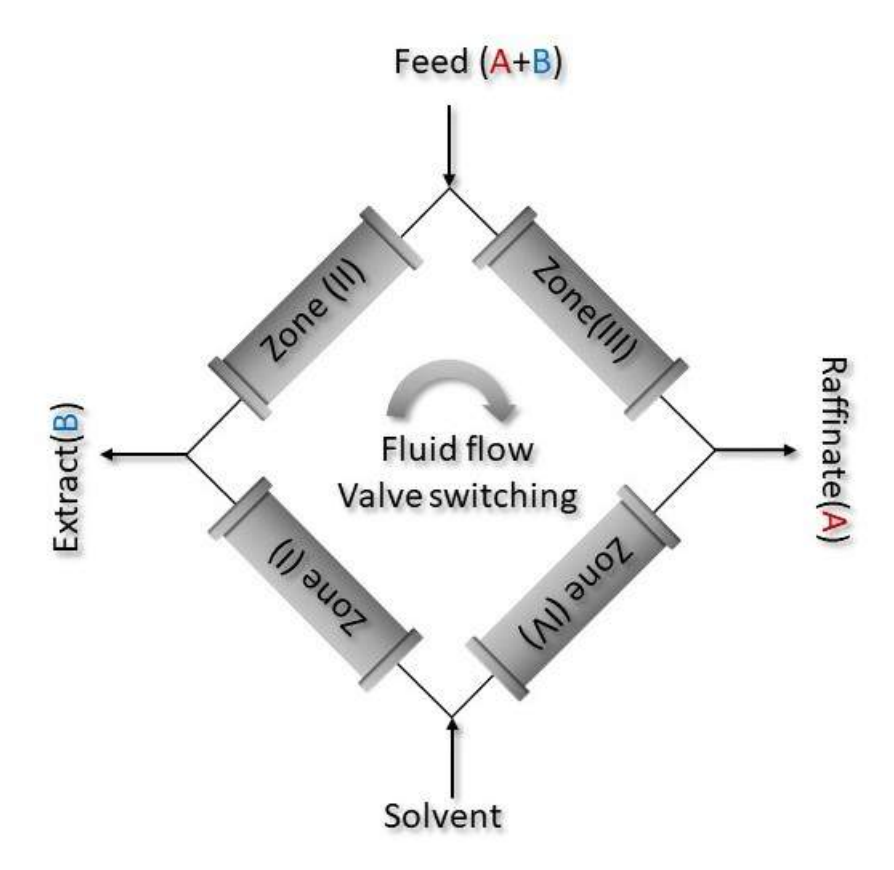


Figure 5.1: Schematic illustration of binary mixture separation using 4-zone  $$\operatorname{SMB}$$ 

In this 4-zone SMB chromatography, there are four distinct zones or sections in the system. Each zone comprises one column, and each column performs a specific function in the separation process. The movement of the solid and liquid phases is precisely controlled to maximize separation efficiency. The feed containing two different components is entering between zones II and III. The less retained component is exiting the system at the raffinate outlet, and the more retained one is at the extract outlet. The solvent enters between zones I and IV. The node balances related to this configuration are:

$$Q_1 = Q_4 + Q_S$$

$$Q_2 = Q_1 - Q_E$$

$$Q_3 = Q_2 + Q_F$$

$$Q_4 = Q_3 - Q_R$$

$$(5.7)$$

In the same way, component node balances can be expressed as follows:

$$c_{i,1}^{in} = \frac{(Q_4 c_{i,4}^{out} + Q_4 c_{i,4}^{out})}{Q_1}$$

$$c_{i,2}^{in} = c_{i,1}^{out}$$

$$c_{i,3}^{in} = \frac{(Q_2 c_{i,2}^{out} + Q_F c_{i,F})}{Q_3}$$

$$c_{i,4}^{in} = c_{i,3}^{out}$$
(5.8)

Streams entering and leaving the system are denoted by the superscripts "in" and "out", respectively. The inlet and outlet ports are switched in the direction of fluid flow to mimic counter-current movements. Moreover, the process of switching is specifically executed by assuming that the internal concentration profiles are maintained within each physical column with every switch. Using the m-values obtained by Equation 5.9, which are dimensionless ratios between the liquid and solid phase flow rates in each column, we are able to maximize productivity for a given minimum purity of the product.

$$m_j = \frac{Q_j^{SMB} t^* - V_c \varepsilon}{V_c (1 - \varepsilon)} = \frac{net \ fluid \ flowrate}{net \ solid \ flowrate}$$
 (5.9)

Where  $m_j$  is the dimension flow rate ratio in column j,  $Q_j$  is the fluid flow rate in column j, and  $V_c$  and  $\varepsilon$  are the column volume and the porosity respectively.

The dynamic behavior of the SMB unit can be calculated numerically with suitable initial and boundary conditions. There are linear and nonlinear solvers in the optimizer toolbox in MATLAB. In this case, we are using fmincon. It is worth noting that the optimization problem is nonlinear and therefore nonconvex, which may lead to multiple local minima. To avoid getting stuck in a suboptimal local minimum the optimization is conducted from multiple starting points. Therefore here a multi-start optimization with 100 starting points and a Sequential Quadratic Programming (SQP) algorithm is implemented.

The objective function to be maximized is the productivity for a given minimum product purity. Our decision variables, x, are the m-values, which are the dimensionless ratios between the liquid and the solid phase flowrates in each column. Maximum productivity is obtained by maximizing the difference between  $m_3$  and  $m_2$ , which is equivalent to find a feasible operating point farthest from the diagonal  $m_2 = m_3$ . At the beginning, the Henry constants are used as the starting point, i.e., the first  $m_3$  and  $m_2$ . Since they are the optimal point of the linear adsorption isotherm for total regeneration, they can be used as the initial guess for the Langmuir adsorption isotherm. The domain for the optimization area is given by  $m_2 \, \varepsilon \, [3,7]$  and  $m_3 \, \varepsilon \, [5.5,9.5]$ . In order to maintain total regeneration,  $m_1$  and  $m_4$  have a safety margin of 10% from Henry constants. A nonlinear inequality constraint of a minimum purity of 0.85 for both products is used for this maximization.

1e-8 is the step tolerance setting. The step tolerance is a threshold used to determine when an optimization algorithm should stop iterating based on the size of the steps taken during each iteration. The initial guess is the components Henry constant  $(H_a, H_b) = (m_2, m_3)$ . These points can be used as initial guesses for the Langmuir adsorption isotherm since they are the optimal points of the linear adsorption isotherm for total separation. The maximization is based on a nonlinear inequality constraint of a minimum purity of 0.85 for both products raffinate and extract. Due to reduced purity, the optimal point was expected to be outside the triangle. The solution using the full model is shown in Figure 5.2.

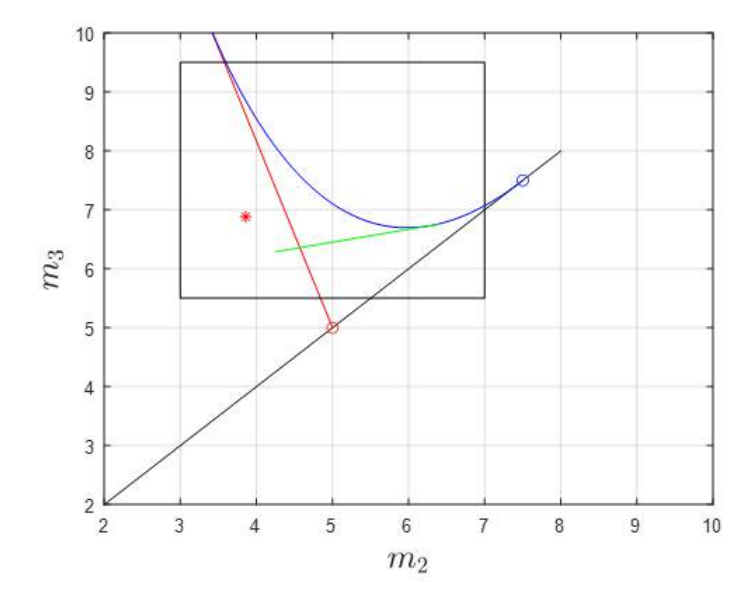


Figure 5.2: Optimal operating point (red star) predicted by the full model (numerical solution) for a minimum purity of 0.85 of both products. Red, blue and green lines define the total separation region according to triangle theory.

The black line or the diagonal is the  $(m_2 = m_3)$  line. The black square also indicates the optimization area. A red star indicates the farthest point from the diagonal that can meet purity requirements. The optimal point is precise dimensions are (3.8578, 6.8826).

### 5.3 Surrogate model

Surrogate modeling is a technique used in engineering, computer science, and other fields to approximate the behavior of complex systems or functions. It involves creating a simplified mathematical model, called a surrogate model, that mimics the behavior of the original system or function. The primary motivation behind surrogate modeling is to reduce the computational cost associated with evaluating the original system or function, which can be time-consuming or resource-intensive. In many fields of engineering and beyond, input-output or response surface models are used as an alternative to computationally expensive rigorous process models. To avoid the computational burden, surrogate models

are used as fast approximations to more accurate simulations [50]. The methods used vary in complexity. As each approach has unique characteristics, the correct choice of a surrogate modeling approach is not trivial. One of the methods is Artificial neural networks, which is used in this work.

#### 5.3.1 Artificial neural network

Solving hyperbolic PDEs repeatedly, sometimes, is necessary to quantitatively model solute movement inside columns. PDE solutions are often approximated numerically by using finite difference, finite element, or finite volume methods due to the limitations of analytical solutions. It can take significant computation time and resources for the numerical solvers to obtain the solutions with desired accuracy, especially if many simulations need to be repeated. In the field of chromatography, surrogate models, such as artificial neural networks (ANN), have been widely used for the rapid optimization of simple processes with simple models[64]. The aim of Artificial Neural Networks (ANN) is to mimic the brain's functions. These structures consist of several so-called neurons, or nodes, which are arranged into groups or layers according to their function. Figure 5.3 shows a visualization of an ANN.

As shown above, an ANN is comprised of three sections: input, hidden, and output layers. The information flow in a feed-forward ANN is limited to one direction, from the left or input to the right or output. The feedback or recurrent ANN, on the other hand, may use an information flow in the opposite direction.

#### 5.4 Algorithm development and dynamics

The objective of this study is to develop a surrogate model that can replace the detailed but expensive full-order SMB model for optimization purposes. A surrogate model is being used in this work, which is based on an artificial neural network. Using Kessler's methodology [38], in this

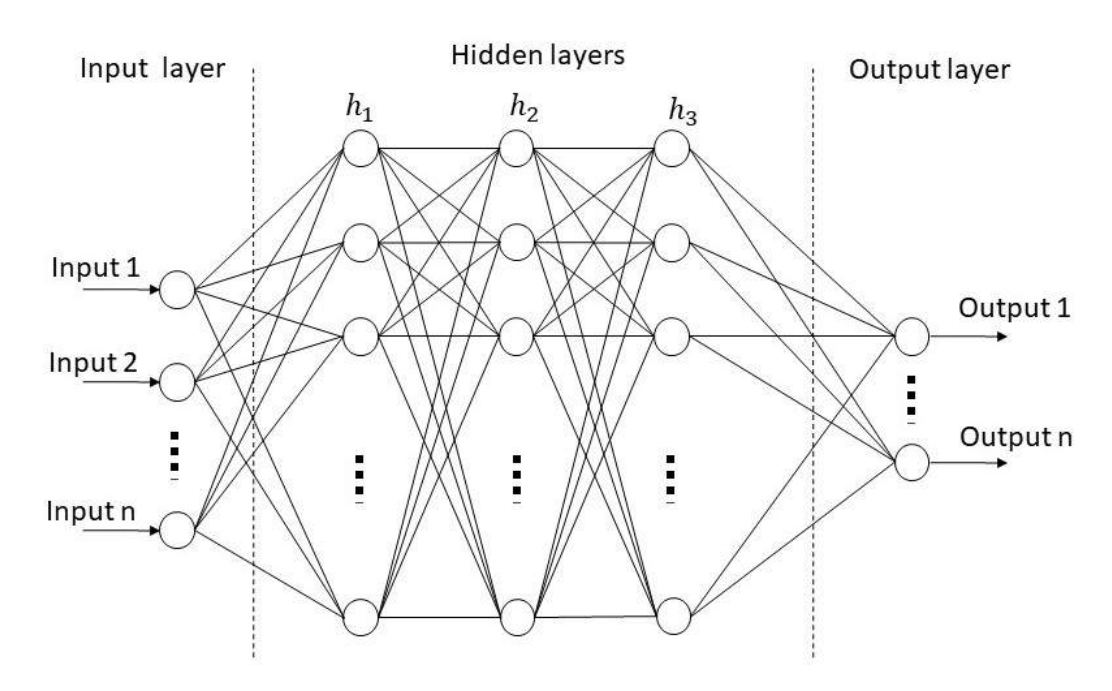


Figure 5.3: Schematic illustration of an artificial neural network

work, a surrogate model based, with an iterative approach is employed. Since this method requires minimal data, it is more efficient numerically.

The goal is to find the most optimal flow rates for the second and third zones in the SMB system. Henry constants define the initial guess, and the area around the initial guess is defined in the same way as the area in full model optimization. The Henry constants are [5,7.5] and the area domain is  $m_2\epsilon[3,7]$  and  $m_3\epsilon[5.5,9.5]$ . This big area is the first area to be explored to find the best possible optimal point as the initial guess for the next calculation. Points within the area are generated using the Halton set algorithm developed by Kocis et al. (1997) [42]. The Halton set generates points using the Halton sequence in a quasi-random form. In order to ensure uniform space-filling, the Halton sequence employs distinct prime bases for each dimension. When it comes to sampling, using space-filling approaches can prevent clustering, as opposed to the random distribution of sampling points.

The locations of these points generated by the Halton set inside the sampling area are taken as m-values  $(m_2, m_3)$ . For every point within the area, the dynamic simulation is used till a cyclic steady state is reached

to evaluate the purity and productivity of the SMB process. This simulation generates output data, including purity and productivity. These values are saved individually for each point, represented by a pair of m-values. To determine the purity of the products and their productivity at every point, the reference model is utilized.

For every iteration, the Halton set is generating 150 points. In order to be considered for further calculation, each point must have a purity greater than 0.85 as determined by the reference model. For surrogate model optimization, only points that meet purity criteria are considered.

In every iteration, the sample points are saved and can be reused if they fall within the sampling area of the subsequent iteration. The number of samples in each iteration may vary, potentially exceeding or falling below the 150 points. A neural network is trained using the data obtained from this calculation. The feed-forward neural network consists of a single layer comprising 15 neurons.

During every iteration, the surrogate model employs the exact same optimization algorithm as the full model, which involves applying the SQP algorithm and multi-starting with 100 random points. The model also employs a step tolerance option set at 1e-8 to determine an optimal point. The calculation process involves comparing the deviation of each iteration's optimal point to the previously calculated optimum. If this deviation exceeds the termination condition of 0.019, the next calculation will commence. However, if the deviation is within the threshold, the final optimal point will be determined. To establish a new sampling region, the formula below uses the current optimal point as the reference point.

$$lb/ub = x_{opt,k-1} \pm \frac{1}{2k}$$
 (5.10)

The integer "k" represents the number of times the iteration is repeated. The center of the current calculation area is determined by the optimal point found in the previous iteration. As a result of Equation 5.10, the area of the sample box is shrinking and the density of samples inside is

increasing at the same time. The algorithm concluded after 4 iterations in the current calculation process. Figure 5.4 depicts the progress.

In the first figure, the red star represents the optimal point in the initial iteration, and the red circle represents the initial guess for starting the calculation. In this visualization, the black dots represent the entire sample data generated by the Halton set. On the other hand, the blue dots indicate the samples that meet the purity requirement as determined by the reference model.

To find the optimal solution, a new area is created using a convex hull that encompasses all the blue dots. The optimizer then searches within this area. The convex hull is a fundamental concept in computational geometry that refers to the smallest convex polygon or polyhedron that encloses a set of points in a given space.

The significance of the shrinking effect is evident only in the initial iteration, highlighting the crucial role of the first sampling region. The significant contrast between the initial and subsequent regions is attributed to the application of Equation 5.10.

According to the second figure, one can see that the area of the field is decreasing at a constant rate. As a result of the reduction in purity requirement that defines the convex hull, the optimal point can be found along its boundary within the greatest distance to the diagonal  $m_2 = m_3$ .

The last figure shows a deviation from the previous optimum that is less than the termination condition and therefore, the calculation stops. The optimal point found using the surrogate model is compared to the one found by the full model.

Surrogate models use the same initial guess point as full-model optimizations. The final optimal point discovered through the surrogate model closely aligns with the optimal point attained through full-model optimization. The reference model calculates the concentration of the extract, as well as the raffinate, and productivity based on the optimal points identified by both models. The results and computational time

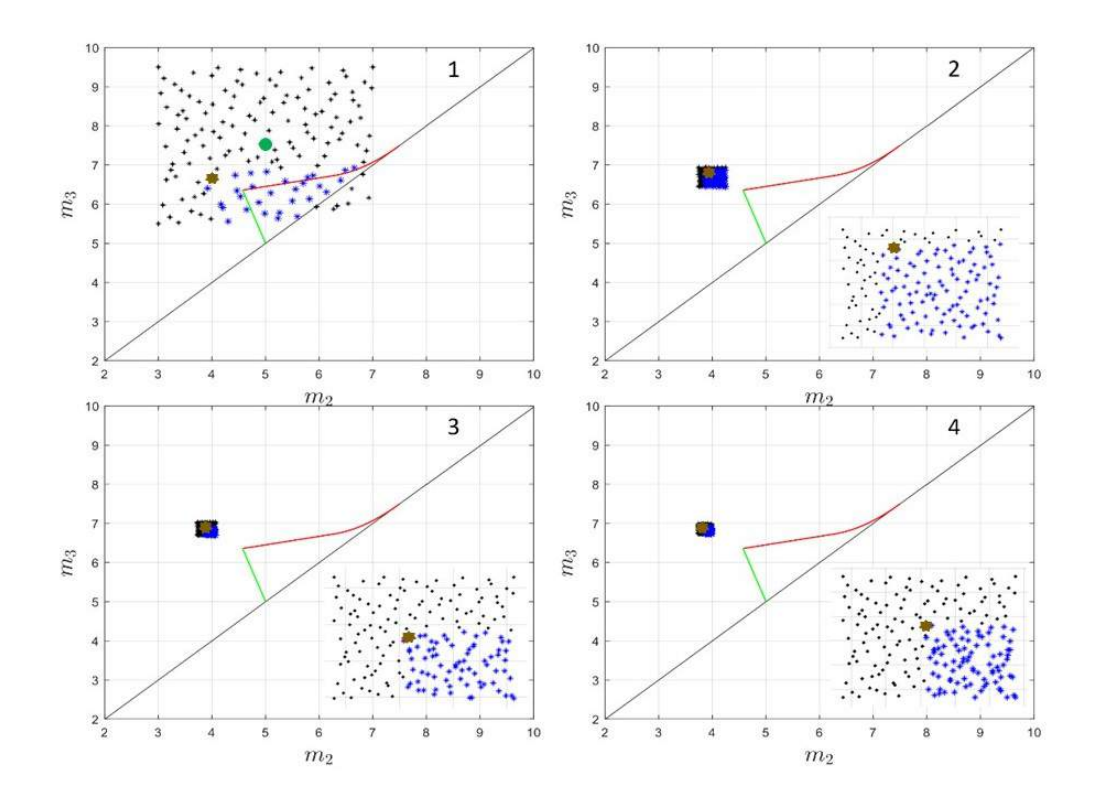


Figure 5.4: Optimal point reached in each iteration and the process of converging towards the final optimum. The green dot in the up left diagram is the starting point.

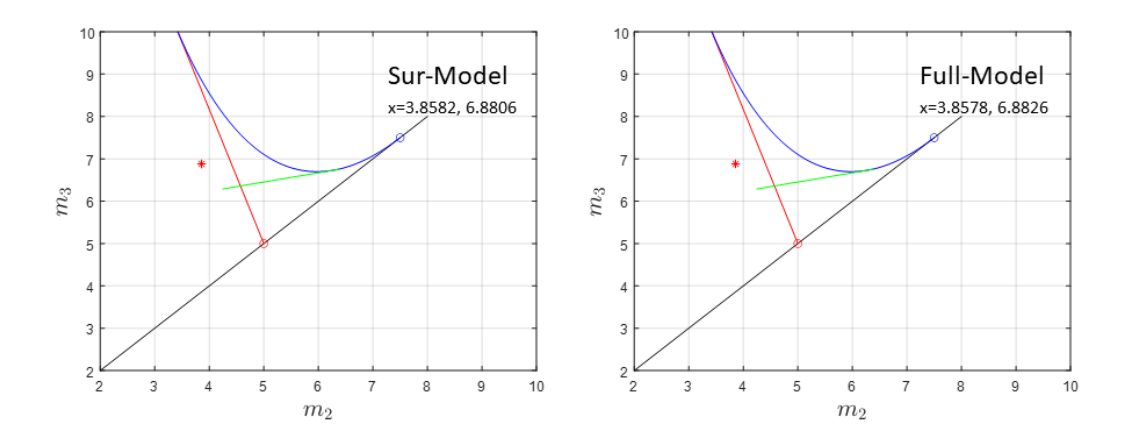


Figure 5.5: Optimal points (x) found by surrogate model and full model.

for both methods are shown in Table 5.1.

The reference model has verified that the purity requirements have been met. Although the optimal point of the full model results in slightly higher productivity compared to the surrogate model, the difference be-

Table 5.1: Comparison of the computational time

method	$x_{opt}$	CPU-time	$pu_{ex}$	$pu_{raf}$	pr
sur-model	3.8582, 6.8806	5423.75  s	0.8501	0.8504	3.0224
full-model	3.8578,  6.8826	$152453~\mathrm{s}$	0.8500	0.8500	3.0249

tween the two is minimal. Although the outcomes are nearly the same, the surrogate model proves to be a more favorable option for the optimization set-up due to its significantly quicker computational time compared to the full model.

#### 5.5 Summary

This chapter introduced a surrogate-based optimization approach for the SMB process. Instead of relying on a time consuming rigorous model, optimization can be achieved through the use of a surrogate model. By applying this approach, the productivity of SMB is optimized with reasonable computational effort. Due to reduced purity, it was anticipated that the optimal point would be located outside the triangle. Based on the optimization set-up presented, the surrogate model is a better option as it has a significantly faster computational time compared to the full model. The methodology suggested could be highly beneficial, especially when deterministic global optimization is employed, as demonstrated in Kessler et al.'s research [38]. However, due to the extensive number of model evaluations required, it was not within the scope of this paper. In future work, the goal is to reduce the amount of solvent used. This can be achieved by minimizing the difference between  $m_1$  and  $m_4$ . In addition, optimization of the SMB with Bi-Langmuir isotherm is also of interest.

## **CHAPTER 6**

# Conclusions and perspectives

In this thesis, new efficient methods for the simulation and optimization of SMB processes are presented. These new techniques speed up the simulation and reduce its computational effort. Avoiding standard numerical solution procedures of the PDEs and ODEs leads to the absence of numerical dispersion. Despite their speed and accuracy, these methods have some limitations. To overcome these limitations, surrogate models are used instead of numerical models for optimization of SMB, which results in a faster optimization with less computational effort. The following summarizes the main results.

#### 6.1 Analytical solution

Based on an ideal equilibrium model, an accurate and fast method for simulating chromatographic columns with linear adsorption isotherms was presented. This method is best suited for chromatographic columns that are highly efficient, with negligible axial dispersion and sharp concentration fronts.

In this method, there are no fixed grid points in the z coordinate representing the column's length. As an alternative, a moving coordinate is assumed, where the component travels through the column at its corresponding velocity. Each component's propagation velocity determines

the distance traveled at each time step.

The proposed approach outperforms the popular cell model-based approaches. It was proven that the method can be applied to binary and ternary SMB processes with center-cut separations and even more challenging, a five-component SMB process. The approach mentioned above can be conveniently extended to other process setups and can be employed in the future for rigorous optimizations and assessment of various process schemes for ternary center-cut separations.

### 6.2 Approximate solution

The analytical method is extended to simulate nonlinear, noncompetitive chromatography. According to the Langmuir adsorption isotherm, higher concentrations travel faster than lower concentrations. In order to determine the concentration profile, it is necessary to calculate the velocity of each concentration value. If higher concentrations attempt to pass lower ones, the shock velocity is calculated, and both concentration values travel together at the same velocity within the column. The accuracy of this solution relies on how the concentration value is discretized. Therefore, the solution being proposed is an approximate solution. The precision of the approximate method improves as the time and concentration vector discretization increase. Initially, the solution is implemented in single-column chromatography and later in 4-zone SMB to evaluate its precision. However, it can also be employed in other chromatographic setups. The concentration profiles and calculation time obtained by the approximate solution are compared to those of the popular cell model.

Despite the approximate method's smaller computational time compared to the cell model, it is able to detect all the concentration profile details in both cases single column and 4-zone SMB. Similar to the analytical solution, this method is also suitable for chromatographic columns with high efficiency and negligible axial dispersion. An extension to competitive isotherms seems possible but more challenging due to the interaction between different components.

#### 6.3 Surrogate-model optimization

Finally, an optimization approach employing a surrogate model for the SMB process was presented. Instead of using a time-consuming rigorous model, optimization is achieved through the use of a surrogate model. The final optimal points calculated by both models demonstrate this approach's effectiveness. By employing the surrogate model, we were able to optimize SMB productivity with a reasonable amount of computational effort. Because of reduced purity, it was anticipated that the optimal point would be outside the triangle.

The productivity, as well as the purity of the extract and raffinate, are calculated by the reference model for the optimal points obtained by both models. As a result, the purity requirements are met. The difference in productivity between the full model's optimal point and the surrogate model is negligible. Although the results are nearly identical, the surrogate model proves to be a superior option due to its significantly faster computational time compared to the full model for the given optimization scenario. In the future, we aim to reduce solvent usage by minimizing the difference between  $m_1$  and  $m_4$ . Moreover, there is also considerable interest in the optimization of the SMB using Bi-Langmuir isotherms.

# **Bibliography**

- [1] G. Agrawal and Y. Kawajiri. "Comparison of various ternary simulated moving bed separation schemes by multi-objective optimization". In: *Journal of Chromatography A* 1238 (2012), pp. 105–113.
- [2] G. Agrawal, B. Sreedhar, and Y. Kawajiri. "Systematic optimization and experimental validation of ternary simulated moving bed chromatography systems". In: *Journal of Chromatography A* 1356 (2014), pp. 82–95.
- [3] B.-M. Andreev, A.-V. Kruglov, and Y.-L. Selivanenko. "Continuous isotope separation by simulated countercurrent moving bed chromatography and ion exchange". In: *Fundamentals of Adsorption*. Springer, 1996, pp. 43–50.
- [4] L. Aumann and M. Morbidelli. "A continuous multicolumn countercurrent solvent gradient purification (MCSGP) process". In: *Bio technology and Bioengineering* 98.5 (2007), pp. 1043–1055.
- [5] D.-C.-S. Azevedo and A.-E. Rodrigues. "Design and optimization of new simulated moving bed plants". In: *Brazilian Journal of Chemical Engineering* 23 (2006), pp. 171–181.
- [6] D.-C.-S. Azevedo and A.-E. Rodrigues. "Design of a simulated moving bed in the presence of mass-transfer resistances". In: AIChE journal 45.5 (1999), pp. 956–966.
- [7] D. Beltscheva, P. Hugo, and A. Seidel-Morgenstern. "Linear two-step gradient counter-current chromatography: analysis based on a recursive solution of an equilibrium stage model". In: *Journal of chromatography A* 989.1 (2003), pp. 31–45.

- [8] G. Bergeot, D. Leinekugel-Le-Cocq, L. Wolff, L. Muhr, and M. Bailly. "Intensification of paraxylene production using a simulated moving bed reactor". In: Oil & Gas Science and Technology–Revue d'IFP Energies nouvelles 65.5 (2010), pp. 721–733.
- [9] J. Blehaut and R.-M. Nicoud. "Recent aspects in simulated moving bed". In: *Analysis* 26.7 (1998), pp. 60–70.
- [10] R. Bochenek, W. Marek, W. Piątkowski, and D. Antos. "Evaluating the performance of different multicolumn setups for chromatographic separation of proteins on hydrophobic interaction chromatography media by a numerical study". In: *Journal of Chromatography A* 1301 (2013), pp. 60–72.
- [11] D.-B. Broughton and C.-G. Gerhold. Continuous sorption process employing fixed bed of sorbent and moving inlets and outlets. US Patent 2,985,589. 1961.
- [12] B.-R. Caes, T.-R. Van Oosbree, F. Lu, J. Ralph, C.-T. Maravelias, and R.-T. Raines. "Simulated moving bed chromatography: separation and recovery of sugars and ionic liquid from biomass hydrolysates". In: *ChemSusChem* 6.11 (2013), pp. 2083–2089.
- [13] V.-P. Chernev, A. Vande Wouwer, and A. Kienle. "Efficient simulation of chromatographic processes using the conservation element/solution element method". In: *Processes* 8.10 (2020), p. 1316.
- [14] C.-B. Ching, D.-M. Ruthven, and K. Hidajat. "Experimental study of a simulated counter-current adsorption system—III. Sorbex operation". In: *Chemical Engineering Science* 40.8 (1985), pp. 1411–1417.
- [15] C.-A.-M. Cristancho, S. Peper, and M. Johannsen. "Supercritical fluid simulated moving bed chromatography for the separation of ethyl linoleate and ethyl oleate". In: *The Journal of Supercritical Fluids* 66 (2012), pp. 129–136.
- [16] C.-A.-M. Cristancho and A. Seidel-Morgenstern. "Purification of single-chain antibody fragments exploiting pH-gradients in simu-

- lated moving bed chromatography". In: Journal of Chromatography A 1434 (2016), pp. 29–38.
- [17] F. Denet, W. Hauck, R.-M. Nicoud, O. Di Giovanni, M. Mazzotti, J.- N. Jaubert, and M. Morbidelli. "Enantioseparation through supercritical fluid simulated moving bed (SF-SMB) chromatography". In: *Industrial & Engineering Chemistry Research* 40.21 (2001), pp. 4603–4609.
- [18] O. Di Giovanni, M. Mazzotti, M. Morbidelli, F. Denet, W. Hauck, and R.-M. Nicoud. "Supercritical fluid simulated moving bed chromatography: II. Langmuir isotherm". In: *Journal of Chromatography A* 919.1 (2001), pp. 1–12.
- [19] G. Dünnebier and K.-U. Klatt. "Modeling of chromatographic separation processes using nonlinear wave theory". In: *IFAC Proceedings Volumes* 31.11 (1998), pp. 499–504.
- [20] M. Fütterer. "On design and control of simulated moving bed plants". In: (2010).
- [21] I. Ghazi, L. Fernandez-Arrojo, A. Gomez De Segura, M. Alcalde, and A. Plou F.-J.and Ballesteros. "Beet sugar syrup and molasses as low-cost feedstock for the enzymatic production of fructo- oligosaccharides". In: *Journal of Agricultural and Food Chemistry* 54.8 (2006), pp. 2964–2968.
- [22] G. Guiochon, A. Felinger, and D.-G. Shirazi. Fundamentals of preparative and nonlinear chromatography. Elsevier, 2006.
- [23] G. Guiochon, B. Lin, et al. *Modeling for preparative chromatogra*phy. Academic press, 2003.
- [24] F.-G. Helfferich and P.-W. Carr. "Non-linear waves in chromatography: I. Waves, shocks, and shapes". In: *Journal of Chromatography* A 629.2 (1993), pp. 97–122.
- B.-J. Hritzko, Y. Xie, R.-J. Wooley, and N.-H.-L. Wang. "Standing-wave design of tandem SMB for linear multicomponent systems".
   In: AIChE journal 48.12 (2002), pp. 2769–2787.

- [26] J.-S. Hur and P.-C Wankat. "Hybrid simulated moving bed and chromatography systems for center-cut separation from quaternary mixtures: Linear isotherm systems". In: *Industrial & Engineering Chemistry Research* 45.25 (2006), pp. 8713–8722.
- [27] S. Javeed, S. Qamar, A. Seidel-Morgenstern, and G. Warnecke. "Efficient and accurate numerical simulation of nonlinear chromatographic processes". In: *Computers & Chemical Engineering* 35.11 (2011), pp. 2294–2305.
- [28] S. Jermann, M. Meijssen, and M. Mazzotti. "Three column intermittent simulated moving bed chromatography: 3. Cascade operation for center-cut separations". In: *Journal of Chromatography A* 1378 (2015), pp. 37–49.
- [29] C. Jiang, F. Huang, and F. Wei. "A pseudo three-zone simulated moving bed with solvent gradient for quaternary separations". In: *Journal of Chromatography A* 1334 (2014), pp. 87–91.
- [30] W. Jin and P.-C. Wankat. "Thermal operation of four-zone simulated moving beds". In: *Industrial & Engineering Chemistry Research* 46.22 (2007), pp. 7208–7220.
- [31] S.-H. Jo, J.-K. Kim, C.-G. Yoo, J.-I. Kim, Y.-M. Koo, and S. Mun. "Comparative Analysis of Single-Cascade Five-Zone and Two-Zone SMB Systems for the Separation of a Ternary Amino Acid Mixture". In: *The Canadian Journal of Chemical Engineering* 85.6 (2007), pp. 874–882.
- [32] S.-H. Kang, J.-H. Kim, and S. Mun. "Optimal design of a tandem simulated moving bed process for separation of paclitaxel, 13-dehydroxybaccatin III, and 10-deacetylpaclitaxel". In: *Process Biochemistry* 45.9 (2010), pp. 1468–1476.
- [33] M. Kaspereit, P. Jandera, M. Škavrada, and A. Seidel-Morgenstern. "Impact of adsorption isotherm parameters on the performance of enantioseparation using simulated moving bed chromatography". In: *Journal of Chromatography A* 944.1-2 (2002), pp. 249–262.

- [34] M. Kaspereit, A. Seidel-Morgenstern, and A. Kienle. "Design of simulated moving bed processes under reduced purity requirements". In: *Journal of Chromatography A* 1162.1 (2007), pp. 2–13.
- [35] S. Katsuo, C. Langel, P. Schanen, and M. Mazzotti. "Extra-column dead volume in simulated moving bed separations: Theory and experiments". In: *Journal of Chromatography A* 1216.7 (2009), pp. 1084–1093.
- [36] Y. Kawajiri and L.-T. Biegler. "Optimization strategies for simulated moving bed and PowerFeed processes". In: *AIChE Journal* 52.4 (2006), pp. 1343–1350.
- [37] L.-C. Keßler and A. Seidel-Morgenstern. "Theoretical study of multicomponent continuous countercurrent chromatography based on connected 4-zone units". In: *Journal of Chromatography A* 1126.1-2 (2006), pp. 323–337.
- [38] T. Keßler. "Global optimization for integrated solvent and process design". In: (2021).
- [39] J.-K Kim, Y. Zang, and P.-C Wankat. "Single-cascade simulated moving bed systems for the separation of ternary mixtures". In: *Industrial & Engineering Chemistry Research* 42.20 (2003), pp. 4849–4860.
- [40] K.-M. Kim, J.-W. Lee, S. Kim, F.-V. Santos da Silva, A. Seidel-Morgenstern, and C.-H. Lee. "Advanced operating strategies to extend the applications of simulated moving bed chromatography". In: Chemical Engineering & Technology 40.12 (2017), pp. 2163–2178.
- [41] D. Kiwala, J. Mendrella, D. Antos, and A. Seidel-Morgenstern. "Center-cut separation of intermediately adsorbing target component by 8-zone simulated moving bed chromatography with internal recycle". In: *Journal of Chromatography A* 1453 (2016), pp. 19–33.
- [42] L. Kocis and W.-J. Whiten. "Computational investigations of low-discrepancy sequences". In: *ACM Transactions on Mathematical Software (TOMS)* 23.2 (1997), pp. 266–294.

- [43] A.-V. Kruglov, B.-M Andreev, and Y.-E. Pojidaev. "Continuous isotope separation in systems with solid phase. II. Separation of nitrogen isotopes with use of ion-exchange resin". In: *Separation Science and Technology* 31.4 (1996), pp. 471–490.
- [44] A.-S. Kurup, K. Hidajat, and A.-K. Ray. "Comparative study of modified simulated moving bed systems at optimal conditions for the separation of ternary mixtures of xylene isomers". In: *Industrial & Engineering Chemistry Research* 45.18 (2006), pp. 6251–6265.
- [45] H.-H. Lee, K.-M. Kim, and C.-H. Lee. "Improved performance of simulated moving bed process using column-modified feed". In: *AIChE journal* 57.8 (2011), pp. 2036–2053.
- [46] J.-W Lee and A. Seidel-Morgenstern. "Solving hyperbolic conservation laws with active counteraction against numerical errors: Isothermal fixed-bed adsorption". In: *Chemical Engineering Science* 207 (2019), pp. 1309–1330.
- [47] J.-W Lee and P.-C. Wankat. "Design of pseudo-simulated moving bed process with multi-objective optimization for the separation of a ternary mixture: Linear isotherms". In: *Journal of Chromatogra-phy A* 1217.20 (2010), pp. 3418–3426.
- [48] R.-J. LeVeque and R.-J. Leveque. *Numerical methods for conservation laws*. Vol. 214. Springer, 1992.
- [49] S. Leweke and E. von Lieres. "Chromatography analysis and design toolkit (CADET)". In: Computers & Chemical Engineering 113 (2018), pp. 274–294.
- [50] S. Li, L. Feng, P. Benner, and A. Seidel-Morgenstern. "Using surrogate models for efficient optimization of simulated moving bed chromatography". In: *Computers & Chemical Engineering* 67 (2014), pp. 121–132.
- [51] E. von Lieres and J. Andersson. "A fast and accurate solver for the general rate model of column liquid chromatography". In: *Computers & Chemical Engineering* 34.8 (2010), pp. 1180–1191.

- [52] Y.-I. Lim, S.-C. Chang, and S.-B. Jørgensen. "A novel partial differential algebraic equation (PDAE) solver: iterative space—time conservation element/solution element (CE/SE) method". In: Computers & Chemical Engineering 28.8 (2004), pp. 1309–1324.
- [53] H. Lorenz, P. Sheehan, and A. Seidel-Morgenstern. "Coupling of simulated moving bed chromatography and fractional crystallisation for efficient enantioseparation". In: *Journal of Chromatography* A 908.1-2 (2001), pp. 201–214.
- [54] M. Mazzotti and A. Rajendran. "Equilibrium theory—based analysis of nonlinear waves in separation processes". In: *Annual Review of Chemical and Biomolecular Engineering* 4 (2013), pp. 119–141.
- [55] M. Mazzotti, G. Storti, and M. Morbidelli. "Optimal operation of simulated moving bed units for nonlinear chromatographic separations". In: *Journal of Chromatography A* 769.1 (1997), pp. 3–24.
- [56] C. Migliorini, M. Mazzotti, and M. Morbidelli. "Continuous chromatographic separation through simulated moving beds under linear and nonlinear conditions". In: *Journal of Chromatography A* 827.2 (1998), pp. 161–173.
- [57] S. Mun. "Effect of a partial-feeding application on product purities and throughput of a five-zone simulated moving bed process for the separation of a ternary nucleoside mixture". In: *Process Biochemistry* 46.4 (2011), pp. 977–986.
- [58] S. Mun. "Enhanced performance of a tandem simulated moving bed process for separation of paclitaxel, 13-dehydroxybaccatin III, and 10-deacetylpaclitaxel by making a difference between the adsorbent particle sizes of the two subordinate simulated moving bed units". In: *Process Biochemistry* 46.6 (2011), pp. 1329–1334.
- [59] S. Mun. "Improving performance of a tandem simulated moving bed process for sugar separation by making a difference in the adsorbents and the column lengths of the two subordinate simulated moving bed units". In: *Journal of Chromatography A* 1277 (2013), pp. 48–57.

- [60] A- Nicolaos, L. Muhr, P. Gotteland, R.-M. Nicoud, and M. Bailly. "Application of equilibrium theory to ternary moving bed configurations (four+ four, five+ four, eight and nine zones): I. Linear case". In: *Journal of Chromatography A* 908.1-2 (2001), pp. 71–86.
- [61] R.-M. Nicoud. *Chromatographic Processes*. Cambridge University Press, 2015.
- [62] J. Nowak. "Separation of Ternary Mixtures by Simulated Moving Bed Chromatography: Theoretical Study and Experimental Validation". PhD thesis. docupoint Barleben, 2013.
- [63] J. Nowak, D. Antos, and A. Seidel-Morgenstern. "Theoretical study of using simulated moving bed chromatography to separate intermediately eluting target compounds". In: *Journal of Chromatography A* 1253 (2012), pp. 58–70.
- [64] S.-M. Pirrung, L.-A. van der Wielen, R.-F. van Beckhoven, E.-J van de Sandt, M.-H. Eppink, and M. Ottens. "Optimization of biopharmaceutical downstream processes supported by mechanistic models and artificial neural networks". In: *Biotechnology Progress* 33.3 (2017), pp. 696–707.
- [65] R. Pishkari, M. Fechtner, T. Keßler, and A. Kienle. "Optimization of Simulated Moving Bed Chromatographic Processes using Surrogate Models". In: Computer Aided Chemical Engineering. Vol. 52. Elsevier, 2023, pp. 343–348.
- [66] R. Pishkari and A. Kienle. "Fast and accurate simulation of simulated moving bed chromatographic processes with linear adsorption isotherms". In: *Computer Aided Chemical Engineering*. Vol. 48. Elsevier, 2020, pp. 487–492.
- [67] A. Rajendran, G. Paredes, and M. Mazzotti. "Simulated moving bed chromatography for the separation of enantiomers". In: *Journal of Chromatography A* 1216.4 (2009), pp. 709–738.
- [68] H.-K. Rhee, R. Aris, and N.-R. Amundson. First-order partial differential equations. Vol. 1. Courier Corporation, 2014.

- [69] H.-K. Rhee, R. Aris, and N.-R. Amundson. *Theory and application of hyperbolic systems of quasilinear equations*. Vol. 2. Courier Corporation, 2001.
- [70] D.-M. Ruthven. *Principles of adsorption and adsorption processes*. John Wiley & Sons, 1984.
- [71] D.-M. Ruthven and C.-B. Ching. "Counter-current and simulated counter-current adsorption separation processes". In: *Chemical Engineering Science* 44.5 (1989), pp. 1011–1038.
- [72] F. Santos da Silva. "Analysis and design of center-cut separations using 8-zone simulated moving bed chromatography". PhD thesis. Otto-von-Guericke-Universität Magdeburg, 2017.
- [73] H. Schmidt-Traub, M. Schulte, and A. Seidel-Morgenstern. *Preparative chromatography*. John Wiley & Sons, 2020.
- [74] M. Schulte, J.-N. Kinkel, R.-M. Nicoud, and F. Charton. "Simulated Moving-Bed Chromatograph-An Efficient Technique to Producing Optically Active Compounds on an Industrial-Scale". In: *Chemie Ingenieur Technik* 68.6 (1996), pp. 670–670.
- [75] A. Seidel-Morgenstern. Mathematische Modellierung der präparativen Flüssigchromatographie. Deutscher Universitätsverlag, 1995.
- [76] A. Seidel-Morgenstern, L. Christian Kessler, and M. Kaspereit. "New developments in simulated moving bed chromatography". In: Chemical Engineering & Technology: Industrial Chemistry-Plant Equipment-Process Engineering-Biotechnology 31.6 (2008), pp. 826–837.
- [77] F.-V.-S. da Silva and A. Seidel-Morgenstern. "Evaluation of center-cut separations applying simulated moving bed chromatography with 8 zones". In: *Journal of Chromatography A* 1456 (2016), pp. 123–136.
- [78] L.-R. Snyder, J.-J. Kirkland, and J.-W. Dolan. *Introduction to modern liquid chromatography*. John Wiley & Sons, 2011.

- [79] G. Storti, R. Baciocchi, M. Mazzotti, and M. Morbidelli. "Design of optimal operating conditions of simulated moving bed adsorptive separation units". In: *Industrial & Engineering Chemistry Research* 34.1 (1995), pp. 288–301.
- [80] G. Storti, M. Masi, R. Paludetto, M. Morbidelli, and S. Carrà. "Adsorption separation processes: countercurrent and simulated countercurrent operations". In: *Computers & Chemical Engineering* 12.5 (1988), pp. 475–482.
- [81] G. Storti, M. Mazzotti, M. Morbidelli, and S. Carrà. "Robust design of binary countercurrent adsorption separation processes". In: *AIChE Journal* 39.3 (1993), pp. 471–492.
- [82] A. Tarafder, L. Aumann, Thomas Müller-S., and M. Morbidelli. "Improvement of an overloaded, multi-component, solvent gradient bioseparation through multiobjective optimization". In: *Journal of Chromatography A* 1167.1 (2007), pp. 42–53.
- [83] P.-C. Wankat. "Simulated moving bed cascades for ternary separations". In: *Industrial & Engineering Chemistry Research* 40.26 (2001), pp. 6185–6193.
- [84] M. Wellhoefer, W. Sprinzl, R. Hahn, and A. Jungbauer. "Continuous processing of recombinant proteins: Integration of inclusion body solubilization and refolding using simulated moving bed size exclusion chromatography with buffer recycling". In: *Journal of Chromatography A* 1319 (2013), pp. 107–117.
- [85] A.-V. Wouwer, P. Saucez, C. Vilas, et al. "Simulation of ode/pde Models With Matlab, Octave and Scilab". In: *Cham: Springer* (2014).
- [86] Z. Zhang, M. Mazzotti, and M. Morbidelli. "Multiobjective optimization of simulated moving bed and Varicol processes using a genetic algorithm". In: *Journal of chromatography A* 989.1 (2003), pp. 95–108.

[87] G. Zhong and G. Guiochon. "Analytical solution for the linear ideal model of simulated moving bed chromatography". In: *Chemical Engineering Science* 51.18 (1996), pp. 4307–4319.